

**FIXED-BED ADSORPTION OF CARBON DIOXIDE ONTO  
AMMONIA-MODIFIED ACTIVATED CARBON:  
EXPERIMENTAL AND MODELING STUDY**

**MOHAMMAD SALEH SHAFEEYAN**

**THESIS SUBMITTED IN FULFILLMENT  
OF THE REQUIREMENTS FOR THE DEGREE OF  
DOCTOR OF PHILOSOPHY**

**FACULTY OF ENGINEERING  
UNIVERSITY OF MALAYA  
KUALA LUMPUR**

**2015**

**UNIVERSITI MALAYA**  
**ORIGINAL LITERARY WORK DECLARATION**

**Name of Candidate:** Mohammad Saleh Shafeeyan (I.C/Passport No: P95425115)

**Registration/Matric No:** KHA110017

**Name of Degree:** DOCTOR OF PHILOSOPHY

**Title of Project Paper/Research Report/Dissertation/Thesis (“this Work”):**

FIXED-BED ADSORPTION OF CARBON DIOXIDE ONTO AMMONIA-MODIFIED  
ACTIVATED CARBON: EXPERIMENTAL AND MODELING STUDY

**Field of Study:** Chemical Engineering

**I do solemnly and sincerely declare that:**

- (1) I am the sole author/writer of this Work;
- (2) This Work is original;
- (3) Any use of any work in which copyright exists was done by way of fair dealing and for permitted purposes and any excerpt or extract from, or reference to or reproduction of any copyright work has been disclosed expressly and sufficiently and the title of the Work and its authorship have been acknowledged in this Work;
- (4) I do not have any actual knowledge nor ought I reasonably to know that the making of this work constitutes an infringement of any copyright work;
- (5) I hereby assign all and every rights in the copyright to this Work to the University of Malaya (“UM”), who henceforth shall be owner of the copyright in this Work and that any reproduction or use in any form or by any means whatsoever is prohibited without the written consent of UM having been first had and obtained;
- (6) I am fully aware that if in the course of making this Work I have infringed any copyright whether intentionally or otherwise, I may be subject to legal action or any other action as may be determined by UM.

**Candidate’s Signature**

**Date:** 23 January 2015

**Subscribed and solemnly declared before,**

**Witness’s Signature**

**Date:** 23 January 2015

**Name:** Dr. Jayakumar Natesan Subramanian Nayagar  
**Designation:** Department of Chemical Engineering,  
Faculty of Engineering, University of Malaya, Kuala Lumpur, 50603, Malaysia  
Tel. /Fax: +60 379675294/ +60 379675319

## ABSTRACT

A commercial granular activated carbon (GAC) adsorbent was modified through an oxidation–amination process in an effort to increase its surface basicity and consequently enhance its CO<sub>2</sub> adsorption capacity. To optimize the amination conditions of activated carbon adsorbents the effects of amination temperature, amination time, and the type of starting materials (variables) on the CO<sub>2</sub> adsorption/desorption capacities of the adsorbents (responses) were investigated using a central composite design. The use of a pre-oxidized sorbent as a starting material and amination at 425 °C for 2.1 h were found to be the optimum conditions for obtaining an efficient carbon dioxide adsorbent. The activated carbon modified at optimum conditions (OXA-GAC) exhibited CO<sub>2</sub> adsorption and desorption capacity values of 26.47 mg/g and 95.4%, respectively. The promising characteristics of the OXA-GAC in terms of adsorption capacity (exhibiting an increase of 44% in capacity compared with the capacity of the GAC at 1 atm and 105 °C) and multicycle durability make it suitable for practical applications.

The equilibrium adsorption isotherms of CO<sub>2</sub> on the GAC and the OXA-GAC were measured using a static volumetric method. CO<sub>2</sub> adsorption measurements were performed at three different temperatures (303, 318, and 333 K) and pressures up to 1 atm. The obtained equilibrium data were fitted to the Freundlich, Sips, and Toth isotherms using a semi-empirical approach to differentiate the contributions of physical and chemical adsorption to the total CO<sub>2</sub> uptake. The Toth semi-empirical equilibrium model provided the best fit to the experimental data, over the entire analyzed ranges of temperature and pressure. The isosteric heats of CO<sub>2</sub> adsorption onto the GAC and OXA-GAC adsorbents were determined using the Clausius–Clapeyron equation. The initial isosteric heats of adsorption of 68 kJ mol<sup>-1</sup> and 23 kJ mol<sup>-1</sup> corresponded to the chemisorption and physisorption of CO<sub>2</sub> on the OXA-GAC adsorbent, respectively, and these values were in

excellent agreement with the zero-coverage heats of adsorption obtained using the temperature-dependent parameters of the proposed model.

The kinetics of CO<sub>2</sub> adsorption on the GAC and OXA-GAC adsorbents over the temperature range of 30–60 °C were studied using the pseudo-first-order, pseudo-second-order, and Avrami kinetic models. The best fit with the experimental kinetic data for both of the studied adsorbents was obtained by applying the Avrami kinetic model. Fixed-bed breakthrough experiments for CO<sub>2</sub> adsorption onto the GAC and OXA-GAC adsorbents were performed by changing the adsorption temperature over the range of 30 to 60 °C and the feed flow rate from 50 to 100 ml min<sup>-1</sup>. The largest values of the CO<sub>2</sub> equilibrium dynamic capacity (0.67 mol kg<sup>-1</sup>) and breakthrough time (10.9 min) over the range of operating conditions investigated were obtained using OXA-GAC adsorbent at 30 °C under a 50 ml min<sup>-1</sup> feed flow rate. To predict the breakthrough behavior of the fixed-bed adsorption of CO<sub>2</sub>, a simple model was developed, including the Toth and Avrami equations to describe the equilibrium and kinetics of adsorption, respectively. The set of coupled differential equations was solved using a numerical approach based on the finite element method implemented in COMSOL Multiphysics software. The validity of the model predictions was evaluated by a comparison with the experimental data. The findings showed that the model predictions successfully fit the experimental data over the studied range of feed gas flow rates and adsorption temperatures.

## ABSTRAK

A penjerap komersial karbon teraktif berbutir (GAC) telah diubahsuai melalui proses pengoksidaan-aminasi dalam usaha untuk meningkatkan permukaan kealkalian dan seterusnya meningkatkan keupayaan penjerapan CO<sub>2</sub>. Untuk mengoptimumkan keadaan ammoksidaan pada penjerap karbon teraktif, kesan suhu aminasi, masa aminasi dan jenis permulaan bahan (pembolehubah) pada penjerapan CO<sub>2</sub>/ kapasiti penyahjerapan penyerap yang diubahsuai (tindakbalas) telah dikaji menggunakan reka bentuk komposit pusat. Penggunaan penyerap pra-teroksida sebagai bahan permulaan dan aminasi pada 425 °C selama 2.1 jam didapati sebagai keadaan optimum untuk mendapatkan penyerap CO<sub>2</sub> yang berkesan. Karbon teraktif diubahsuai pada keadaan optimum telah menunjukkan penjerapan CO<sub>2</sub> dan nilai kapasiti penyahjerapan sebanyak 26.47 mg /g dan 95.4%. Ciri-ciri yang menggalakkan terhadap OXA-GAC dari segi kapasiti penjerapan (mempamerkan peningkatan sebanyak 44% dalam kapasiti berbanding dengan kapasiti GAC pada 1 atm and 105 °C) dan daya tahan pusingan perlbagai menjadikan ia sesuai untuk aplikasi praktikal.

Keseimbangan isoterma penjerapan CO<sub>2</sub> pada GAC dan penjerap yang optimum (OXA-GAC) telah diukur dengan menggunakan kaedah isipadu statik. Pengukuran penjerapan CO<sub>2</sub> telah dijalankan pada tiga suhu yang berbeza (303, 318, dan 333 K) dan pada tekanan sehingga 1 atm. Data keseimbangan diperolehi dipadankan dengan Freundlich, Sips dan Toth isoterma menggunakan pendekatan semi-empirikal untuk membezakan sumbangan penjerapan fizikal dan kimia untuk jumlah pengambilan CO<sub>2</sub>. Keseimbangan separa empirik Toth model disediakan sangat sepadan untuk data ujikaji, bagi sepanjang analysis untuk julat suhu dan tekanan. Saringan isosteric penjerapan CO<sub>2</sub> pada penjerap ammonia-diubahsuai dan pada penjerap yang tidak dirawat telah ditentukan dengan menggunakan persamaan Clausius-Clapeyron. Saringan awal isosteric penjerapan adalah 68 kJ mol<sup>-1</sup> dan 23 kJ mol<sup>-1</sup> sepadan dengan chemisorption dan physisorption CO<sub>2</sub> pada penjerap yang

diubah suai, dan nilai-nilai ini sangat sepadan dengan penjerapan saringan sifar-liputan diperolehi menggunakan parameter bersandar suhu kepada model yang dicadangkan.

Kinetik penjerapan CO<sub>2</sub> pada GAC dan OXA-GAC penjerap pada julat suhu 30-60 °C telah dikaji menggunakan pseudo-tertib pertama, pseudo-tertib kedua, dan Avrami model kinetik. Yang sepadan dengan data kinetik eksperimen untuk kedua-dua penjerap dikaji telah diperolehi dengan menggunakan model kinetik Avrami. “Fixed-bed breakthrough” eksperimen bagi penjerapan CO<sub>2</sub> ke atas GAC dan OXA-GAC penjerap yang dilakukan dengan menukar suhu penjerapan ke lingkungan julat 30 hingga 60 °C dan kadar aliran masuk dari 50-100 ml min<sup>-1</sup>. Nilai terbesar kapasiti dinamik keseimbangan CO<sub>2</sub> (0.67 mol kg<sup>-1</sup>) dan masa “breakthrough” (10.9 min) ke atas pelbagai keadaan operasi yang disiasat telah diperolehi dengan menggunakan OXA-GAC penjerap pada 30 °C di bawah aliran 50 ml min<sup>-1</sup> kadar aliran masuk. Untuk meramalkan keadaan “breakthrough” daripada penjerapan “fixed-bed” CO<sub>2</sub>, model yang mudah telah dibangunkan, termasuk Toth dan Avrami persamaan untuk menggambarkan keseimbangan dan kinetik penjerapan, masing-masing. Beberapa set persamaan pembezaan telah diselesaikan dengan menggunakan pendekatan yang berangka berdasarkan kaedah unsur terhingga dilaksanakan dalam perisian COMSOL Multifizik. Kesahihan ramalan model telah dinilai oleh perbandingan dengan data uji kaji. Keputusan kajian menunjukkan bahawa ramalan model berjaya sepadan dengan data uji kaji pada julat yang dikaji pada kadar aliran gas masuk dan suhu penjerapan.

*To my beloved parents, for their patient, encouragement and full support*  
*To My Beloved Wife, Rahil, For Her Constant Support, Understanding & Love*

## **ACKNOWLEDGEMENTS**

I extend my immense gratitude to my advisor, Prof. Dr. Wan Mohd Ashri Wan Daud. He is always willing to help me to go through difficulties I have encountered. His insightful comments and helpful suggestions are important in the making of the thesis. Without his guidance, support and patience this dissertation would not have been possible.

I am also very grateful to Ahmad shamiri and Amirhossein Houshmand. Their advice regarding the experimental techniques and the analysis of the data was truly invaluable, and it contributed greatly to both the quality of this work and my professional development.

Finally, many, many thanks are extended to my beloved brother and sisters for their never-ending love, support, and encouragement throughout my study overseas.



## TABLE OF CONTENTS

TITLE PAGE .....	i
ORIGINAL LITERARY WORK DECLARATION FORM.....	ii
ABSTRACT.....	iii
ABSTRAK.....	v
ACKNOWLEDGEMENTS.....	viii
TABLE OF CONTENTS.....	ix
LIST OF FIGURES.....	xiii
LIST OF TABLES.....	xv
LIST OF SYMBOLS AND ABBREVIATIONS.....	xvii
CHAPTER 1: INTRODUCTION .....	1
1.1 Background .....	1
1.2 Research objectives .....	3
1.3 Thesis organization .....	4
CHAPTER 2: LITERATURE REVIEW .....	6
2.1 Introduction.....	6
2.2 Overview of the prediction of adsorption column dynamics.....	9
2.3 Development and analysis of a mathematical model.....	32
2.3.1 Fluid phase material balance.....	32
2.3.2 Complexity of kinetic models .....	34
2.3.2.1 Local equilibrium model.....	35
2.3.2.2 Mass transfer resistance models.....	38
2.3.3 Energy balance .....	56
2.3.3.1 Gas phase energy balance.....	56

2.3.3.2	Solid phase energy balance.....	58
2.3.3.3	Wall energy balance.....	59
2.3.4	Momentum balance.....	61
CHAPTER 3: MATERIALS AND METHODS.....		64
3.1	Introduction.....	64
3.2	The application of response surface methodology to optimize the amination of activated carbon for the preparation of carbon dioxide adsorbents .....	64
3.2.1	Adsorbent materials.....	64
3.2.2	Ammonia modification.....	64
3.2.3	Experimental design and method of analysis.....	66
3.2.4	CO <sub>2</sub> adsorption/desorption measurements.....	72
3.3	A semi-empirical model to predict adsorption equilibrium of carbon dioxide on ammonia modified activated carbon .....	73
3.3.1	Adsorbent materials.....	73
3.3.2	Equilibrium CO <sub>2</sub> adsorption measurements .....	73
3.3.3	Adsorption isotherm equations.....	74
3.4	Modeling of carbon dioxide adsorption onto ammonia-modified activated carbon: Kinetic analysis and breakthrough behavior .....	76
3.4.1	Adsorbent materials.....	76
3.4.2	Kinetic adsorption measurements.....	76
3.4.3	Fixed-bed adsorption experiments .....	77
3.4.4	Model description and solution methodology .....	79
3.4.4.1	Kinetic models .....	79
3.4.4.2	Modeling dynamic column breakthrough experiments.....	84
3.4.4.3	Solution methodology.....	87

CHAPTER 4: RESULTS AND DISCUSSION .....	88
4.1 Introduction.....	88
4.2 The application of response surface methodology to optimize the amination of activated carbon for the preparation of carbon dioxide adsorbent.....	92
4.2.1 Evaluation of CO <sub>2</sub> adsorption and desorption capacity .....	92
4.2.1.1 Effect of amination variables on the CO <sub>2</sub> adsorption capacity.....	96
4.2.1.2 Effect of amination variables on the CO <sub>2</sub> desorption capacity.....	99
4.2.2 Investigation of the optimum amination conditions.....	102
4.2.3 Reusability of the sorbent prepared under optimum conditions .....	105
4.3 A semi-empirical model to predict adsorption equilibrium of carbon dioxide on ammonia modified activated carbon .....	106
4.3.1 Adsorption equilibrium study .....	106
4.3.2 Equilibrium isotherms modeling.....	109
4.3.3 Isothermic heat of adsorption .....	117
4.4 Modeling of carbon dioxide adsorption onto ammonia-modified activated carbon: Kinetic analysis and breakthrough behavior .....	122
4.4.1 Adsorption kinetics .....	122
4.4.2 Column breakthrough experiments and model validation .....	130
4.4.2.1 Effect of temperature on the breakthrough profile of CO <sub>2</sub> adsorption.....	132
4.4.2.2 Effect of feed flow rate on the breakthrough curve for the adsorption of CO <sub>2</sub> .....	137
4.4.2.3 Validation of the proposed model.....	139
CHAPTER 5: CONCLUSION AND RECOMMENDATIONS .....	141

5.1 Conclusion .....	141
5.2 Recommendations .....	143
REFERENCES.....	144
LIST OF PUBLICATIONS.....	164

## LIST OF FIGURES

Figure 2.1	Schematic diagram showing various resistances to the transport of adsorbate as well as concentration profiles through an idealized bidisperse adsorbent particle demonstrating some of the possible regimes. ....	47
Figure 3.1	Schematic diagram of the experimental setup for the ammonia modification.....	66
Figure 3.2	Schematic of the experimental system used for the column breakthrough measurements.....	79
Figure 4.1	Response surface plot of CO <sub>2</sub> adsorption capacity for (a) pre-heat treated, and (b) pre-oxidized adsorbent.....	99
Figure 4.2	Response surface plot of CO <sub>2</sub> desorption capacity for (a) pre-heat treated, and (b) pre-oxidized adsorbent.....	101
Figure 4.3	Contour plot of (a) CO <sub>2</sub> adsorption capacity and (b) CO <sub>2</sub> desorption capacity as a function of amination temperature and time for pre-oxidized adsorbents.....	104
Figure 4.4	Overlay plot of the optimal region for pre-oxidized adsorbents.....	105
Figure 4.5	Cyclical adsorption and desorption of CO <sub>2</sub> at 105 °C by the optimal activated carbon adsorbent.....	106
Figure 4.6	Experimental adsorption isotherms of CO <sub>2</sub> on (a) modified and (b) untreated activated carbon measured at 30, 45 and 60 °C.....	108
Figure 4.7	Calculated adsorption isotherms for CO <sub>2</sub> chemisorption onto the modified adsorbent at 30, 45 and 60 °C.....	111
Figure 4.8	Graphical evaluation of the fit of the experimental equilibrium data to the proposed model for the modified adsorbent, whose parameters are presented in Tables 4.6 and 4.7. The surface is the global isotherm model, and the black and white circles show the experimental data at 303, 318 and 333 K.....	117

Figure 4.9	Adsorption isosteres of CO <sub>2</sub> for (a) modified and (b) untreated adsorbent in the temperature range from 303 to 333 K. The points were calculated by numerical interpolation, and the lines represent the linear fit. All of the isosteres are marked with the corresponding amount of CO <sub>2</sub> adsorbed in units of (cm <sup>3</sup> STP/g).....	119
Figure 4.10	Concentration dependence of the isosteric enthalpy for CO <sub>2</sub> adsorption on the GAC and the OXA-GAC .....	121
Figure 4.11	Experimental CO <sub>2</sub> adsorption onto modified and untreated adsorbents at (a) 30 °C, (b) 45 °C, and (c) 60 °C along with the corresponding fit to kinetic models.....	123
Figure 4.12	Arrhenius plots for the estimation of the CO <sub>2</sub> adsorption activation energies on the GAC and OXA-GAC adsorbents.....	129
Figure 4.13	Effect of temperature on breakthrough curves of CO <sub>2</sub> adsorption onto (a) GAC and (b) OXA-GAC adsorbents at a 50 ml min <sup>-1</sup> feed flow rate and (c) GAC and (d) OXA-GAC at a 100 ml min <sup>-1</sup> feed flow rate.....	134
Figure 4.14	The efficiency of the adsorption bed for the breakthrough experiments with GAC and OXA-GAC adsorbents at varying adsorption temperatures and feed flowrates.....	136
Figure 4.15	Effect of feed flow rate on breakthrough curves of CO <sub>2</sub> adsorption onto GAC and OXA-GAC adsorbents at (a) 30 °C (b) 45 °C and (c) 60 °C.....	138
Figure 4.16	Verification of the proposed model with experimental breakthrough curves at three representative operating conditions.  Discrete symbols are experimental data, and solid lines are predictions by the model....	140

## LIST OF TABLES

Table 2.1	Summary of the dynamics models for fixed-bed adsorption of CO <sub>2</sub> .....	12
Table 3.1	Independent numerical variables and their levels (actual and coded).....	67
Table 3.2	Experimental design layout and experimental results of the responses.....	70
Table 3.3	Physical properties of the adsorbent and characteristics of the adsorption bed along with the operating conditions used for the fixed-bed experiments .....	79
Table 3.4	Optimal values of the proposed Toth equilibrium isotherm parameters.....	82
Table 3.5	Correlations used for estimation of the model parameters.....	86
Table 4.1	Analysis of variance (ANOVA) for the CO <sub>2</sub> adsorption capacity .....	93
Table 4.2	Analysis of variance (ANOVA) for the CO <sub>2</sub> desorption capacity .....	94
Table 4.3	Predicted and experimental values of the studied responses obtained at optimum conditions.....	105
Table 4.4	Freundlich isotherm parameters with $R^2$ and ARE for each independent mechanism at temperatures of 303, 318, and 333 K .....	114
Table 4.5	Sips isotherm parameters with $R^2$ and ARE for each independent mechanism at temperatures of 303, 318, and 333 K .....	114
Table 4.6	Toth isotherm parameters with $R^2$ and ARE for each independent mechanism at temperatures of 303, 318, and 333 K .....	115
Table 4.7	Optimal values of the proposed Toth temperature-dependent parameters.....	116
Table 4.8	The calculated parameters of the kinetic models and associated $R^2$ and $\Delta q$ (%) for the CO <sub>2</sub> adsorption onto GAC at different temperatures.....	128
Table 4.9	The calculated parameters of the kinetic models and associated $R^2$ and $\Delta q$ (%) for the CO <sub>2</sub> adsorption onto OXA-GAC at different temperatures .....	128

Table 4.10 Breakthrough curve characteristic parameters under different operating conditions.....132



## LIST OF SYMBOLS AND ABBREVIATIONS

$a_a$	Ratio of the external surface area to the volume of the column wall
$a_s$	Ratio of the particle external surface area to volume
$a_w$	Ratio of the internal surface area to the volume of the column wall
ANOVA	Analysis Of Variance
ARE	Average Relative Error
BET	Brunauer, Emmette and Teller
$Bi$	Biot number
$c$	Adsorbate concentration in the fluid phase
$c_p$	Adsorbate concentration in the macropore
$C$	Total concentration in the bulk phase
$C_g$	Gas phase heat capacity
$C_s$	Adsorbent heat capacity
$C_w$	Column wall heat capacity
CCD	Central Composite Design
$d_{ext}$	Column external diameter
$d_{int}$	Column internal diameter
$d_p$	Particle mean diameter
$D_m$	Molecular diffusivity
$D_p$	Macropore diffusivity
$D_z$	Effective axial dispersion coefficient
$D_\mu$	Micropore diffusivity
$D_{\mu}^{\infty}$	Micropore diffusivity at infinite dilution
DDW	Distilled Deionized Water

DF	Degree of Freedom
$E_a$	Activation energy
$g$	Gravity acceleration
GAC	Granular Activated Carbon
$h_{ext}$	External convective heat transfer coefficient
$h_f$	Film heat transfer coefficient
$h_w$	Internal convective heat transfer coefficient
$-\Delta H$	Isotheric heat of adsorption
HTA	Pre-heat-treated GAC
IUPAC	International Union of Pure and Applied Chemistry
$k_A$	Avrami kinetic constant
$k_b$	Barrier transport coefficient
$k_{ext}$	Column external air conductivity
$k_f$	External film mass transfer coefficient
$k_F$	Pseudo-first-order kinetic rate constant
$k_g$	Gas phase thermal conductivity
$k_w$	Column wall conductivity
$K$	Linear driving force rate coefficient
$K_s$	Pseudo-second-order kinetic rate constant
$L$	Bed length
LDF	Linear driving force model
$L_{MTZ}$	Length of the Mass Transfer Zone
$LUB$	Length of Unused Bed
$M$	Molecular weight
MFC	Mass Flow Controller

MRA	Multiple Regression Analysis
OFAT	One Factor At Time
OXA	Pre-oxidized GAC
OXA-GAC	Optimal adsorbent
$p$	Partial pressure
$P$	Total pressure
$P/P_0$	Relative pressure
$Pr$	Prandtl number
$q$	Adsorbed concentration
$\bar{q}$	Average adsorbed phase concentration in the micropore
$\bar{q}$	Average concentration in adsorbent particle
$q^*$	Adsorbed phase concentration in equilibrium with the fluid phase concentration
$q_m$	Maximum loading capacity
$\Delta q$	Normalized standard deviation
$r$	Distance along the microparticle radius
$r_p$	Mean macropore radius
$R^2$	Regression coefficient
$R$	Universal gas constant
$Ra$	Rayleigh number
$R_c$	Microparticle radius
$Re$	Reynolds
$R_p$	Macroparticle radius
RSM	Response Surface Methodology
$Sc$	Schmidt

SS	Sum of Squares
STP	Standard Temperature and Pressure
$t$	Time
TC	Thermocouple
TGA	Thermo Gravimetric Analyser
$u$	Fluid velocity
$U$	External overall heat transfer coefficient
$y$	Mole fraction
$z$	Distance along the bed length
3D	Three Dimensional
$\varepsilon_b$	Bed void fraction
$\varepsilon_p$	Adsorbent porosity
$\rho_p$	Particle density
$\rho_g$	Gas phase density
$\rho_w$	Column wall density
$\mu m$	Micrometre
$\sigma^2$	Residual Mean Square
$\tau$	Pore tortuosity factor
$\lambda_L$	Effective axial heat dispersion
$\nu$	Kinematic viscosity
$\alpha$	Thermal diffusivity
$\mu$	Gas mixture viscosity
$\Phi$	Column efficiency

## CHAPTER 1: INTRODUCTION

### 1.1 Background

Global warming and related environmental damage associated with emissions of carbon dioxide (CO<sub>2</sub>), the most significant greenhouse gas, have long been recognized to represent a potential serious threat to the future of the earth's environment (Bezerra, Oliveira, Vieira, Cavalcante, & Azevedo, 2011; Jadhav et al., 2007). The primary source of anthropogenic CO<sub>2</sub> emissions is the combustion of fossil fuels such as coal or natural gas for the production of electricity. Because fossil fuels are likely to remain the predominant energy source all over the world, CO<sub>2</sub> emissions must be reduced to mitigate the unfettered release of this greenhouse gas into the atmosphere (Garcés, Villarroel-Rocha, Sapag, Korili, & Gil, 2013; Siriwardane, Shen, Fisher, & Poston, 2001). As a result, various CO<sub>2</sub> separation techniques, such as liquid solvent absorption, membrane separation, cryogenic separation, and adsorption processes including pressure/vacuum swing adsorption (PSA/VSA) and temperature swing adsorption (TSA), are currently under investigation (Gomes & Yee, 2002; Xu, Song, Andresen, Miller, & Scaroni, 2002). Currently, absorption with amine-based absorbents is the preferred technology for the large-scale separation of CO<sub>2</sub> from the flue-gas streams of fossil-fuel-based power plants. However, this method suffers from several significant drawbacks that impede its implementation, including low efficiency, high energy consumption during the regeneration process, a high equipment corrosion rate, oxidative degradation of the amines, and flow problems caused by viscosity (Rinker, Ashour, & Sandall, 2000; Veawab, Tontiwachwuthikul, & Chakma, 1999). The development of alternative, lower lower-cost, energy-efficient CO<sub>2</sub> removal technologies is therefore important. The separation and purification of gas mixtures by adsorption is a potential option because of

its ease of operation, high adsorption capacity, minimal environmental impact, low cost, and efficient recovery of the solute compared to conventional absorption with liquid solvents (Cavenati, Grande, & Rodrigues, 2004; Serna-Guerrero, Belmabkhout, & Sayari, 2010a). Particularly, pressure-swing adsorption (PSA) has a number of attractive characteristics, such as its applicability over a relatively wide range of temperature and pressure conditions, its low energy requirements, and its low capital investment costs (Delgado, Uguina, Sotelo, Ruiz, & Gomez, 2006; Mutasim & Bowen, 1991). The last three decades have seen a tremendous growth in research into and commercial applications of CO<sub>2</sub> removal from various flue-gas mixtures by PSA processes (Siriwardane et al., 2001; Yong, Mata, & Rodrigues, 2002).

The development of an easily regenerated and durable adsorbent with fast adsorption/desorption kinetics, a high selectivity and a high adsorption capacity will undoubtedly enhance the competitiveness of adsorptive separation for CO<sub>2</sub> capture in flue-gas applications (Lu et al., 2009; Su, Lu, Kuo, & Zeng, 2010). Among all adsorbents, activated carbon offers several advantages as a CO<sub>2</sub> adsorbent: an inherent affinity for CO<sub>2</sub>, an easy-to-design pore structure, insensitivity to moisture, ease of regeneration, stability over a large number of cycles, and an appealing low cost (Bezerra et al., 2011; Sjostrom & Krutka, 2010). Most of the processes that produce CO<sub>2</sub> in product streams occur at elevated temperatures (up to 100 °C), and the stream must be cooled before separation takes place. Therefore, developing an adsorbent with a high adsorption capacity at relatively high temperatures can drastically reduce the cooling cost of separation and make CO<sub>2</sub> capture from power plants feasible (Maroto-Valer, Tang, & Zhang, 2005; Xu et al., 2002).

The CO<sub>2</sub> adsorption performance of activated carbon is well known to be strongly influenced by modification of the surface chemical properties of the activated carbon (Arenillas, Smith, Drage, & Snape, 2005; M. G. Plaza et al., 2009; Shafeeyan, Daud,

Houshmand, & Shamiri, 2010). Inspired by the current liquid-phase amine scrubbing technology, researchers have incorporated different basic nitrogen functional groups onto the carbon surface for CO<sub>2</sub> removal from gaseous mixtures at relatively high temperatures (Przepiórski, Skrodzewicz, & Morawski, 2004; Zhijuan Zhang, Xu, Wang, & Li, 2010). This approach is expected to exploit the strong chemical interactions between CO<sub>2</sub> and the attached basic nitrogen functionalities on the surface, as well as the low energy requirements, to regenerate the solid adsorbent (Drage et al., 2007; Knowles, Delaney, & Chaffee, 2006; Maroto-Valer et al., 2005; Plaza, Pevida, Arenillas, Rubiera, & Pis, 2007). Several authors have proposed modifying activated carbon with gaseous ammonia in the presence or absence of oxygen as a suitable technique to produce efficient CO<sub>2</sub> adsorbents that maintain high uptakes despite moderately high temperatures (Pevida, Plaza, et al., 2008; Plaza et al., 2009; Plaza, Rubiera, Pis, & Pevida, 2010).

## **1.2 Research objectives**

The purpose of this research is to investigate the fixed-bed adsorption of CO<sub>2</sub> onto ammonia-modified activated carbon. More specifically, the objectives of this study are:

- Optimize the amination conditions of activated carbon adsorbents in an effort to maximize their CO<sub>2</sub> adsorption/desorption capacities.
- Study the adsorption equilibrium of carbon dioxide onto the ammonia modified and untreated activated carbon adsorbents and develop an appropriate semi-empirical isotherm model.
- Study the kinetics of CO<sub>2</sub> adsorption on the ammonia modified and untreated activated carbon adsorbents at different temperatures and develop an appropriate kinetic model.

- Develop a model that consists of an appropriate equilibrium and kinetics equations to predict the breakthrough behavior of the fixed-bed adsorption of CO<sub>2</sub>.

### **1.3 Thesis organization**

This thesis consists of five chapters dealing with different aspects related to the topic of research.

- CHAPTER 1: This chapter briefly introduces the importance of CO<sub>2</sub> capture and sequestration from point source emissions as a potential way to mitigate unfettered release of greenhouse gases into the atmosphere. The objectives of the study are also presented.
- CHAPTER 2: This chapter presents a review of efforts over the last three decades toward mathematical modeling of the fixed-bed adsorption of carbon dioxide. The nature of various gas–solid equilibrium relationships as well as different descriptions of the mass transfer mechanisms within the adsorbent particle are reviewed. In addition to mass transfer, other aspects of adsorption in a fixed bed, such as heat and momentum transfer, are also studied. Both single- and multi-component CO<sub>2</sub> adsorption systems are discussed in the review.
- CHAPTER 3: This chapter explains all the experiments procedures for the modification and characterization of activated carbon samples. Details on the raw material, equipment, and other related procedures are also presented.
- CHAPTER 4: This chapter presents results and data obtained from laboratory experiments. In this chapter the results are presented in three parts. Part 1 investigates the application of response surface methodology in predicting and



optimizing the amination conditions of activated carbon adsorbent toward CO<sub>2</sub> adsorption. Part 2 investigates the adsorption equilibrium of carbon dioxide onto the ammonia modified and untreated activated carbon adsorbents and develops a semi-empirical equilibrium model able to distinguish the contributions of physical and chemical adsorption to the total CO<sub>2</sub> uptake. Part 3 studies the kinetics of CO<sub>2</sub> adsorption on the ammonia modified and untreated activated carbon adsorbents. To predict the breakthrough behavior of the fixed-bed adsorption of CO<sub>2</sub>, the focus of Part 3 is to develop a dynamic model that consists of an Avrami equation to describe the kinetics of adsorption and a semi-empirical Toth equation to represent the gas–solid equilibrium isotherm. In addition, a comprehensive discussions and explanations on experimental results are presented.

- CHAPTER 5: The conclusions constructed from the results and discussion chapter are explained part by part. The recommendations and suggestions for future works are also presented.

## CHAPTER 2: LITERATURE REVIEW

### 2.1 Introduction

Concerns over the gradual increase in the atmospheric concentration of CO<sub>2</sub> and its impact on climate change have prompted a global research effort to capture CO<sub>2</sub> from point source emissions and stabilize its concentration in the atmosphere (Gomes & Yee, 2002; Grande & Rodrigues, 2008; Plaza et al., 2007). The most important sources of CO<sub>2</sub> emissions are power plants that generate electricity from fossil fuels (coal, oil, and natural gas) (Dantas et al., 2011; Grande, Lopes, Ribeiro, Loureiro, & Rodrigues, 2008; Grande & Rodrigues, 2008; Kikkinides, Yang, & Cho, 1993; Mulgundmath, Jones, Tezel, & Thibault, 2012; Park, Beum, Kim, & Cho, 2002). Therefore, it is critical to separate and recover carbon dioxide from the flue gases emitted by power plants to avoid excess CO<sub>2</sub> emissions (Chou & Chen, 2004; Ko, Siriwardane, & Biegler, 2005; Mulgundmath et al., 2012). Various separation techniques, such as liquid solvent absorption, membrane separation, cryogenic techniques, and adsorption over solid sorbents, are increasingly used to reduce CO<sub>2</sub> emissions (Gomes & Yee, 2002; Takamura, Narita, Aoki, Hironaka, & Uchida, 2001). At present, the most widely used technology for the removal of CO<sub>2</sub> from gaseous mixtures is amine absorption (Delgado et al., 2006; Leci, 1996). However, this process is energy-intensive during the regeneration of solvent and is also plagued by extensive corrosion of the process equipment (Chue, Kim, Yoo, Cho, & Yang, 1995; Gray et al., 2004; Gray et al., 2005; Ko et al., 2005). It is therefore important to explore economical and energy-efficient alternative approaches for CO<sub>2</sub> separation (Grande et al., 2008; Xu, Song, Miller, & Scaroni, 2005).

Recently, it was reported that the cost associated with CO<sub>2</sub> capture can be reduced below the cost of conventional absorption with liquid solvents by using adsorption separation technologies (Ho, Allinson, & Wiley, 2008; Radosz, Hu, Krutkramelis, & Shen, 2008).

Several technological advances in the field of CO<sub>2</sub> capture by adsorption have been developed around the world, demonstrating the attractiveness of this technique for post-combustion treatment of flue gas (Dantas et al., 2011; Dantas et al., 2011; Grande et al., 2008). Two main adsorption technologies are viewed as feasible for CO<sub>2</sub> separation and purification on a large scale: pressure/vacuum swing adsorption (PSA/VSA) and temperature swing adsorption (TSA) (Chue et al., 1995; Clause, Bonjour, & Meunier, 2004; Plaza et al., 2009; Plaza, Garcia, Rubiera, Pis, & Pevida, 2011). Recent developments have demonstrated that PSA is a promising option for separating CO<sub>2</sub> due to its ease of applicability over a relatively wide range of temperature and pressure conditions, its low energy requirements, and its low capital investment costs (Agarwal, Biegler, & Zitney, 2010b; Cen & Yang, 1985; Delgado et al., 2006; Gomes & Yee, 2002). Many studies concerning CO<sub>2</sub> removal from various flue gas mixtures by means of PSA processes have been addressed in the literature (Agarwal et al., 2010b; Chaffee et al., 2007; Chou & Chen, 2004; Chue et al., 1995; Grande et al., 2008; Ho et al., 2008; Kikkinides et al., 1993; Ko, Siriwardane, & Biegler, 2003; Mulgundmath et al., 2012; Na, Koo, Eum, Lee, & Song, 2001; Reynolds, Ebner, & Ritter, 2005; Sircar & Kratz, 1988; Xiao et al., 2008). Prior to the design of an adsorption process, selecting an appropriate adsorbent with high selectivity and working capacity, as well as a strong desorption capability, is key to separating CO<sub>2</sub>. As a result, a wide variety of adsorbents, such as activated carbons, synthetic zeolites, carbon molecular sieves, silicas, and metal oxides, have been investigated in recent years for this purpose (Chue et al., 1995; Dantas et al., 2011; Dantas et al., 2011; Moreira, Soares, Casarin, & Rodrigues, 2006; Plaza et al., 2011; Xu et al., 2005).

The design of an appropriate adsorption process requires the development of a model that can describe the dynamics of adsorption on a fixed bed with the selected adsorbent (Dantas et al., 2011; Dantas et al., 2011; Delgado, Uguina, Sotelo, & Ruiz, 2006; Lua &

Yang, 2009). The absence of an accurate and efficient adsorption cycle simulator necessitates the use of data from experimental units to develop new processes. This empirical design of an adsorption column through extensive experimentation on process development units tends to be expensive and time consuming (Siahpoosh, Fatemi, & Vatani, 2009). A predictive model using independently established equilibrium and kinetic parameters may provide, in principle, a method of estimating the column dynamic capacity without extensive experimentation. A fixed-bed column mathematical simulation that considers all relevant transport phenomena is therefore required to obtain a better understanding of the behavior of new adsorbents during the adsorption/desorption cycles and for optimization purposes. Moreover, these models are capable of estimating the breakthrough curve and temperature profile for a certain constituent in the bulk gas at all locations within the packed column. This experimentally verified model is then used to conduct an extensive study to understand the effects of various process parameters on the performance of the PSA cycle. These are the main reasons why the mathematical modeling of adsorption processes has attracted a great deal of attention among researchers.

In general, prediction of column dynamics behavior requires the simultaneous solution of a set of coupled partial differential equations (PDEs) representing material, energy, and momentum balances over a fixed-bed with the appropriate boundary conditions (Hwang, Jun, & Lee, 1995). Because the simultaneous solution of a system of PDEs is tedious and time consuming, the use of simplified models capable of satisfactorily predicting fixed-bed behavior is desirable. Many attempts have been made to evaluate and develop simplifying assumptions to decrease computational time and facilitate optimization studies. A review of the literature reveals the development of simplifying assumptions mainly on the representation of mass transfer phenomena within the adsorbent particles as an alternative pathway to simplify fixed-bed adsorption calculations. Modeling and

optimization of the fixed-bed adsorption of CO<sub>2</sub> has developed over the past three decades and is still of great interest to investigators. This review presents a fairly extensive survey of previous studies on the mathematical modeling of the CO<sub>2</sub> adsorption process in a packed column. Various models for gas-solid adsorption equilibria as well as different descriptions of the mass transfer mechanisms within the adsorbent particle are reviewed. In addition to concentration variation, other aspects of adsorption in a fixed bed, such as temperature and pressure variations, are also studied. The purpose of this study was to investigate the mathematical models capable of simulating the dynamic behavior of the fixed-bed adsorption of carbon dioxide.

## **2.2 Overview of the prediction of adsorption column dynamics**

In most adsorption processes, the adsorbent is in contact with a fluid in a packed bed. An understanding of the dynamics behavior of such systems is therefore required for rational process design and optimization (Rutherford & Do, 2000a). The dynamics behavior of an adsorption column system can be classified based on the nature of the gas-solid equilibrium relationship of fluid constituents and the complexity of the mathematical model required for describing the mechanism by which the mass transfer from the fluid to the solid phase occurs (Ruthven, 1984). The gas-solid adsorption equilibrium indicates the limiting capacity for solute separation from the gas phase into the solid phase. It is the most important process that controls the dynamics behavior of a packed column so that the general nature of a mass transfer zone is determined entirely by the equilibrium isotherm. Therefore, due to variations in the composition/temperature with respect to time and location within the adsorption column and the consequent effects on the adsorption equilibrium relation, a comprehensive gas-solid equilibrium model is needed. Several authors have reported experimental evidence of these effects in a column packed with microporous adsorbents (Carta, 2003). The complexity of the mathematical model, in

turn, depends on the concentration level, the choice of rate equation, and the choice of flow model (Ruthven, 1984). In addition, temperature changes may also affect the concentration profiles, particularly for high-concentration feeds in which the heat of adsorption generates thermal waves in both axial and radial directions. Therefore, apart from the mass transfer effects on adsorption rate, the effects of heat generation and heat transfer in the adsorbent bed must also be considered (Rezaei & Grahn, 2012). Moreover, the axial pressure along the bed may not be constant. As a consequence, a momentum balance also has to be included in the model. Table 2.1 provides a comprehensive classification scheme of the summary of the fixed-bed column mathematical models for carbon dioxide adsorption developed over the last three decades. All of the models assume that the gas phase follows the ideal gas law. The flow pattern is described by the plug flow or axially dispersed plug-flow model. It is further assumed that the radial gradients of concentration and, where applicable, temperature and pressure are negligible (with the exception of models 4 and 20). The assumption that the radial gradient is negligible has been widely accepted in many other studies (Jee, Park, Haam, & Lee, 2002; Kim, Bae, Choi, & Lee, 2006; Kim, Moon, Lee, Ahn, & Cho, 2004). The majority of the models reviewed here include the effects of the finite mass transfer rate, resulting in a theoretical representation that more closely approaches a real process. Most of the aforementioned models use a linear driving force approximation to describe the gas-solid mass transfer mechanism. Some of these models consider the effects of heat generation and heat transfer in the adsorbent bed, which may affect the adsorption rates. Moreover, in modeling the non-isothermal operation of adsorption processes occurring in packed beds, it is also commonly assumed that the heat transfer resistance between the gas and the solid phases is negligible and that they reach thermal equilibrium instantaneously. With the exception of models 15-17, 21, 24, 26-27, 29-30, 31, and 33, the pressure drop across the adsorbent bed is neglected, and the column is assumed to operate at constant

pressure. Most of the adsorption equilibrium is described using non-linear isotherms such as the Langmuir isotherm or a hybrid Langmuir-Freundlich isotherm; only rarely have linear isotherms been used.

Table 2.1: Summary of the dynamics models for fixed-bed adsorption of CO<sub>2</sub>

No.	Model assumptions					Application	Solution method	Results and comments	Ref.
	Equilibrium relationship	Flow pattern	Mass transfer rate model	Heat effects	Others				
1	Linear equilibrium isotherm	Plug flow	Local equilibrium model	Isothermal	No radial variation in concentration. Negligible pressure drop. Trace system*.	PSA separation of carbon dioxide from a He-CO <sub>2</sub> mixture using silica gel	Analytical results from a linear mathematical model obtained by the method of characteristics.	The model provided a qualitative or semi quantitative process description. Due to neglecting the effects of mass transfer resistance some of the detailed behavior differed from experimental results.	(Shenda lman & Mitchell , 1972)
2	A hybrid Langmuir-Freundlich isotherm	Plug flow	Local equilibrium/ Linear driving force (LDF) approximation model	Non-isothermal	No radial variations in concentration and temperature. Thermal equilibrium between the fluid and particles.	Separation of coal gasification products containing H <sub>2</sub> , CO, CH <sub>4</sub> , H <sub>2</sub> S, and CO <sub>2</sub> by PSA using activated carbon	The model was solved using an implicit finite difference method which was stable and convergent.	Poor comparison with experimental data for the predictive equilibrium model. The major discrepancy was in the CO <sub>2</sub> concentration. The results of the LDF model were in fair agreement with the experimental data. Mass transfer coefficient for CO <sub>2</sub> was determined empirically.	(Cen & Yang, 1985)

(continued on next page)



‘Table 2.1, continued’

No.	Model assumptions					Application	Solution method	Results and comments	Ref.
	Equilibrium relationship	Flow pattern	Mass transfer rate model	Heat effects	Others				
3	Linear equilibrium isotherm	Axial dispersed plug flow	LDF approximation with non-constant coefficient	Isothermal	Negligible radial gradient of concentration. Negligible pressure drop. Trace system.	PSA separation of carbon dioxide from a He-CO <sub>2</sub> mixture using silica gel	The solution to the model equations was obtained by orthogonal collection and using finite difference methods with consistent results.	The theoretical curves based on the assumption of inverse dependence of the mass transfer coefficient with the pressure provided a good representation of the experimental results.	(Raghavan, Hassan, & Ruthven, 1985)
4	Linear equilibrium isotherm	Axial dispersed plug flow	Pore diffusion model	Non-isothermal	Negligible radial concentration gradient. Radial temperature profile in the column/uniform temperature over the column cross-section. Negligible axial pressure gradient. Constant temperature of the column wall.	Theoretical and experimental studies on the CO <sub>2</sub> capture in a column packed with activated carbon particles	Analytical solution was performed in the Laplace domain under the condition of a semi-infinite column.	The central-axis-thermal waves measured at various axial locations in the column were in good agreement with those predicted.	(Kaguei, Shemilt, & Wakao, 1989; Kaguei, Yu, & Wakao, 1985)

(continued on next page)

'Table 2.1, continued'

No.	Model assumptions					Application	Solution method	Results and comments	Ref.
	Equilibrium relationship	Flow pattern	Mass transfer rate model	Heat effects	Others				
5	A hybrid Langmuir-Freundlich isotherm	Plug flow	Local equilibrium model. Pore/surface diffusion models	Non-isothermal	Negligible radial gradients in temperature and concentrations. Thermal equilibrium between the fluid and particles. Negligible pressure drop in the bed.	Separation of gas mixtures containing CO <sub>2</sub> , CH <sub>4</sub> , and H <sub>2</sub> (one-third each by volume) by PSA using activated carbon	The models were solved numerically by employing finite difference method.	The Knudsen plus surface diffusion model provided the best fit when compared to the experimental data. Due to the assumption of infinite pore diffusion rate, the ILE model predicted a later breakthrough plus a lower concentration for CO <sub>2</sub> .	(Doong & Yang, 1986)
6	Langmuir isotherm	Plug flow	LDF approximation model with a cycle time dependent coefficient	Isothermal	Negligible radial concentration gradient. Negligible pressure drop.	PSA separation of a CO <sub>2</sub> (50%)-CH <sub>4</sub> (50%) mixture using a carbon molecular sieve	The model was solved using an implicit backward finite difference scheme, which was both stable and convergent.	The model predictions were reasonable and the average difference between the model prediction and experimental result was within 3.0%.	(Kapoor & Yang, 1989)

(continued on next page)

‘Table 2.1, continued’

No.	Model assumptions					Application	Solution method	Results and comments	Ref.
	Equilibrium relationship	Flow pattern	Mass transfer rate model	Heat effects	Others				
7	Langmuir isotherm	Plug flow	Local equilibrium model	Non-isothermal (adiabatic)	No radial variations in concentration and temperature. Thermal equilibrium between the fluid and particles. Negligible pressure drop.	Separation of carbon dioxide from binary gas mixtures (CO <sub>2</sub> /N <sub>2</sub> , CO <sub>2</sub> /CH <sub>4</sub> , and CO <sub>2</sub> /H <sub>2</sub> ) using BPL carbon and 5A zeolite	A set of PDEs was reduced to ODEs and solved by using the numerical technique of finite differences.	The adiabatic simulation of the blowdown step showed that an isothermality assumption is inadequate for process design. However, it could be an excellent tool for predicting the column behavior and trends in a semi quantitative manner.	(R. Kuma r, 1989)
8	Langmuir isotherm	Plug flow	LDF approximation Model	Non-isothermal	Negligible radial temperature and concentration gradients/ Thermal equilibrium between the gas and solid phases. Negligible pressure drop through the bed.	CO <sub>2</sub> capture from a mixture of N <sub>2</sub> (90%)- CO <sub>2</sub> (10%) by PSA using 5A molecular sieve	The nonlinear rate equations were solved using Runge-Kutta-Merson method. Adsorbate concentration and temperature profiles were predicted using an implicit backward difference approximation.	A comparison of experimental breakthrough and temperature profiles with model predictions revealed that the model reproduced the experimental data satisfactorily, which indicates that the assumptions the model is based on are valid for this system.	(Muta sim & Bowe n, 1991)

(continued on next page)

‘Table 2.1, continued’

No.	Model assumptions					Application	Solution method	Results and comments	Ref.
	Equilibrium relationship	Flow pattern	Mass transfer rate model	Heat effects	Others				
9	Langmuir isotherm	Axial dispersed plug flow	LDF approximation model	Isothermal	No radial variations in concentration. Negligible pressure gradient across the bed.	Investigation of adsorption and desorption breakthrough behaviors of CO and CO <sub>2</sub> on activated carbon	A set of PDEs was solved by the method of orthogonal collection. The resulting set of ODEs was solved numerically in the time domain by using DGEAR of the International Mathematical and Statistical Library (IMSL) which employs Gear’s stiff method with variable order and step size.	The experimental adsorption and desorption curves were predicted fairly well by the LDF model and the pressure dependent mass transfer coefficients calculated from a single component system provided a reasonably good representation of adsorption and desorption data for a multi component system.	(Hwang & Lee, 1994)
10	Langmuir isotherm/ Ideal adsorbed solution theory (IAST)	Plug flow	LDF approximation model	Non-isothermal	No radial concentration and temperature gradients. Negligible axial pressure gradient.	Fixed-bed adsorption of a N <sub>2</sub> (85%)-CO <sub>2</sub> (15%) mixture using a of X-type zeolite	A set of differential equation with the initial and boundary conditions were solved by using the solver LSODA.	A comparison between concentration and temperature history curves with theoretical results revealed that the presented model could predict the dynamic behavior of the adsorption bed, even though a slight deviation was observed after the maximum point.	(Kim, Chue, Kim, Cho, & Kim, 1994)

(continued on next page)

‘Table 2.1, continued’

No.	Model assumptions					Applicati on	Solution method	Results and comments	Ref.
	Equilibrium relationship	Flow pattern	Mass transfer rate model	Heat effects	Others				
11	Langmuir isotherm	Plug flow	LDF approximation model with lumped mass transfer coefficient	Non-adiabatic, adiabatic, and isothermal	Negligible radial velocity, temperature, and concentration gradients. Negligible pressure gradient across the bed.	Fixed-bed adsorption of carbon dioxide (with helium as the carrier gas) on activated carbon	A set of PDEs was solved by the numerical method of lines. The resulting set of ODEs was solved by using the subroutine DIVPAG of the IMSL library, while the non-linear algebraic equation was solved by using the subroutine DNEQNF of the same library.	The model provided a good representation of the experimental breakthrough and temperature curves. Since the mass transfer coefficients were determined by fitting the experimental data, the disadvantage of this model is the determination of a new value for the effective mass transfer coefficient for each run.	(Hwang et al., 1995)
12	Extended Langmuir-Freundlich isotherm	Plug flow	LDF approximation model with a single lumped mass transfer coefficient	Non-isothermal	Negligible radial gradients in temperature and concentrations. Thermal equilibrium between the fluid and particles. Negligible pressure drop in the bed.	Separation of a binary mixture H <sub>2</sub> (70%)-CO <sub>2</sub> (30%) by PSA using zeolite 5A	A set of PDAEs representing the packed column were solved by a flux corrected third-order upwind method. Numerical oscillation, which often appears when a convection equation is solved, is eliminated by the flux corrected scheme.	The predicted values matched significantly with the experimental results at shorter adsorption time. The errors at longer adsorption time was attributed to a partial breakthrough of mass transfer zone during cocurrent depressurization and/or blowdown/purge steps.	(Yang, Han, Cho, Lee, & Lee, 1995)

(continued on next page)

‘Table 2.1, continued’

No.	Equilibrium relationship	Flow pattern	Model assumptions			Application	Solution method	Results and comments	Ref.
			Mass transfer rate model	Heat effects	Others				
13	Langmuir isotherm	Plug flow	LDF approximation model	Isothermal	No radial variation in concentration. Negligible pressure drop. Trace system.	Removal and concentration of CO <sub>2</sub> dilute gas from air by PSA using three types of commercial molecular-sieve zeolites (13X, 5A, and 4A)	A set of equations describing the system was solved by Euler's method.	Good agreement between the model and the experimental results was obtained particularly for values of between the ratio of feed/enriched product flow rates = 3 and 6. Also, at the point the ratio of feed/lean product flow rates <2, where the solute balance was not satisfactory, the agreement was not quite good.	(Diagnose, Goto, & Hirose, 1996)
14	Langmuir isotherm	Plug flow	LDF approximation model	Non-isothermal	No radial concentration and temperature gradients. Thermal equilibrium between the gas phase and adsorbents. Negligible axial pressure gradient.	Layered-bed PSA separation of a typical cracked gas mixture (H <sub>2</sub> , CH <sub>4</sub> , CO, and CO <sub>2</sub> ) using activated carbon followed by zeolite 5A	To solve a set of coupled PDAEs, the spatial derivatives were divided using a backward difference scheme, and the resulting ordinary differential equations were solved with the GEAR method.	The agreement between the experimental and theoretical prediction was good that indicate validity of the present model. The overall mass transfer coefficients were obtained by fitting the breakthrough data. The experimental effluent temperature was much lower than the model prediction because the model did not take into account the heat loss to the end of the column.	(Park, Kim, & Cho, 2000; Park, Kim, Cho, Kim, & Yang, 1998)

(continued on next page)

‘Table 2.1, continued’

No.	Equilibrium relationship	Flow pattern	Model assumptions			Application	Solution method	Results and comments	Ref.
			Mass transfer rate model	Heat effects	Others				
15	Extended Langmuir-Freundlich isotherm	Axial dispersed plug flow	LDF approximation model with a single lumped mass transfer coefficient	Non-isothermal	Negligible radial gradients of concentration, pressure and temperature. Thermal equilibrium between the fluid and particles. Pressure drop along the bed was calculated by the Ergun equation.	Layered bed PSA separation of a coke oven gas containing H <sub>2</sub> , CH <sub>4</sub> , CO, N <sub>2</sub> , and CO <sub>2</sub> using activated carbon and zeolite 5A	A set of coupled PDEs was solved using a finite difference method. The spatial dimension was discretized by using a second-order central difference and a second-order backward difference for the second-order and the first-order space derivatives, respectively.	In spite of the frozen solid-phase model, the utilized LDF model could predict a transient variation of the effluent stream during pressurization and depressurization steps and simulated results of the dynamic model agreed well with the PSA experimental results. The experimental data resulted in slightly higher recovery than predicted (4% error).	(Lee, Yang, & Ahn, 1999)
16	Langmuir-Freundlich isotherm	Axial dispersed plug flow	LDF approximation model	Non-isothermal	No radial variations in temperature, pressure, and concentration. The Ergun equation was used to estimate the pressure drop.	Packed bed adsorption of carbon dioxide, nitrogen, and water on molecular sieve 5A	A set of partial differential equations was solved using finite differences and Newmans’s method.	The model provided a reasonable fit to experimental adsorption data. However, comparing the experimental data with the model prediction suggested that a 2D model is required for accurate simulation of the average column breakthrough concentration.	(Mohamadi nejad, Knox, & Smith, 2000)

(continued on next page)

‘Table 2.1, continued’

No.	Model assumptions					Application	Solution method	Results and comments	Ref.
	Equilibrium relationship	Flow pattern	Mass transfer rate model	Heat effects	Others				
17	Langmuir isotherm	Axial dispersed plug flow	Local equilibrium model/ LDF model based on pore diffusion	Non-isothermal	No radial concentration, pressure and temperature gradients. Pressure distribution was described by the Ergun equation. Thermal equilibrium between the gas and particles.	High temperature carbon dioxide adsorption on hydrotalcite adsorbent	The equations were solved in the gPROMS modelling environment. The spatial discretization method of orthogonal collocation on finite elements was employed.	The LDF model was found to give a good description of the adsorption and desorption data especially for high feed CO <sub>2</sub> concentrations. The ILE model failed to give an adequate description of the desorption kinetics.	(Ding & Alpay, 2000)
18	Langmuir isotherm	Plug flow	LDF approximation Model	Isothermal	Negligible radial gradient of concentration. Negligible pressure drop.	CO <sub>2</sub> recovery from boiler exhaust gas (containing CO <sub>2</sub> and N <sub>2</sub> ) by PSA using Na-X and Na-A type zeolites	A set of equations describing the system was discretized in space and the resulting set of ordinary differential equations with a variable time step was solved.	Both simulation and experimental results showed the same trend of the recovery efficiency and the CO <sub>2</sub> concentration of the recovery gas with respect to the variation of the feed gas flow rate.	(Takamura et al., 2001)

(continued on next page)



‘Table 2.1, continued’

No.	Model assumptions					Application	Solution method	Results and comments	Ref.
	Equilibrium relationship	Flow pattern	Mass transfer rate model	Heat effects	Others				
19	Extended Langmuir isotherm	Plug flow	LDF approximation model	Non-isothermal (adiabatic)	Negligible gradients in radial concentration and temperature. Negligible pressure drop.	CO <sub>2</sub> recovery from a flue gas (containing 83% N <sub>2</sub> , 13% CO <sub>2</sub> , and 4% O <sub>2</sub> ) by PSA using zeolite 13X	A MATLAB function based on sequential quadratic programming (SQP) method was used to solve the constrained nonlinear programming optimization problem.	The analysis of breakthrough curves showed good agreement with simulation data. However, analysis of temperature changes in the adsorption beds revealed some discrepancy between simulations and experiments.	(Choi et al., 2003)
20	Ideal adsorption solution theory (IAST)	Non-Darcian flow model (2D flow)	LDF approximation model	Non-isothermal	Variations in temperature, concentration, and velocity along the radial direction of column.	Carbon dioxide adsorption from a mixture of (CO <sub>2</sub> , N <sub>2</sub> , and H <sub>2</sub> O) in a column packed with zeolite 5A	A set of coupled PDEs was discretized by first- or second-order differences in time and spatial dimensions. The set of discretized finite difference equations was solved simultaneously by the implicit method of Newman.	The model prediction of breakthrough curves definitely matched the obtained experimental data. The temperature profile results of 2D model also estimated the experimental data fairly well. The few degree discrepancy between the model and experimental data was attributed to prediction of heat transfer coefficients.	(Mohamad, Knox, & Smith, 2003)

(continued on next page)

'Table 2.1, continued'

No.	Equilibrium relationship	Flow pattern	Model assumptions			Application	Solution method	Results and comments	Ref.
			Mass transfer rate model	Heat effects	Others				
21	O'Brien–Myers isotherm	Axial dispersed plug flow	LDF approximation model with an adjustable mass transfer coefficient	Adiabatic, near-adiabatic, and isothermal effects	Negligible radial and angular gradients in concentration, temperature and velocity. Thermal equilibrium between the gas and the adsorbent. The momentum equation represented by Ergun's equation.	Adsorption of a 30% CO <sub>2</sub> –10% C <sub>2</sub> H <sub>6</sub> mixture in nitrogen (inert carrier gas) by TSA using Amborsorb 600 adsorbent	To solve a set of differential equations, the numerical method of lines was retained. For the spatial discretization, a finite volumes scheme with two staggered grids was chosen: one for the velocity and one for the temperature, pressure and concentrations (gas and adsorbed phases). The set of PDAEs obtained was integrated by employing an integrator (DASPK 2.0).	For low mass transfer coefficients (<0.01) the numerical breakthrough curves were too dispersive when compared to the experimental ones. For higher values, the numerical curves were identical the ones to the others and agreed well with the experimental measurements.	(Clausse et al., 2004)

(continued on next page)

‘Table 2.1, continued’

No.	Model assumptions					Application	Solution method	Results and comments	Ref.
	Equilibrium relationship	Flow pattern	Mass transfer rate model	Heat effects	Others				
22	Extended Langmuir isotherm	Axial dispersed plug flow	Local equilibrium model	Non-isothermal	The concentration and temperature gradients in the radial direction and the pressure drop in the bed were neglected. Instantaneous thermal equilibrium between the solid and gas phases.	CO <sub>2</sub> removal from a flue gas (containing 80% N <sub>2</sub> and 20% CO <sub>2</sub> ) by VSA using zeolite 13X	The PDEs were converted to ODEs by the method of lines with adaptive grid points. The estimation of the spatial derivatives was made from the upwind difference, and the cubic spline approximation was used to estimate the flow rates in the adsorptive bed. The concentration, temperature, and adsorption quantity were integrated with respect to the time in the bed by LSODE of ODEPACK software.	Comparison of the simulation results of the CO <sub>2</sub> concentration and the CO <sub>2</sub> recovery with experimental results indicated that the data trends were similar although the simulation values were slightly lower than the experimental data. The difference was attributed to the application of an imprecise adsorptive isotherm.	(Chou & Chen, 2004)

(continued on next page)

‘Table 2.1, continued’

No.	Equilibrium relationship	Flow pattern	Model assumptions			Application	Solution method	Results and comments	Ref.
			Mass transfer rate model	Heat effects	Others				
23	Langmuir isotherm	Axial dispersed plug flow	LDF approximation model	Isothermal	No radial variations in concentration.	Prediction of the dynamics of CO <sub>2</sub> breakthrough in a carbon monolith column	The system of partial differential algebraic equations (PDAEs) was coded in gPROMS software to obtain a numerical model.	The model that included the detailed structure of the monolith provided an excellent match to experimental results whereas the model based on the equivalent single channel approach incorrectly predicted higher separation efficiencies at different concentrations.	(Ahn & Brandani, 2005)
24	Multisite Langmuir isotherm	Axial dispersed plug flow	A double LDF approximation model to express macropore and micropore diffusion equations	Non-isothermal (adiabatic)	Negligible heat, mass, and momentum transport in the radial direction of the column. Pressure drop was described using Ergun equation.	Separation of a mixture of CH <sub>4</sub> (55%)-CO <sub>2</sub> (45%) by VSA-PSA technology using a Takeda carbon molecular sieve 3K	The fixed-bed model was solved in gPROMS (PSE Enterprise, London, U.K.) using orthogonal collocation method on finite elements with 25 finite elements and 2 interior collocation points per element.	The proposed model was able to predict well the behavior of the binary mixture in a fixed bed. Darken’s law provided a successful correction of the micropore diffusion coefficients in the nonlinear regions of the isotherms.	(Cavenati, Grande, & Rodrigues, 2005)

(continued on next page)

‘Table 2.1, continued’

No.	Model assumptions					Application	Solution method	Results and comments	Ref.
	Equilibrium relationship	Flow pattern	Mass transfer rate model	Heat effects	Others				
25	Langmuir isotherm	Axial dispersed plug flow	LDF approximation model	Isothermal	Negligible radial concentration gradient. Negligible pressure drop.	Adsorption of carbon dioxide from mixtures of CO <sub>2</sub> diluted in helium onto a hydrotalcite-like Al-Mg compounds in a fixed bed	A set of PDAEs was solved using the PDECOL package in the FORTRAN language, which is based on the method of orthogonal collocation of finite elements for partial differential equations in double precision.	The dispersion and mass transfer coefficients were calculated by theoretical correlations and the model described quite very well the dynamics of CO <sub>2</sub> adsorption in a fixed bed.	(Mor eira et al., 2006 )
26	Extended Langmuir-Freundlich isotherm	Axial dispersed plug flow	General LDF model with constant diffusivity/ Modified LDF model with concentration-dependent diffusivity	Non-isothermal	Negligible radial concentration and temperature gradients. Thermal equilibrium between fluid and particles. The pressure drop along the bed was calculated by the Ergun equation.	PSA separation of a mixture of CH <sub>4</sub> /CO <sub>2</sub> (50/50 vol %) using Takeda 3A carbon molecular sieve	The gPROMS modeling tool developed by Process Systems Enterprise Ltd. was used to obtain the solution of the dynamic simulation of the model.	Compared with the LDF model with constant diffusivity the experimental breakthrough curves and adsorption dynamics, was well-predicted by using the proposed non-isothermal and non-adiabatic modified LDF model with concentration-dependent diffusivity.	(Ki met al., 2006 )

(continued on next page)

'Table 2.1, continued'

No.	Equilibrium relationship	Flow pattern	Model assumptions			Application	Solution method	Results and comments	Ref.
			Mass transfer rate model	Heat effects	Others				
27	Extended Langmuir isotherm	Axial dispersed plug flow	LDF approximation model with a single lumped mass transfer coefficient	Non-isothermal	Negligible gradients in radial concentration and temperature. Thermal equilibrium between the gas and particles. The momentum balance represented by Ergun's equation.	Fixed-bed adsorption of binary gas mixtures (CO <sub>2</sub> /He, CO <sub>2</sub> /N <sub>2</sub> , and CO <sub>2</sub> /CH <sub>4</sub> ) onto silicalite pellets, sepiolite, and a basic resin	The complete model was solved numerically using the PDECOL program that uses orthogonal collocation on finite elements technique.	The model described adequately the breakthrough curves for the experiments with low CO <sub>2</sub> concentration, whereas the error was higher for the runs with higher CO <sub>2</sub> concentration. The quality of the prediction was improved introducing interaction factors in this model, because of the strong interactions between the adsorbed CO <sub>2</sub> molecules.	(Delgado et al., 2006; Delgado, Maria A. Uguina, Sotelo, Beatriz Ruiz, & Marcio Rosario, 2007)

(continued on next page)

‘Table 2.1, continued’

No.	Equilibrium relationship	Flow pattern	Model assumptions			Application	Solution method	Results and comments	Ref.
			Mass transfer rate model	Heat effects	Others				
28	Langmuir Isotherm	Axial dispersed plug flow	A double LDF approximation model	Non-isothermal	Negligible radial variations in concentration and temperature. Thermal equilibrium between the gas and solid phases. Negligible pressure drop.	Adsorption of a mixture of CH <sub>4</sub> (70%)-CO <sub>2</sub> (30%) in a column packed with bidisperse adsorbent (5A zeolite)	Orthogonal collocations were used as a spatial discretization method. The resulting ordinary differential-algebraic system of equations was solved by the DDASPG integration subroutine (IMSL library), based on the Petzold–Gear BDF method.	The presented model fitted well with experimental data, for both outlet composition and bed temperature. This indicated that the approximations proposed in this study give a good representation of the intra-particle mass transfer.	(Lein ekuge l-le-Cocq, Tayak out-Fayol le, Le Gorre c, & Jallut, 2007)
29	Multi-site Langmuir isotherm	Axial dispersed plug flow	A rigorous description for macropore diffusion model as well as an LDF approximation for micropore diffusions	Non-isothermal	No radial variations in temperature, pressure, and concentration. The pressure drop was described by Darcy’s law.	Low-concentration CO <sub>2</sub> removal from flue gas streams by electric swing adsorption using monolith	The mathematical model was solved using gPROMS 3.01 (PSE Enterprise, United Kingdom).	The results showed that both adsorption and desorption curves were not symmetrical, which cannot be accurately described by the employed mathematical model. This was attributed to the channels with different sizes in the boundaries of the honeycomb.	(Gran de & Rodrigue, 2008)

(continued on next page)

‘Table 2.1, continued’

No.	Model assumptions					Application	Solution method	Results and comments	Ref.
	Equilibrium relationship	Flow pattern	Mass transfer rate model	Heat effects	Others				
30	Virial isotherm model	Axial dispersed plug flow	A double LDF approximation model to express macropore and micropore diffusion equations	Non-isothermal	No mass, heat or velocity gradients in the radial direction. Thermal equilibrium between the gas and solid phases. The momentum balance represented by Ergun’s equation.	Separation of gas mixtures containing CO <sub>2</sub> , CH <sub>4</sub> , CO, N <sub>2</sub> and H <sub>2</sub> by PSA using activated carbon	The numerical solutions were performed with gPROMS (PSE Enterprise, UK) using the orthogonal collocation on finite elements as the numerical method.	A good agreement was observed between the experimental and the predicted concentration history at the end of the column and also the temperature evolution within the column. A deviation between the adsorbed amount obtained experimentally and the predicted by the model was lower than 10%.	(Grande et al., 2008)
31	Toth isotherm	Axial dispersed plug flow	LDF approximation model with a single lumped mass transfer coefficient	Non-isothermal (adiabatic/non-adiabatic)	Negligible radial concentration and temperature gradients. The momentum balance represented by Ergun’s equation.	Fixed-bed adsorption of binary gas mixtures (CO <sub>2</sub> /He and CO <sub>2</sub> /N <sub>2</sub> ) using activated carbon and zeolite 13X	The mathematical model was solved using the commercial software gPROMS (Process System Enterprise Limited, UK). The orthogonal collocation method on finite elements was used with six finite elements and three collocation points in each element of the adsorption bed.	The model acceptably reproduced the experimental data for the different feed concentrations and temperatures. By using the Toth equation for pure components, the simulated curve fitted well the experimental data, whereas a deviation was observed for multicomponent.	(Dantas et al., 2009; Dantas et al., 2011; Dantas et al., 2011)

(continued on next page)



‘Table 2.1, continued’

No.	Equilibrium relationship	Flow pattern	Model assumptions			Application	Solution method	Results and comments	Ref.
			Mass transfer rate model	Heat effects	Others				
32	Virial isotherm model / Multisite Langmuir isotherm	Axial dispersed plug flow	A rigorous description of macropore and micropore diffusion models	Isothermal	Negligible radial concentration gradient. Constant velocity within the column.	Adsorption of CO <sub>2</sub> on pitch-based activated carbon	Simulations of the presented mathematical model were performed in gPROMS (PSE Enterprise, UK) using the orthogonal collocation on finite elements.	An exponential dependence of the micropore diffusivity with temperature was shown to correctly describe the experimental data within the temperature range studied.	(Shen, Grande, Li, Yu, & Rodrigues, 2010)

(continued on next page)

'Table 2.1, continued'

No.	Model assumptions					Application	Solution method	Results and comments	Ref.
	Equilibrium relationship	Flow pattern	Mass transfer rate model	Heat effects	Others				
33	Dual-site Langmuir isotherm	Plug flow	LDF approximation with lumped mass transfer coefficient	Non-isothermal	No radial variations in temperature, pressure, and concentration. The gas and the solid phases are in thermal equilibrium. The pressure drop along the bed was calculated by the Ergun equation.	CO <sub>2</sub> capture from an 85%–15% N <sub>2</sub> -CO <sub>2</sub> feed mixture using PSA cycles/CO <sub>2</sub> capture from a synthesis gas feed mixture (55% H <sub>2</sub> and 45% CO <sub>2</sub> ) using PSA cycles	A complete discretization approach that uses the finite volume method was applied in both spatial and time domains, and the resulting large-scale nonlinear programming problem (NLP) was solved using an interior point NLP solver.	The results indicated the potential of the superstructure approach to predict PSA cycles with up to 98% purity and recovery of CO <sub>2</sub> . Verifications of the accuracy of the discretization scheme showed this approach is reasonably accurate in capturing the dynamics of PSA systems governed by hyperbolic PDAEs and steep adsorption fronts, and can be used for PSA systems with efficient NLP solvers.	(Agarwal, Biegler, & Zitney, 2010a; Agarwal et al., 2010b)

(continued on next page)

'Table 2.1, continued'

No.	Model assumptions					Application	Solution method	Results and comments	Ref.
	Equilibrium relationship	Flow pattern	Mass transfer rate model	Heat effects	Others				
34	Langmuir isotherm	Axial dispersed plug flow	LDF approximation model for external fluid film mass transfer / A rigorous description of pore diffusion model for intra-particle mass transfer	Non-isothermal	Negligible radial temperature and concentration gradients. Negligible pressure drop.	Fixed bed adsorption of carbon dioxide from a CO <sub>2</sub> -N <sub>2</sub> gas mixture (10% CO <sub>2</sub> in 90% N <sub>2</sub> ) using zeolite 13X	-	The curvature of the concentration breakthrough curve including the noted tailing was predicted with good accuracy. Energy profile was predicted with lower accuracy. However, the point at which the temperature breakthrough occurs was estimated with good accuracy which is the most important factor for industrial applications.	(Mulgund math et al., 2012)

\* The adsorbable component is present at only low concentration in an inert carrier.

## 2.3 Development and analysis of a mathematical model

The fixed-bed column mathematical models are used to predict the transient behavior of the concentration and temperature profiles for any defined changes in the initial parameters such as feed concentration, temperature, and flow rate. A complete mathematical model capable of describing the dynamics behavior of a fixed-bed adsorption system is established based on a set of fairly complex partial differential and algebraic equations (PDAEs) constructed from conservation of mass, energy, and momentum and augmented by appropriate transport rate equations and equilibrium isotherms (Hwang et al., 1995). The models used to represent a PSA process differ mainly in the form of the mass transfer rate, the form of the equilibrium isotherm, thermal effects, and the pressure drop along the bed. General descriptions of the above-mentioned items are presented in the following subsections. Many mathematical models for gas-solid adsorption in an adsorption column have been published over the past few decades, and there is still interest in developing a description of the dynamic evolution of such systems (Afzal, Rahimi, Ehsani, & Tavakoli, 2010; Leinekugel-le-Cocq et al., 2007).

### 2.3.1 Fluid phase material balance

The transient gas-phase component mass balance, which includes the axial dispersion term, convection flow term, accumulation in the fluid phase, and source term caused by the adsorption process on the adsorbent particles, can be represented by the following equation for a differential control volume of the adsorption column (Ruthven, 1984; Yang, 1987):

$$-D_{zi} \frac{\partial^2 c_i}{\partial z^2} + \frac{\partial}{\partial z}(uc_i) + \frac{\partial c_i}{\partial t} + \left(\frac{1-\varepsilon_b}{\varepsilon_b}\right)\rho_p \frac{\partial q_i}{\partial t} = 0 \quad (2-1)$$

where  $c_i$  represents the adsorbate concentration in the fluid phase;  $z$  is the distance along the bed length;  $u$  is the fluid velocity;  $t$  denotes time;  $\varepsilon_b$  is the bed void fraction;  $\rho_p$  is the

particle density;  $\bar{q}_i$  denotes average concentration of component  $i$  in adsorbent particle, which forms a link between the fluid and solid phase mass balance equations; and the effects of all mechanisms that contribute to axial mixing are lumped into a single effective axial dispersion coefficient,  $D_{zi}$ , which can be estimated using the following correlation (Da Silva, Silva, & Rodrigues, 1999; Ruthven, 1984; Wakao & Funazkri, 1978; Welty, Wicks, Wilson, & Rorrer, 2000; Yang, 1987):

$$\frac{\varepsilon_b D_{zi}}{D_{mi}} = 20 + 0.5 Sc Re \quad (2-2)$$

where  $D_{mi}$  is the molecular diffusivity of component  $i$  and  $Sc$  and  $Re$  are the Schmidt and Reynolds numbers, respectively.

The above equation, Eq. (2-1), is used to find the distribution of gas composition along the bed. Assuming no radial dependence of concentration and solid loading,  $c_i$  and  $\bar{q}_i$ , represent cross-sectional average values (these variables are functions of  $t$  and  $z$ ).

The well-known Danckwert's boundary conditions for a dispersed plug flow system can be assumed as follows (Khalighi, Farooq, & Karimi, 2012; Wehner & Wilhelm, 1956):

$$D_{zi} \left. \frac{\partial c_i}{\partial z} \right|_{z=0} = -u \Big|_{z=0} (c_i \Big|_{z=0^-} - c_i \Big|_{z=0}) \quad (2-3)$$

$$\left. \frac{\partial c_i}{\partial z} \right|_{z=L} = 0 \quad (2-4)$$

where  $c_i \Big|_{z=0^-}$  represents the feed composition for component  $i$  and  $L$  is the bed length.

In the above model, Eq. (2-1), if the flow pattern is represented as plug flow, axial dispersion can be neglected, and therefore the term  $-D_{zi} \left( \frac{\partial^2 c_i}{\partial z^2} \right)$  can be dropped, reducing Eq. (2-1) to a first-order hyperbolic equation. This is a reasonable approximation, particularly for large industrial units, for which the term representing the axial dispersion is very small compared to the convection term (Simo, Brown, & Hlavacek, 2008).

As a result of pressure and temperature variations, gas density and hence gas velocity vary along the bed. The following equation expressing the overall material balance for the bulk phase in the adsorption column is used to compute the velocity distribution through the bed (Ko et al., 2005):

$$-D_{zi} \frac{\partial^2 C}{\partial z^2} + \frac{\partial(uC)}{\partial z} + \frac{\partial C}{\partial t} + \left(\frac{1-\varepsilon_b}{\varepsilon_b}\right) \rho_p \sum_{i=1}^n \frac{\partial \bar{q}_i}{\partial t} = 0 \quad (2-5)$$

where  $C$  is the total concentration in the bulk phase and  $n$  is the number of components.

Applying the ideal gas law ( $c_i = \frac{y_i P}{RT_g}$ ), the overall mass balance equation can be expressed

as follows (Ahn, Yang, & Lee, 2001; Lee et al., 1999):

$$\begin{aligned} & -D_{zi} \frac{\partial^2 P}{\partial z^2} + \frac{\partial P}{\partial t} + P \frac{\partial u}{\partial z} + u \frac{\partial P}{\partial z} + PT_g \left[ -D_{zi} \frac{\partial^2 (1/T_g)}{\partial z^2} + \frac{\partial (1/T_g)}{\partial t} + u \frac{\partial (1/T_g)}{\partial z} \right] \\ & -2D_{zi} T_g \frac{\partial (1/T_g)}{\partial z} \frac{\partial P}{\partial z} + \left(\frac{1-\varepsilon_b}{\varepsilon_b}\right) \rho_p RT_g \sum_{i=1}^n \frac{\partial \bar{q}_i}{\partial t} = 0 \end{aligned} \quad (2-6)$$

where  $y_i$  is the mole fraction of component  $i$  in the gas phase,  $P$  is the total pressure,  $T_g$  is the gas temperature and  $R$  is the universal gas constant.

### 2.3.2 Complexity of kinetic models

The term  $\frac{\partial \bar{q}_i}{\partial t}$  in Eq. (2-1) represents the overall rate of mass transfer for component  $i$  (at time  $t$  and distance  $z$ ) averaged over a particle. The mass balance for an adsorbent particle yields the adsorption rate expression, which may be written as

$$\frac{\partial \bar{q}_i}{\partial t} = f(q_i, c_i) \quad (2-7)$$

For an isothermal system, the expressions for the concentration profiles in both phases,  $[c_i(z,t), \bar{q}_i(z,t)]$ , is given by the simultaneous solution of Eqs. (2-1) and (2-7), subject to the initial and boundary conditions imposed on the column. For non- isothermal systems, an energy balance must also be taken into account. In this case, all equations are coupled because, in general, both the equilibrium concentration and the rate coefficients are temperature dependent.

Although the mass transfer rate expression, Eq. (2-7), was written here as a single equation, it commonly consists of a set of equations comprising one or more diffusion equations with their associated boundary conditions. It is worth noting that a kinetic model is basically a mass balance that involves different variables describing mass transfer mechanisms within the adsorbent particle (Chahbani & Tondeur, 2000). A variety of mass transfer kinetic models with different degrees of complexity can be found in the literature. Mass transfer kinetic models can be classified into two main categories based on the assumption of local equilibrium or the existence of mass transfer resistance between the adsorbent particle and the fluid phase. They are introduced in the following subsections.

### **2.3.2.1 Local equilibrium model**

This model is expressed by the existence of an instantaneous local equilibrium (ILE) between the solid and fluid concentrations. If the mass transfer rate is relatively rapid, one may assume that local equilibrium is always maintained between the gas phase and the adsorbed phase within the particle at all points in the column. In other words, the local equilibrium assumption relates to the negligible effect of mass transfer resistance through the particles. As a result, it is assumed that, in this model, the adsorptive quantity is equal to the equilibrium adsorptive quantity:

$$\frac{\partial q_i}{\partial t} = \frac{\partial q_i^*}{\partial t} \quad (2-8)$$

In the above equation  $q_i^*$  is the adsorbed phase concentration of species  $i$  in equilibrium with the fluid phase concentration.

Equilibrium theory is aimed at identifying the general features of the dynamic response of the column without detailed calculations, as the overall pattern of the response is governed by the form of the equilibrium relationship rather than by kinetics. However, in practice, because axial mixing and mass transport resistances are neglected, breakthrough curves predicted by equilibrium models fail to give quantitatively satisfactory results and give only approximate representations of the behavior observed (Hwang et al., 1995). Although such systems are not common in practice, their analytical solution can provide useful information about the process dynamics and system behavior, which is quite valuable for preliminary design and analysis, leading to a greater understanding of the behavior of more complex systems.

Based on the classification presented in Table 2-1, the simplest case to consider is an isothermal system with no axial dispersion in which a trace level component is adsorbed from a non-adsorbing carrier gas with the assumption of negligible mass transfer resistance (model 1). Because the adsorbable component is present at a low concentration (trace level assumption), variation in the fluid velocity across the mass transfer zone is considered to be negligible, and the superficial velocity calculated based on the flow at the inlet can be treated as a constant. For these systems, the differential gas phase mass balance, Eq. (2-1), reduces to

$$u \frac{\partial c_i}{\partial z} + \frac{\partial c_i}{\partial t} + \left( \frac{1 - \varepsilon_b}{\varepsilon_b} \right) \rho_p \frac{\partial q_i^*}{\partial t} = 0 \quad (2-9)$$



Analytical determination of the concentration front in a packed adsorption column is limited to a few simple cases. Using a linear equilibrium isotherm, it is possible to obtain an analytical solution for isothermal or adiabatic systems with non-disperse behavior. Assuming a constant pattern profile, an improved analytical solution was obtained for the system that used a nonlinear equilibrium isotherm such as the Langmuir isotherm, but there are some assumptions that restrict its application (Yang, 1987). In the case of the PSA processes, the first analytical solution of the equilibrium model was obtained by (Shendalman & Mitchell, 1972) for the separation of CO<sub>2</sub> from a He-CO<sub>2</sub> mixture using silica gel as an adsorbent (model 1). They implemented the linear equilibrium relation for isothermal adsorption of a trace-level component in a one-dimensional system with no axial dispersion. The assumption of linear equilibrium for one adsorbable component permitted them to obtain a solution to the equations by the characteristic method. However, the experimental data revealed rather large deviations from the equilibrium theory predictions, suggesting that effects of mass transfer resistance are likely important. (Chan, Hill, & Wong, 1981) extended the local equilibrium theory to the separation of two-component gaseous mixtures via the PSA process in an isothermal system in which both the carrier and the impurity are adsorbed. They analytically studied the assumption of instant equilibrium between the adsorbate and the adsorbent when the more strongly adsorbed component is present at a trace level and the linear isotherms for both components were considered. Later, Fernandez & Kenney (1983) and Knaebel & Hill (1985) solved the model for binary mixtures with linear adsorption isotherms, and Serbezov and Sotirchos (1997) extended the solution to multicomponent mixtures with linear adsorption isotherms.

### 2.3.2.2 Mass transfer resistance models

The modeling of transport equations in a packed column strongly depends on the mechanism by which the mass transfer from the fluid to the solid phase occurs. In fact, equilibrium theory is confined to systems in which the adsorptive selectivity depends on a difference in equilibrium and is not useful for systems in which separation is based on kinetic selectivity (Hassan, Ruthven, & Raghavan, 1986). An example of kinetic adsorptive separation is the separation of a CO<sub>2</sub>/CH<sub>4</sub> mixture using a carbon molecular sieve, in which the separation is achieved by the large difference in diffusion rates between the two components (Diagne et al., 1996). Therefore, in modeling a real practical non-equilibrium packed column, the effects of mass transfer resistance between the fluid and the particle and within the particle must be considered (Hwang et al., 1995). In an attempt to construct a theoretical representation that more closely approximates a real process, researchers have developed dynamic models that consider effects due to dispersion and a finite mass transfer rate.

The mass transfer of solute from bulk gas into the solid phase is driven by equilibrium isotherms, whereas the mass balance equation inside the adsorbent particle depends on the adsorbent structure. At the microscopic level, the diffusion of the adsorbate into the adsorbent particles before adsorption onto the micropore surface (or adsorption onto the macropore surface, if no micropores exist) involves different transfer mechanisms. The adsorbate molecules initially must cross the external film surrounding each adsorbent particle and then diffuse through and along the porous structure of the adsorbent, as illustrated in Fig. 2.1. Depending on the specific system and the conditions, any one of the three different types of potential resistance to mass transfer may be dominant, and more than one resistance may be significant. These three potential resistances are the external fluid film resistance and the intraparticle diffusional resistances, the macropore diffusional resistance and the micropore diffusional resistance (LeVan, Carta, & Yon,

1999). In general, the mass transfer process through such a heterogeneous system can be expressed by detailed models identifying the film resistance around the solid particles and macropore/micropore resistances inside the particles. The most general case in adsorption process modeling is the case of macropore/micropore diffusion with external film resistance. Consequently, the discussion in the following subsections will focus on the case of the bidisperse pore-diffusion model with clearly distinct macropore/micropore diffusion.

#### 2.3.2.2.1 *External fluid film resistance*

External fluid film mass transfer is defined based on the concentration difference across the boundary layer surrounding each adsorbent particle and is strongly affected by the hydrodynamic conditions outside the particles (as characterized by the system's Sherwood, Reynolds, and Schmidt numbers) (LeVan et al., 1999). Indeed, it is supposed that the mass transfer resistance between the bulk phase and the macro-porous gas phase is localized to an external film around the adsorbent particles. By assuming steady-state conditions at the fluid-solid interface, the mass transfer rate across the external film is supposed to be equal to the diffusive flux at the particle surface (Farooq, Qinglin, & Karimi, 2001). In fact, because no accumulation of adsorbates is allowed, the film transfer and macropore diffusion can be treated as sequential steps, and mass conservation assumption is applicable. It can be expressed as the following equation (Jin, Malek, & Farooq, 2006; LeVan et al., 1999):

$$\frac{\partial \bar{q}_i}{\partial t} = \frac{3k_{fi}}{R_p} (c_i - c_{pi}|_{(t,R_p)}) = \frac{3}{R_p} \varepsilon_p D_{pi} \left. \frac{\partial c_{pi}}{\partial R} \right|_{(t,R_p)} \quad (2-10)$$

where  $k_{fi}$  is the external film mass transfer coefficient,  $R_p$  is the macroparticle radius,  $c_{pi}$  is the adsorbate concentration in the macropore, which is a function of radial position in

the particle,  $\varepsilon_p$  is the adsorbent porosity,  $D_{pi}$  is the macropore diffusivity, and  $R$  is the distance along the macroparticle radius.

The external film mass transfer coefficient,  $k_{fi}$ , around the particles can be estimated from the following correlation, which is applicable over a wide range of conditions (Wakao & Funazkri, 1978):

$$Sh = \frac{2k_{fi}R_p}{D_{mi}} = 2 + 1.1Sc^{1/3}Re^{0.6} \quad (2-11)$$

In most gas adsorption studies, the intraparticle diffusional resistance is normally much greater than the external fluid film resistance (intraparticle transport of the adsorbate is the slower step). Therefore, it is reasonable to assume negligible gas-side resistance and simulate adsorption systems based on a diffusion model (Carta & Cincotti, 1998; S. Farooq et al., 2001; Raghavan et al., 1985). An accurate kinetic model that accounts for the intraparticle diffusional resistances can provide reliable simulations of kinetically controlled PSA processes. Indeed, neglecting intraparticle mass transfer kinetics leads to significant deviations from the exact solution (Chahbani & Tondeur, 2000).

#### 2.3.2.2.2 *Macropore diffusional resistance*

Diffusion in sufficiently large pores (macro- and mesopores) such that the diffusing molecules escape from the force field of the adsorbent surface is often referred to as macropore diffusion (or pore diffusion). Depending on the relative magnitude of the pore diameter and the mean free path of the adsorbate molecules, transport in a macropore can occur by different mechanisms (Karger & Ruthven, 1992). For gas phase diffusion in small pores at low pressure, when the molecular mean free path is much greater than the pore diameter, Knudsen diffusion dominates the transport mechanism. In this case, the resistance to mass transfer mainly arises from collisions between the diffusing molecules and the pore wall. The Knudsen diffusivity ( $D_{ki}$ ) is independent of pressure and varies

only weakly with temperature as follows (Karger & Ruthven, 1992; Ruthven, 1984; Suzuki, 1990; Yang, 1987):

$$D_{ki} = 9700 r_p \sqrt{\frac{T}{M}} \quad (2-12)$$

where  $r_p$  is the mean macropore radius in cm,  $T$  is the temperature, and  $M$  is the molecular weight of the adsorbate.

By contrast, when the molecular mean free path is small relative to the pore diameter, the bulk molecular diffusion will be the dominant transport mechanism and can be estimated from the Chapman-Enskog equation (Bird, Stewart, & Lightfoot, 2002; Ribeiro et al., 2008; Ruthven, 1984; Sherwood, Pigford, & Wilke, 1975) for binary systems or the Stefan–Maxwell equation for multi-component systems (Suzuki, 1990). In the case of molecular diffusion, the collisions between diffusing molecules are the main diffusional resistance. For the intermediate case, both mechanisms are of comparable significance, and thus the combined effects of the Knudsen and the molecular diffusion constitute the rate-controlling mechanism. The effective macropore diffusivity ( $D_p$ ) is obtained from the Bosanquet equation (Grande et al., 2008; Yang, 1987):

$$\frac{1}{D_{pi}} = \tau \left( \frac{1}{D_{ki}} + \frac{1}{D_{mi}} \right) \quad (2-13)$$

where  $\tau$  is the pore tortuosity factor.

As discussed above, in macropore diffusion, transport occurs within the fluid-filled pores inside the particle (LeVan et al., 1999; Ruthven, 1984). In this situation, a differential mass balance equation for species  $i$  over a spherical adsorbent particle may be written as follows (Do, 1998b; Gholami & Talaie, 2009; Jin et al., 2006; LeVan et al., 1999; Qinglin, Farooq, & Karimi, 2003):

$$\frac{\partial c_{pi}}{\partial t} + \left(\frac{1-\varepsilon_p}{\varepsilon_p}\right) \frac{\partial \bar{q}_i}{\partial t} = \frac{1}{R^2} \frac{\partial}{\partial R} \left( R^2 D_{pi} \frac{\partial c_{pi}}{\partial R} \right) \quad (2-14)$$

This equation is used to determine the composition of the gas penetrating macropore volume at each radial position. In the above equation,  $\bar{q}_i$  is the average adsorbed phase concentration of component  $i$  in the micropore, which is related to the adsorbate flux at the micropore mouth by either equation 2-18 or 2-19, depending on the expression of the dominant transport mechanism in the micropore. The corresponding boundary conditions for macropore balance are as follows (Do, 1998b; Gholami & Talaie, 2009; Jin et al., 2006; LeVan et al., 1999; Qinglin, Farooq, et al., 2003; Qinglin, Sundaram, & Farooq, 2003):

$$\left\{ \begin{array}{l} \frac{\partial c_{pi}}{\partial R} \Big|_{(t,0)} = 0 \end{array} \right. \quad (2-15)$$

*The external fluid – film resistance can be reflected in the boundary condition as follows :*

$$\left\{ \begin{array}{l} \varepsilon_p D_{pi} \frac{\partial c_{pi}}{\partial R} \Big|_{(t,R_p)} = k_{fi} (c_i - c_{pi} \Big|_{(t,R_p)}) \end{array} \right. \quad (2-16)$$

*or  $c_{pi}(t, R_p) = c_i$  for no external film resistance (when pure adsorbate is fed to the column)* (2-17)

#### *Micropore diffusional resistance*

In very small pores in which the pore diameter is not much greater than the molecular diameter, the adsorbing molecules can never escape from the force field of the pore wall, even at the center of the pore. Such a mechanism, in which transport may occur by an activated process involving jumps between adsorption sites, is often called micropore diffusion (also known as solid diffusion) (LeVan et al., 1999; Ruthven, 1984). In this situation, the intraparticle gas phase is neglected, and diffusion through it is supposed to be null (Chahbani & Tondeur, 2000). Consequently, the material balance equation in the

micropores does not contain any gas phase accumulation term. As illustrated in Fig. (2.1), transport in the micropores may occur by three different mechanisms: barrier resistance (confined at the micropore mouth), distributed micropore interior resistance, and the combined effects of both resistances (Cavenati et al., 2005; S. Farooq et al., 2001; Srinivasan, Auvil, & Schork, 1995).

The mass transfer rate across the micropore mouth can be expressed by the following equations (Buzanowski & Yang, 1989; Jin et al., 2006; LeVan et al., 1999; Qinglin, Sundaram, et al., 2003):

$$\frac{\partial \bar{q}_i}{\partial t} = k_{bi} (q_i^* - \bar{q}_i) \quad \text{when the gas diffusion is controlled by the barrier resistance} \quad (2-18)$$

$$\text{or } = \frac{3}{R_c} D_{\mu i} \left. \frac{\partial q_i}{\partial r} \right|_{(t, R_c)} \quad \text{when the distributed micropore interior resistance is dominant} \quad (2-19)$$

where  $k_{bi}$  is the barrier transport coefficient,  $R_c$  is the microparticle radius,  $q_i$  is the distributed adsorbate concentration in the micropore,  $D_{\mu i}$  is the micropore diffusivity of component  $i$ , and  $r$  is the distance along the microparticle radius.

The strong dependence of the micropore diffusivity on concentration can be expressed using Darken's equation (Cavenati et al., 2005; Chihara, Suzuki, & Kawazoe, 1978; Do, 1998a; Kawazoe, Suzuki, & Chihara, 1974; Khalighi et al., 2012; Ruthven, Farooq, & Knaebel, 1994):

$$D_{\mu i} = D_{\mu i}^{\infty} \left. \frac{d \ln(p_i)}{d \ln(q_i)} \right|_T \quad (2-20)$$

where  $D_{\mu i}^{\infty}$  is the micropore diffusivity of component  $i$  at infinite dilution and  $p_i$  is the partial pressure of component  $i$ , which is in equilibrium with the adsorbed concentration in the micropore.

The temperature dependence of the corrected diffusivity and the surface barrier mass transfer coefficients follows an Arrhenius-type form, as described by the following (Cavenati et al., 2005; Gholami & Talaie, 2009; Grande & Rodrigues, 2004; Grande & Rodrigues, 2005; Khalighi et al., 2012; Qinglin, Sundaram, et al., 2003):

$$D_{\mu i}^{\infty} = D_{\mu i}^0 \exp\left(-\frac{E_{ai}}{R_g T_s}\right) \quad (2-21)$$

$$k_{bi} = k_{bi}^0 \exp\left(-\frac{E_{bi}}{R_g T_s}\right) \quad (2-22)$$

where  $D_{\mu i}^0$  and  $k_{bi}^0$  are the temperature-independent pre-exponential constants,  $R_g$  is the universal gas constant,  $T_s$  is the solid temperature, and  $E_{ai}$  and  $E_{bi}$  are the activation energy of micropore diffusion and the activation energy of surface barrier resistance for component  $i$ , respectively.

When the resistance distributed in the micropore interior dominates the transport of species  $i$ , the mass balance equation for micropore diffusion is the following (Jin et al., 2006; LeVan et al., 1999; Qinglin, Sundaram, et al., 2003):

$$\frac{\partial q_i}{\partial t} = \frac{1}{r^2} \frac{\partial}{\partial r} \left( r^2 D_{\mu i} \frac{\partial q_i}{\partial r} \right) \quad (2-23)$$

The corresponding boundary conditions for the microparticle balance are as follows (Jin et al., 2006; LeVan et al., 1999; Qinglin, Sundaram, et al., 2003):

$$\left\{ \begin{array}{l} \frac{\partial q_i}{\partial r} \Big|_{(t,0)} = 0 \quad (2-24) \\ \text{when a combination of barrier and distributed micropore interior resistances is} \\ \text{dominant,} \\ \text{the barrier resistance can be reflected in the boundary condition as follows:} \\ \frac{3}{R_c} D_{\mu i} \frac{\partial q_i}{\partial r} \Big|_{(t,R_c)} = k_{bi} (q_i^* - q_i|_{(t,R_c)}) \quad (2-25) \\ \text{or } q_i(t, R_c) = q_i^* \quad \text{for no barrier resistance} \quad (2-26) \end{array} \right.$$



The adsorbed amount at a certain time for component  $i$  based on particle volume can be calculated by volume integration of the concentration profiles in the macropores and micropores (Jin et al., 2006; Khalighi et al., 2012; Qinglin, Farooq, et al., 2003; Qinglin, Farooq, & Karimi, 2004; Qinglin, Sundaram, et al., 2003):

$$\bar{q}_i = \varepsilon_p \frac{3}{R_p^3} \int_0^{R_p} c_{pi} R^2 dR + (1 - \varepsilon_p) \frac{3}{R_p^3} \int_0^{R_p} \bar{q}_i R^2 dR \quad (2-27)$$

where:

$$\bar{q}_i = \frac{3}{R_c^3} \int_0^{R_c} q_i r^2 dr \quad (2-28)$$

In most kinetically selective processes, the controlling resistance for the uptake of sorbates is typically diffusion in the micropores (Cavenati et al., 2005; S. Farooq et al., 2001; Lamia et al., 2008). Micropore diffusion can contribute significantly to the overall intraparticle mass transport, primarily due to the higher concentration of the adsorbed phase, although the mobility of molecules in the adsorbed phase is generally much smaller than in the gas phase (Kapoor & Yang, 1990). Doong & Yang (1986) reported that micropore diffusion contributed as much as 50% to the total flux in the activated carbon pores during the PSA separation of CO<sub>2</sub>, H<sub>2</sub>, and CH<sub>4</sub> (model 5). Liu and Ruthven (1996) gravimetrically measured the diffusion of CO<sub>2</sub> in a carbon molecular sieve sample and concluded that the data were consistent with the barrier resistance model at lower temperatures, while the distributed micropore interior resistance model adequately fitted the data at higher temperatures. They found that the results suggested a dual resistance model with varying importance of the two components depending on pressure and temperature. In another study, Rutherford and Do (2000b) fitted the uptake of CO<sub>2</sub> in a sample of a carbon molecular sieve (Takeda 5A) using a model based on distributed diffusional resistance in the micropore interior. The model simulation results were in fair agreement with the experimental data. Qinglin et al. (2003a) and Qinglin et al. (2003b)

investigated the diffusion of carbon dioxide in three samples of carbon molecular sieve adsorbent. They indicated that transport of gases in the micropores of these samples is controlled by a combination of barrier resistance at the micropore mouth followed by a distributed pore interior resistance acting in series. The proposed dual resistance model was shown to be able to fit the experimental results over the entire range covered in that study. Cavenati et al. (2005) studied diffusion of CO<sub>2</sub> on the carbon molecular sieve 3K and reported that the initial difficulty associated with diffusion due to the surface barrier resistance was not observed in the uptake of CO<sub>2</sub>. A successful description of diffusion in micropores was achieved using the distributed micropore interior resistance model without the need for the surface barrier resistance model at the mouth of the micropore (model 24). They attributed the absence of surface barrier resistance to performing the activation protocol at a higher temperature. Shen et al. (2010) studied diffusion of CO<sub>2</sub> on pitch-based activated carbon beads using diluted breakthrough experiments performed at different temperatures. To simulate the breakthrough curves, they developed a mathematical model based on a rigorous description of macropore and micropore diffusion with a nonlinear adsorption isotherm and assumed that the process was isothermal (model 32). The experimental results demonstrated that micropore resistances control the diffusion mechanism within the adsorbent. More recently, Mulgundmath et al. (2012) investigated concentration and temperature profiles of CO<sub>2</sub> adsorption from a CO<sub>2</sub>-N<sub>2</sub> gas mixture in a dynamic adsorption pilot plant unit to better understand the adsorbent behavior. A dynamic model based on an exact description of pore diffusion was developed for the simulation of non-isothermal adsorption in a fixed-bed (model 34). The proposed model was able to adequately predict the experimental data at all three ports for the duration of the experiment.

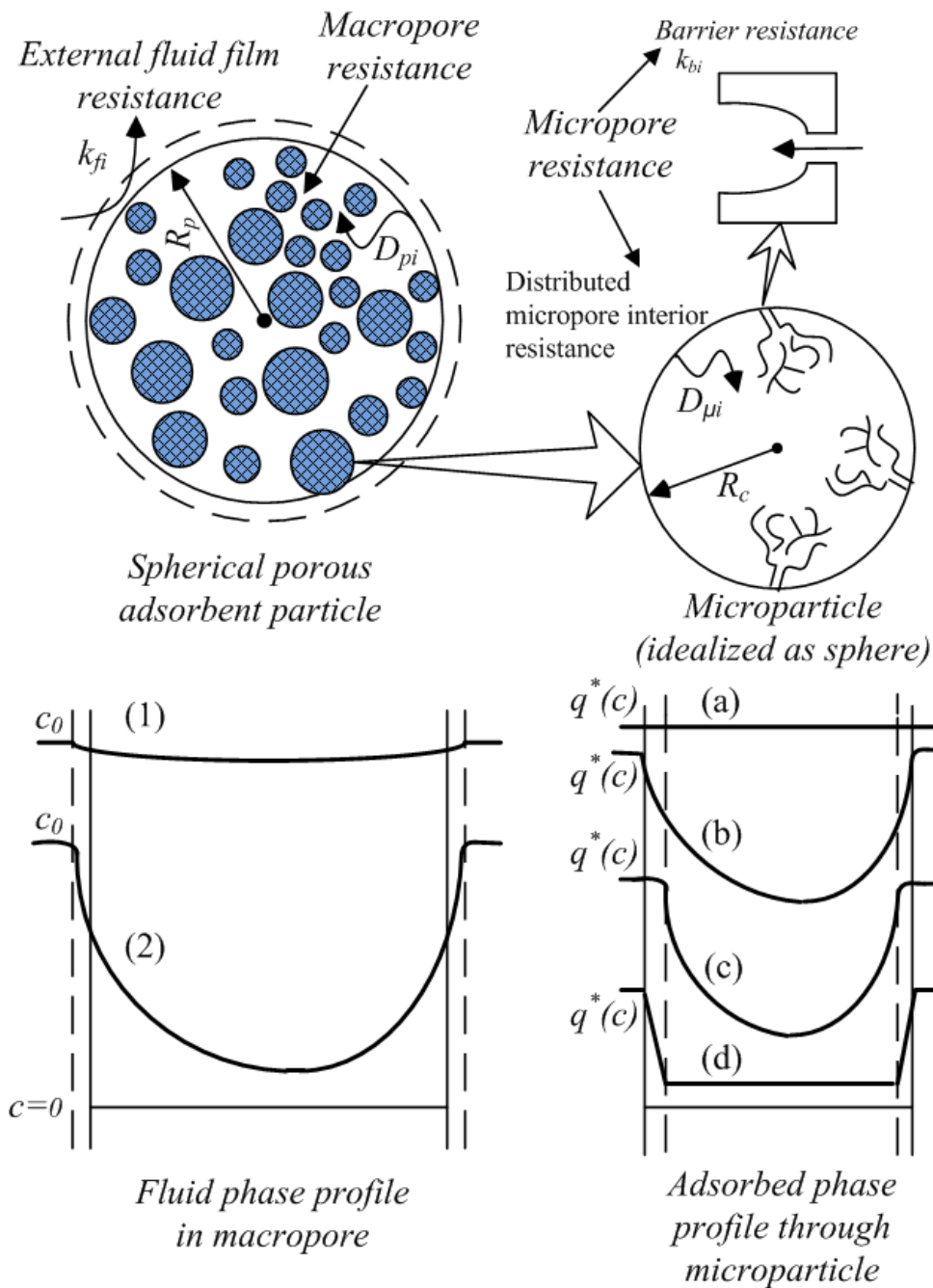


Figure 2.1: Schematic diagram showing various resistances to the transport of adsorbate as well as concentration profiles through an idealized bidisperse adsorbent particle demonstrating some of the possible regimes: (1)+(a) rapid mass transfer, equilibrium through particle; (1)+(b) micropore diffusion control with no significant macropore or external resistance; (1)+(c) transport controlled by the resistance at the micropore interior; (1)+(d) controlling resistance at the surface of the microparticles; (2)+(a) macropore diffusion control with some external resistance and no resistance within the microparticle; (2)+(b) all three resistances (micropore, macropore, and film) are significant; (2)+(c) diffusional resistance within the macroparticle with some external film resistance together with a restriction at the micropore interior (2)+(d) diffusional resistance within the macroparticle in addition to a restriction at the micropore mouth with some external film resistance.

### 2.3.2.2.3 *Linear driving force model*

Although the diffusional models are closer to reality, due to the mathematical complexities associated with such equations for the exact description of intraparticle diffusion in adsorbent particles, simpler rate expressions are often desirable (Carta & Cincotti, 1998; Zhang & Ritter, 1997). Simplified models are generally adopted by using an expression of the particle uptake rate, which does not involve the spatial coordinates. The approximations express the mass exchange rate between the adsorbent and its surroundings in terms of the mean concentration in the particle, regardless of the actual nature of the resistance to mass transfer (Lee & Kim, 1998). Simplifying assumptions should increase the practical applicability of the model without reduction of accuracy. The most frequently applied approximate rate law is the so-called linear driving force (LDF) approximation, which was first proposed by Glueckauf and Coates (1947). They originally suggested that the uptake rate of a species into adsorbent particles is proportional to the linear difference between the concentration of that species at the outer surface of the particle (equilibrium adsorption amount) and its average concentration within the particle (volume-averaged adsorption amount):

$$\frac{\partial \bar{q}_i}{\partial t} = k_i (q_i^* - \bar{q}_i) \quad (2-29)$$

As can be seen, the overall resistance to mass transfer is lumped into a single effective linear driving force rate coefficient,  $k_i$ . Glueckauf demonstrated that the LDF overall mass transfer coefficient for spherical particles was equal to  $15D_e/R_p^2$  (Glueckauf, 1955). The above equation has been shown to be valid for dimensionless times  $(D_e t/R_p^2) > 0.1$ , where  $D_e$  is the effective diffusivity (accounts for all mass transfer resistances) and  $t$  is the time of adsorption or desorption (Yang, 1987). Although the LDF model deals with the average concentrations of the adsorbate within the adsorbent particle, (Liaw, Wang, Greenkorn, & Chao, 1979) demonstrated that the same value for  $k_i$  could be simply obtained by

assuming a parabolic concentration profile within the particle. This assumption was later shown to be acceptable, as the exact solution to the concentration profile has almost always been found to be a parabolic function (Do & Rice, 1986; Patton, Crittenden, & Perera, 2004; Tsai, Wang, & Yang, 1983; Tsai, Wang, Yang, & Desai, 1985; Yang & Doong, 1985). Sircar and Hufton (2000a) demonstrated that the LDF model approximation is in accordance with any continuous intraparticle concentration profile within a spherical particle when a numerical constant other than 15 is used in the expression of the LDF rate coefficient. The literature includes many attempts to develop new correlations for the accurate prediction of the overall LDF rate constant (Gholami & Talaie, 2009). When both the macropore and the micropore diffusions are dominant, the overall LDF mass transfer coefficient can be expressed by defining a single effective diffusivity related to both macropore and micropore diffusivities. The following correlation was proposed by Farooq and Ruthven (1990), in which more than one mass transfer resistance (i.e., film, macropore, and micropore resistances) is considered significant:

$$\frac{1}{k_i} = \frac{R_p q_0}{3k_{fi} c_0} + \frac{R_p^2 q_0}{15 \varepsilon_p D_{pi} c_0} + \frac{R_c^2}{15 D_{\mu i}} \quad (2-30)$$

where  $q_0$  is the value of  $q$  at equilibrium with  $c_0$  at feed temperature.

The above equation is actually an extension of the Glueckauf approximation, which, apart from validity for a linear isothermal system, is also known to work reasonably well for nonlinear systems.

Recently, the Stefan-Maxwell approach (Do & Do, 1998; Liow & Kenney, 1990) or the dusty gas model (Mendes, Costa, & Rodrigues, 1995; Atanas Serbezov & Sotirchos, 1998) has been proposed to describe adsorption kinetics. However, Sircar & Hufton (2000b) indicated that the LDF model is adequate to capture gas adsorption kinetics because in the estimation of the final process performance, the detailed characteristics of

a local adsorption kinetic model are lumped during repeated integrations (Agarwal et al., 2010a, 2010b). Indeed, although this adsorption rate model is rather simple, it can predict the experimental data with satisfactory accuracy (Yang & Lee, 1998). Consequently, this approximation has found widespread application in modeling fixed-bed and cyclic CO<sub>2</sub> adsorption processes (Hwang & Lee, 1994; Raghavan et al., 1985).

A dynamic model that included finite mass transfer resistance based on a linear driving force assumption was first developed by (Mitchell & Shendalman, 1973) for the isothermal removal of CO<sub>2</sub> (a strongly adsorbed component in a trace amount) from He (an inert product) using silica gel. However, the model was found to provide a poor representation of the experimental data. Cen and Yang (1985) performed separation of a five-component gas mixture containing H<sub>2</sub>, CO, CH<sub>4</sub>, H<sub>2</sub>S, and CO<sub>2</sub> by PSA. Both equilibrium and LDF models were employed to develop a mathematical model for simulating the PSA process (model 2). The results predicted by the equilibrium model, particularly for CO<sub>2</sub> concentration, were in poor agreement with the experimental data, indicating the significant role of mass transfer resistance in CO<sub>2</sub> adsorption/desorption. The simulation results of the LDF model were in generally good agreement with the experimental data. (Raghavan et al., 1985) simulated an isothermal PSA separation of a trace amount of an adsorbable species from an inert carrier using a linear equilibrium isotherm and with the assumption of a linear driving force for mass transfer resistance (model 3). The theoretically predicted behavior of the system was shown to provide a good fit with the experimental data of (Mitchell & Shendalman, 1973) for the CO<sub>2</sub>-He-silica gel system. The major difference between this model and the model of (Mitchell & Shendalman, 1973) is the assumption of an inverse dependence of the effective mass transfer coefficient on the total pressure. Such behavior is to be expected for a system in which the uptake is controlled by external film or pore diffusional resistance (Raghavan et al., 1985).

Kapoor and Yang (1989) also studied the kinetic separation of a CO<sub>2</sub>/CH<sub>4</sub> mixture on a carbon molecular sieve. The experimental results were simulated using a linear driving force model approach with a cycle time-dependent LDF rate coefficient (model 6). The cycle time-dependent LDF coefficient included all mass transfer resistances such as film and intraparticle diffusion and was determined by matching the model simulation results with the experimental results. However, the experimental estimates of this parameter differed considerably from the predictions of a priori correlations developed by (Nakao & Suzuki, 1983) and (Raghavan, Hassan, & Ruthven, 1986). (Diagne et al., 1996) developed a new PSA process with the intermediate feed inlet position operated with dual refluxes for separation of CO<sub>2</sub> dilute gas from air. They studied the influence of different CO<sub>2</sub> feed concentrations and feed inlet positions on CO<sub>2</sub> product concentration. An isothermal model based on LDF approximation was developed (model 13) to explore the effects of various combinations of the operating variables and to analyze semi-quantitatively the effects of the main characteristic parameters such as the dimensionless feed inlet position and the stripping-reflux ratio. Good agreement between the model prediction and the experimental results was obtained.

In another study, low-concentration CO<sub>2</sub> separation from flue gas was performed by PSA using zeolite 13X as the adsorbent (Choi et al., 2003). To further assess the effects of adsorption time and reflux ratio on product purity and the recovery, dynamic modeling of the PSA process based on an LDF approximation was developed (model 19). The comparison of the numerical simulation-based and experimental results demonstrated that the model adequately describes the experimental breakthrough curves and temperature changes in the bed. (Delgado et al., 2006; Delgado et al., 2007) investigated the fixed-bed adsorption of binary gas mixtures (CO<sub>2</sub>/He, CO<sub>2</sub>/N<sub>2</sub>, and CO<sub>2</sub>/CH<sub>4</sub>) onto silicalite pellets, sepiolite, and a basic resin. The experimental breakthrough curves were simulated by a model based on the LDF approximation for the mass transfer that considered the energy

and momentum balances and used the extended Langmuir equation to describe the adsorption equilibrium isotherm (model 27). They proposed a lumped mass transfer coefficient instead of considering two mass transfer resistances in a bidisperse adsorbent. A comparison between the experimental and theoretical curves demonstrated that the model reproduces the experimental data satisfactorily for the different feed concentrations, flow rates, and temperatures used. More recently, (Dantas et al., 2011) studied the fixed-bed adsorption of carbon dioxide from CO<sub>2</sub>/N<sub>2</sub> mixtures on a commercial activated carbon. A model based on the LDF approximation for the mass transfer that considered the energy and momentum balances was used to simulate the adsorption kinetics of carbon dioxide (model 31). They considered an overall LDF mass transfer coefficient in which the effects of film, macropore, and micropore resistances were assumed to be significant. The proposed LDF model acceptably reproduced the experimental data for the different feed concentrations/temperatures and was suitable for describing the dynamics of CO<sub>2</sub> adsorption from the mixtures. The importance of the external and internal mass transfer resistances was determined by performing a sensitivity analysis, which concluded that micropore resistances are not very important in the studied system. Moreover, it was deduced that, in the case of macropore resistances only, the molecular diffusivity is predominant.

If one neglects diffusion through macropores, the mass transfer rate through micropore volumes can be simplified by applying the LDF model approximation, which is mathematically equivalent to the modeling of transport through a barrier resistance confined at the micropore mouth (Cavenati et al., 2005; Grande & Rodrigues, 2007; Srinivasan et al., 1995):



$$\frac{\partial \bar{q}_i}{\partial t} = K_{\mu i} (q_i^* - \bar{q}_i) \quad (2-31)$$

$$K_{\mu i} = \frac{1}{\frac{1}{k_{bi}} + \frac{R_c^2}{15D_{\mu i}}} \quad (2-32)$$

where  $K_{\mu i}$  is the LDF constant for mass transfer in the micropores for component  $i$  (Grande & Rodrigues, 2007).

When there is no surface barrier resistance in the mouth of the micropores, the first term in the denominator of Eq. (2-32) vanishes (Cavenati et al., 2005). This model, which has been referred to as the LDFS model, is simply obtained from Eq. (2-23) if the intraparticle concentration profile of the adsorbate is assumed to be parabolic (Carta & Cincotti, 1998; Chahbani & Tondeur, 2000; Do & Rice, 1986; Liaw et al., 1979; Siahpoosh et al., 2009). The mathematically simple LDF approximation permits the direct use of the averaged adsorbed concentration in the interior of the adsorbent particle and thus eliminates the need for the integration step at the particle level, in contrast to the solid diffusion model (Chahbani & Tondeur, 2000; S. Sircar & Hufton, 2000b).

If the adsorbed-phase diffusion is neglected, a similar linear driving force model based on the gaseous phase can be used to approximate the diffusive process in macropore resistance as follows (Khalighi et al., 2012):

$$\varepsilon_p \frac{\partial \bar{c}_{pi}}{\partial t} + \rho_p \frac{\partial \bar{q}_i}{\partial t} = K_{pi} (c_i - \bar{c}_{pi}) \quad (2-33)$$

$$K_{pi} = \varepsilon_p \frac{15D_{pi}}{R_p^2} \frac{Bi_i}{Bi_i + 1} \quad (2-34)$$

where  $K_{pi}$  is the LDF constant for mass transfer in the macropores for component  $i$ ,  $\bar{c}_{pi}$  is the mean intraparticle gas phase concentration of species  $i$ , and  $Bi_i = R_p k_{fi} / (5\varepsilon_p D_{pi})$  is the mass Biot number, which represents the ratio of internal macropore to external film resistances.

As can be seen, the proposed effective LDF rate coefficient,  $K_{pi}$ , is a combination of external fluid film transport, molecular, and Knudsen diffusions in the macropores. This model, which has been referred to as the LDFG model, can be derived from the pore diffusion model, Eq. (2-14), based on the assumption of a parabolic gas-phase concentration profile in the particle (Chahbani & Tondeur, 2000; Leinekugel-le-Cocq et al., 2007; Atanas Serbezov & Sotirchos, 2001; Yang & Doong, 1985). Such a space-independent expression for the adsorption rate can transform the PDE expressing mass conservation for gas penetrating pores into an ODE, and therefore the solutions are mathematically simpler and faster than the solution of the diffusion models.

(Lai & Tan, 1991) developed approximate models for pore diffusion inside the particle with a nonlinear adsorption isotherm based on a parabolic concentration profile assumption for the summation of the gas and adsorbed phases. They developed a rate expression model that depends on the slope of the adsorption isotherm at the external surface of the sorbent. (Ding & Alpay, 2000) studied high-temperature CO<sub>2</sub> adsorption and desorption on hydrotalcite adsorbent at a semi-technical scale of operation. They presented a dynamic model based on a linear driving force approximation to describe intraparticle mass transfer processes (model 17). To address the importance of intraparticle mass transfer resistances during different steps of operation, they also developed an adsorption model based on ILE assumption between the gas and adsorbed phases. Overall, they concluded that although the ILE model failed to give an adequate description of the desorption kinetics, the LDF model based on pore diffusion and accounting for the non-linearity of the isotherm provides an adequate approximation of the adsorption and desorption processes. (Grande & Rodrigues, 2008) studied the operation of an electric swing adsorption process for low-concentration CO<sub>2</sub> removal from flue gas streams using an activated carbon honeycomb monolith as an adsorbent. To explore the dynamics behavior of the system, the authors developed a mathematical

model that included bidisperse resistances within the porous structure of the monolith (model 29). A rigorous description and a linear driving force approximation were employed for macropore and micropore diffusion, respectively. Adsorption/desorption breakthrough experiments were performed to determine the validity of the proposed mathematical model. A comparison of simulated breakthroughs and experimental data showed that the dynamic model incorporating mass, energy, and momentum balances agreed well with the experimental results.

If macropore or the adsorbed-phase diffusion cannot be ignored, the mass transfer rate expression can be expressed using a double LDF model, through which the macropore and the micropore diffusion are both represented by LDF approximations taken in series (Da Silva et al., 1999; Doong & Yang, 1987; Kim, 1990; Leinekugel-le-Cocq et al., 2007; Mendes, Costa, & Rodrigues, 1996). Cavenati et al. (2005) studied the separation of a methane-carbon dioxide mixture in a column packed with bidisperse adsorbent (carbon molecular sieve 3K). To reduce the computational time required for the simulations, macropore and micropore diffusion equations were described using a bi-LDF simplification instead of the mass balances in macropores and in micropores (model 24). They assumed that the macropore diffusivity and surface barrier resistance at the mouth of the micropore are not a function of the adsorbed phase concentration, whereas the Darken law describes micropore diffusivity dependence with concentration. To confirm the validity of the mathematical model and the proposed bi-LDF approximation for the prediction of experimental data, a fixed-bed experiment of the binary mixture was performed. The results indicated that the proposed mathematical model was able to adequately predict the behavior of the binary mixture in a fixed bed. Leinekugel-le-Cocq et al. (2007) presented a simplified intraparticle model based on a non-isothermal double LDF approximation to simulate breakthroughs of a CH<sub>4</sub>/CO<sub>2</sub> mixture in a fixed bed of bidisperse adsorbent (5A zeolite). A bidisperse double LDF model was proposed that

considered both macropore and micropore diffusion by LDF approximations taken in series (model 28). A comparison of the model predictions with the experimental data revealed that the approximated model proposed in this study yields a good representation of the intraparticle mass transfer.

### **2.3.3 Energy balance**

As mentioned earlier, adsorption is an exothermic process, and temperature changes may affect the adsorption equilibrium relation and, in some cases, adsorption rates. Therefore, the effects of heat generation and heat transfer in the adsorbent bed must be considered to accurately predict packed column dynamics. Some publications have addressed non-isothermal adsorption of CO<sub>2</sub> in a fixed bed either as a single adsorbate or multi-component mixture, which are summarized in Table 2.1. The amplitude of the temperature variation depends primarily on the heat of adsorption, the throughput, and the heat transfer characteristics of the packed adsorbed column (Farooq, Hassan, & Ruthven, 1988; Ruthven, 1984). The generated heat is conducted to the surface of the particles and then is transferred to the gas phase by a convection mechanism. To take into account the energy transfer, three different control volumes may be considered: gas, solid, and column wall.

#### **2.3.3.1 Gas phase energy balance**

The variation of gas temperature with respect to time arises from the transfer of energy due the axial conductive solid-phase heat flux to the gas phase along the  $z$  direction as well as the energy transfer by convection through the bed due to the bulk movement of gas. Therefore, the energy balance for the gas phase, which includes the heat transfer between the flowing fluid and the surface of the solid adsorbent through a laminar film

and the energy transferred to the wall of the column, may be written as the following (Rezaei & Grahn, 2012; Ruthven, 1984):

$$-\lambda_L \frac{\partial^2 T_g}{\partial z^2} + \rho_g C_g \frac{\partial(uT_g)}{\partial z} + \rho_g C_g \frac{\partial T_g}{\partial t} + \left(\frac{1-\varepsilon_b}{\varepsilon_b}\right) h_f a_s (T_g - T_s) + \frac{4h_w}{\varepsilon_b d_{int}} (T_g - T_w) = 0 \quad (2-35)$$

The above equation is used to find the distribution of gas temperature along the bed, where  $T_g$  represents the bulk gas temperature;  $C_g$  is the heat capacity of the gas;  $\rho_g$  is the bulk density of the gas;  $h_f$  denotes the film heat transfer coefficient between the gas and the adsorbent;  $a_s$  expresses the ratio of the particle external surface area to volume;  $T_s$  denotes the solid temperature;  $h_w$  is the internal convective heat transfer coefficient between the gas and the column wall;  $d_{int}$  is the column internal diameter;  $T_w$  denotes the wall temperature; and  $\lambda_L$  is the effective axial heat dispersion, which can be estimated using the following correlation (Grande & Rodrigues, 2005; Wakao & Funazkri, 1978; Yang, 1987):

$$\frac{\lambda_L}{k_g} = 7 + 0.5PrRe \quad (2-36)$$

where  $k_g$  is the thermal conductivity of the gas mixture and  $Pr$  is the Prandtl number.

The Chilton–Colburn analogy can be applied (in analogy with Eq. (2-11)) to estimate the convective film heat transfer coefficient between the gas and the adsorbent,  $h_f$  (Chilton & Colburn, 1934). It can be estimated through the following correlation, which is particularly applicable at higher Reynolds numbers (Wakao, Kaguei, & Funazkri, 1979):

$$Nu = \frac{2h_f R_p}{k_g} = 2 + 1.1Pr^{1/3}Re^{0.6} \quad (2-37)$$

The following correlation can be applied for the estimation of the internal convective heat transfer coefficient,  $h_w$  (Dantas et al., 2009; Dantas et al., 2011; Dantas et al., 2011):

$$Nu_w = \frac{h_w d_{int}}{k_g} = 12.5 + 0.048 Re \quad (2-38)$$

The following boundary conditions are assumed:

$$\lambda_L \left. \frac{\partial T_g}{\partial z} \right|_{z=0} = -\rho_g C_g u \left. (T_g \right|_{z=0^-} - T_g \left|_{z=0} ) \quad (2-39)$$

$$\left. \frac{\partial T_g}{\partial z} \right|_{z=L} = 0 \quad (2-40)$$

where  $T_g \left|_{z=0^-}$  is feed temperature.

### 2.3.3.2 Solid phase energy balance

For the solid phase, a separate energy balance equation can be assumed that considers the accumulation term, the film heat transfer term, and the heat generated by the adsorption of the adsorbate, as shown by the following (Do, 1998b):

$$\rho_p C_s \frac{\partial T_s}{\partial t} = h_f a_s (T_g - T_s) + \sum_{i=1}^n (-\Delta H_i) \frac{\partial q_i}{\partial t} \quad (2-41)$$

where  $\rho_p$  is the particle density,  $C_s$  represents the heat capacity of the adsorbent and  $(-\Delta H_i)$  is the isosteric heat of adsorption for the  $i$  component at zero coverage, which can be calculated by using the Clausius-Clapeyron equation (Yang, Lee, & Chang, 1997).

When the external heat transport limitations are negligible, it is a reasonable approximation to neglect the occurrence of temperature gradients in the particles and consider the gas phase and the surface of the adsorbing particles to be isothermal (Ribeiro, Grande, Lopes, Loureiro, & Rodrigues, 2008). In this case, a single temperature equation, which is obtained from the overall local balance in the bed (combining Eqs. (2-35) and (2-41) into one), is sufficient to describe the energy transport in the bed (Hu & Do, 1995; Atanas Serbezov & Sotirchos, 1998). However, some experimental studies have demonstrated the occurrence of temperature differences between the gas phase and the

surface of the adsorbent particles (Haul & Stremming, 1984; Lee & Ruthven, 1979; Ruthven, Lee, & Yucel, 1980). This situation is particularly relevant when an adsorption process occurs at a relatively high rate such that the time needed for the released heat to be transported to the bulk phase may not be sufficient and, consequently, significant temperature gradients are encountered in the interior of the particle (Atanas Serbezov & Sotirchos, 1998).

### 2.3.3.3 Wall energy balance

Finally, the energy balance for the column wall, which includes the wall heat-transfer to the external environment and to the gas phase inside the column, can be expressed as follows (Da Silva et al., 1999):

$$\rho_w C_w \frac{\partial T_w}{\partial t} = h_w a_w (T_g - T_w) + U a_a (T_\infty - T_w) \quad (2-42)$$

where  $C_w$  and  $\rho_w$  represent the heat capacity and the density of the column wall, respectively;  $a_w$  represents the ratio of the internal surface area to the volume of the column wall (Da Silva et al., 1999; Dantas et al., 2009; Huang & Fair, 1988);  $a_a$  denotes the ratio of the external surface area to the volume of the column wall;  $U$  is the external overall heat transfer coefficient from the wall to ambient air; and  $T_\infty$  is the ambient temperature.

The external overall heat transfer coefficient,  $U$ , can be estimated through following correlation (Incropera & Witt, 1996):

$$\frac{1}{U} = \frac{1}{h_w} + \frac{d_{\text{int}}}{k_w} \ln\left(\frac{d_{\text{ext}}}{d_{\text{int}}}\right) + \frac{d_{\text{int}}}{d_{\text{ext}} h_{\text{ext}}} \quad (2-43)$$

where  $k_w$  is the column wall conductivity;  $d_{\text{ext}}$  is the column external diameter; and  $h_{\text{ext}}$  is the external convective heat transfer coefficient that can be estimated using the following correlation (Incropera & Witt, 1996):

$$\frac{h_{ext}L}{k_{ext}} = 0.68 + \frac{0.67Ra^{1/4}}{[1 + (0.492/Pr)^{9/12}]^{4/9}} \quad (2-44)$$

In the above equation,  $k_{ext}$  is the column external air conductivity and  $Ra = g\beta \frac{(T_w - T_\infty)}{\nu\alpha} L^3$  is the Rayleigh number, where  $g$  is the gravity acceleration;  $\beta$  is the thermal expansion coefficient; and  $\nu$  and  $\alpha$  are the air kinematic viscosity and thermal diffusivity at the film temperature  $((T_w + T_\infty)/2)$ , respectively.

If the area of heat transfer from the fluid to the wall is an order of magnitude larger than the area in the axial direction, the contribution of the axial heat conduction along the column wall can be neglected (Ahn, Lee, Seo, Yang, & Baek, 1999; Ahn et al., 2001; Mohamadinejad et al., 2000). In the above wall energy balance equation (Eq. 2-42), the resistance of the metal wall to radial heat transfer has been considered in the overall heat transfer coefficient,  $U$ , which makes this value lower than that of the individual convection heat transfer coefficient between the wall and the surroundings (Grande & Rodrigues, 2005).

In an industrial-scale process in which the column length-to-diameter ratio is not large, the heat loss through a wall and heat accumulation in the wall are considered negligible in comparison to the amount of heat caused by the heat of adsorption, resulting in operation close to adiabatic behavior (Lee et al., 1999). In such a situation, the overall heat transfer coefficient,  $U$ , and therefore the last term in Eq. (2-42) can be dropped (Bastos-Neto, Moeller, Staudt, Bohm, & Glaser, 2011). In the case of an isothermal system, an instantaneous thermal equilibrium is assumed to exist between the gas and solid phases ( $T_g = T_s$ ) or between the gas, solid, and column wall ( $T_g = T_s = T_w$ ), depending on the system's conditions. Under such assumptions, the original three energy balances of the complete model discussed above (Eqs. 2-35, 2-41, and 2-42) are reduced to two equations and one equation, respectively.



### 2.3.4 Momentum balance

As the bulk fluid flows through the void spaces between adsorbent particles, it experiences a pressure drop due to viscous energy losses and a drop in kinetic energy.

The momentum balance considers the terms of pressure drop and velocity changes across the packed bed and relates them by the Ergun equation (Alpay, Kenney, & Scott, 1993; Z. P. Lu, Loureiro, Rodrigues, & LeVan, 1993; Yang, Park, Chang, Ko, & Lee, 1998):

$$\frac{\partial P}{\partial z} = -K_D u - K_V u^2 \quad (2-45)$$

where  $K_D$  and  $K_V$  are parameters corresponding to the viscous and kinetic pressure loss terms, respectively. For low particle Reynolds numbers (e.g.,  $<5$ ), the kinetic contribution to the total pressure loss is negligible, and Eq. (2-45) reduces to Darcy's law (Ding & Alpay, 2000). Semi-empirical relationships for  $K_D$  and  $K_V$  have been derived by Ergun (Macdonald, El-Sayed, Mow, & Dullien, 1979) as follows:

$$K_D = \frac{150\mu(1-\varepsilon_b)^2}{\varepsilon_b^3 d_p^2} \quad (2-46)$$

$$K_V = \frac{1.75(1-\varepsilon_b)\rho_g}{\varepsilon_b^3 d_p} \quad (2-47)$$

where  $P$  is the total pressure,  $\mu$  is the gas mixture viscosity, and  $d_p$  is the particle mean diameter.

The existence of the pressure drop in packed beds affects the system performance by reducing the working capacity. Conventional gas separation processes using packed beds of beads or granules suffer predominantly from high pressure drop and mass transfer resistance when higher throughputs are required, leading to lower productivity and recovery and higher power consumption. In order to overcome these drawbacks, novel adsorbent structures such as monoliths, laminates, and foams structures are considered as alternate candidates for the replacement of conventional adsorbent configurations as they

offer the advantage of allowing increased throughput and reduced pressure drops (Rezaei & Webley, 2010). In recent years, monolithic adsorbents have garnered considerable attention for CO<sub>2</sub> capture from the gas streams (Brandani, Rouse, Brandani, & Ruthven, 2004; Grande & Rodrigues, 2008; Mosca, Hedlund, Ridha, & Webley, 2008; Ribeiro et al., 2008). A detailed review of these alternate structures and their merits was recently conducted by (Rezaei & Webley, 2010).

The pressure drop of the monolithic and laminate structures can be expressed by the following equation using the Hagen–Poiseuille equation (Rezaei & Webley, 2009):

$$\frac{\Delta P}{L} = \frac{32\mu}{d^2 \varepsilon_b} u \quad (2-48)$$

where  $d$  is the channel dimension.

In the case of foam adsorbents, the pressure drop can be estimated using the equation presented by Richardson et al. (Richardson, Peng, & Remue, 2000):

$$\frac{\Delta P}{L} = \frac{\alpha s^2 (1-\varepsilon)^2}{\varepsilon_b^3} \mu u + \frac{\beta s (1-\varepsilon)}{\varepsilon_b^3} \rho_g u^2 \quad (2-49)$$

where the first term represents flow resistance from viscous forces, the second term is the inertial or turbulent contributions, and  $\alpha$ ,  $\beta$ ,  $s$  can be calculated using following expressions:

$$\alpha = 9.73 \times 10^2 d_p^{0.743} (1 - \varepsilon_b)^{-0.0982} \quad (2-50)$$

$$\beta = 3.68 \times 10^2 d_p^{-0.7523} (1 - \varepsilon_b)^{0.07158} \quad (2-51)$$

$$s = \frac{12.979 [1 - 0.971(1 - \varepsilon_b)^{0.5}]}{d_p (1 - \varepsilon_b)^{0.5}} \quad (2-52)$$

Clearly, other momentum balance equations that model the pressure drop in a structured packing could also be applied.

A detailed description of the differential mass and heat balance equations for the different adsorbent structures can be found elsewhere (Grande et al., 2006; Rezaei & Grahn, 2012; Rezaei & Webley, 2009).

## **CHAPTER 3: MATERIALS AND METHODS**

### **3.1 Introduction**

The following sections give information about the materials and the procedures used in developing an efficient adsorbent for CO<sub>2</sub> separation. Details of adsorbent modification, characterization and evaluation of their adsorption performance are also described here. Commercial granular activated carbon (GAC) used in this research was supplied by BRAVO GREEN SDN BHD. All the gases were of purity greater than 99.99% and were supplied by Air Products.

### **3.2 The application of response surface methodology to optimize the amination of activated carbon for the preparation of carbon dioxide adsorbents**

#### **3.2.1 Adsorbent materials**

The commercial palm-shell-based granular activated carbon (referred to as GAC) was used as a starting material for the preparation of CO<sub>2</sub> adsorbent. The precursor was ground and passed through a US mesh size 20-35 (850-500 µm) prior to all further treatments. To eliminate fines, the GAC was then thoroughly washed with distilled-deionized water (DDW), dried at 105 °C for 24 h to remove moisture, and stored in a desiccator under vacuum. The following is a brief outline of the process used to modify these samples.

#### **3.2.2 Ammonia modification**

In this work, two different types of adsorbents were used as starting materials: GACs that were either pre-heat-treated under nitrogen or pre-oxidized with air. These adsorbents are referred to as HTA and OXA, respectively. To produce carbon adsorbents with different amounts and types of N-containing functionalities, the ammonia treatment was performed for different times and at different temperatures for both adsorbents. The ammonia modification of HTA was achieved by placing approximately 1 g of activated carbon in

a tubular quartz reactor under a  $75 \text{ cm}^3\text{min}^{-1}$  flow of nitrogen. The temperature of the reactor was increased at a rate of  $10 \text{ }^\circ\text{C min}^{-1}$  until it reached a final modification temperature (selected temperatures from 200 to 1000  $^\circ\text{C}$ ). The feed gas (nitrogen) was then changed to reactive gas (pure ammonia) at the same flow rate. During this treatment, the samples were maintained at the final temperature for a period of time (between 1 and 3 h) and then cooled down to 100  $^\circ\text{C}$  at the same cooling rate ( $10 \text{ }^\circ\text{C min}^{-1}$ ). Finally, the flow was changed back to  $\text{N}_2$  until room temperature was reached. For the modification of OXA samples, approximately 1 g of sample was placed into a quartz reactor. Air was introduced, and the reactor was heated ( $10 \text{ }^\circ\text{C min}^{-1}$ ) to 400  $^\circ\text{C}$ . This temperature was selected for air oxidation because it was reported to be the optimum temperature at which to add surface oxygen groups (Mangun, Benak, Daley, & Economy, 1999; Polovina, Babić, Kaluderović, & Dekanski, 1997; Saha, Tai, & Streat, 2001). The sample was held at this temperature for 2.5 h and then cooled down to room temperature before the gas was switched to pure ammonia. Both the air and  $\text{NH}_3$  flow rates were set to  $75 \text{ cm}^3 \text{ min}^{-1}$ . Next, the sample was heated in an ammonia atmosphere with a heating rate of  $10 \text{ }^\circ\text{C min}^{-1}$  until the desired temperature was reached. The ammonia treatment was then performed with the same reaction conditions described above. The schematic diagram of the apparatus for the ammonia modification is shown in Figure 3.1.

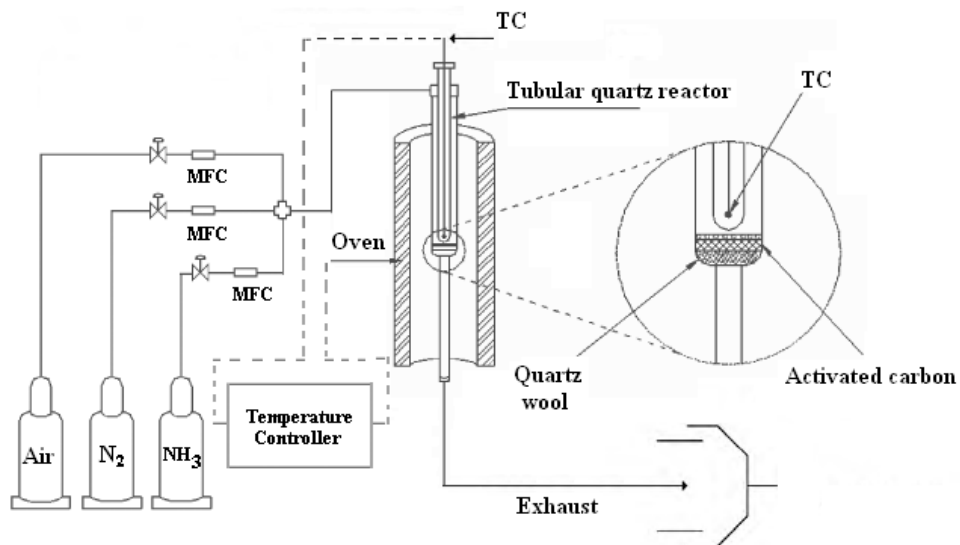


Figure 3.1: Schematic diagram of the experimental setup for the ammonia modification  
MFC, mass flow controller; TC, thermocouple

### 3.2.3 Experimental design and method of analysis

The conventional approach for optimizing multifactor experiments, one-factor-at-a-time method (OFAT), involves varying a single factor while all other factors are kept fixed for a particular set of experiments. This approach is time-consuming and incapable of reaching the true optimum because possible interaction effects between the variables are not taken into consideration (Frigon & Mathews, 1997; Ghafari, Aziz, Isa, & Zinatizadeh, 2009; Kusic, Jovic, Kos, Koprivanac, & Marin, 2010; Montgomery, 2005). The RSM statistical method has been proposed to optimize parameters with a minimal number of experiments and to analyze the interaction between the parameters (Azargohar & Dalai, 2005; Khuri & Cornell, 1996; Myer & Montgomery, 2002). RSM has already proven to be a reliable statistical tool in the investigation of chemical treatment processes (Can, Kaya, & Algur, 2006; Ghafari et al., 2009; Gönen & Aksu, 2008; Hameed, Tan, & Ahmad, 2008; Körbahti & Rauf, 2008a, 2008b; Kusic et al., 2010; Ölmez, 2009; Sahu, Acharya, & Meikap, 2009; Zhanmei Zhang & Zheng, 2009). Accordingly, in this study, Design-Expert 8.0.5 software (trial version) was used to generate experimental designs, statistical analyses, and regression models and to optimize the sorbent modification

conditions. Central composite design with a quadratic model and  $\alpha = 0.5$  was coupled with response surface methodology to statistically design experiments and analyze data. In the present work, the effects of three independent variables, including two numerical variables (i.e., amination temperature between 200 and 1000 °C ( $X_1$ ) and amination times between 1 and 3 h ( $X_2$ )), both at five levels, and one categorical variable (i.e., the use of HTA or OXA as the starting material ( $X_3$ )) were investigated using central composite design. These variables, along with their respective regions of interest, were chosen based on the literature and preliminary studies (Pevida, Plaza, et al., 2008; Plaza et al., 2009; Plaza, Rubiera, et al., 2010; Przepiórski et al., 2004; Shafeeyan et al., 2010). Table 3.1 presents the range and levels of the independent numerical variables in terms of actual and coded values. The numerical variables in actual form ( $X_1, X_2$ ) were converted to their coded form ( $x_1, x_2$ ) using the following equation (Amini, Younesi, & Bahramifar, 2009; Banik, Santhiagu, & Upadhyay, 2007; Soloman, Ahmed Basha, Velan, Balasubramanian, & Marimuthu, 2009):

$$x_i = \frac{(X_i - X_0)}{\Delta X} \quad (3 - 1)$$

where  $x_i$  is the dimensionless coded value of the  $i$ th independent variable, and  $X_i, X_0$ , and  $\Delta X$  correspond to the actual value, actual value at the center point, and the step change of the  $i$ th variable, respectively.

Table 3.1: Independent numerical variables and their levels (actual and coded)

Independent numerical variables	Symbol	Coded variable levels				
		-1	-0.5	0	+0.5	+1
Amination temperature, (° C)	$X_1$	200	400	600	800	1000
Amination time, (h)	$X_2$	1	1.5	2	2.5	3

For each categorical variable, 13 experiments were performed in randomized order (to minimize the effects of the uncontrolled factors), including five replications at the design center to obtain an accurate estimation of the experimental error (Table 3.2). The CO<sub>2</sub> sorption capacity ( $Y_S$ ) and desorption capacity ( $Y_D$ ) of the resulting adsorbents were taken as the two responses of the designed experiments. A quadratic polynomial equation was developed to predict the dependent variables (chosen responses) as a function of independent variables (factors) and their interactions, as given by Eq. (3-2) (Aksu & Gönen, 2006; Can et al., 2006; Yetilmezsoy, Demirel, & Vanderbei, 2009):

$$Y = \beta_0 + \sum_{i=1}^n \beta_i x_i + \sum_{i=1}^n \beta_{ii} x_i^2 + \sum_{i=1}^n \sum_{j=1}^n \beta_{ij} x_i x_j + \varepsilon \quad (3-2)$$

In this equation,  $Y$  is the predicted responses;  $\beta_0$  is the constant;  $x_i, x_j$  are the coded value of the independent variables;  $\beta_i$  is the linear term coefficient;  $\beta_{ii}$  is quadratic term efficient;  $\beta_{ij}$  is the interaction term coefficient,  $\varepsilon$  is the random error, and  $n$  is the number of factors studied.

An analysis of variance (ANOVA) was applied to evaluate the fitness of the model and identify the interactions between the amination variables and the responses. The goodness of fit of the polynomial model was expressed by the coefficients of determination,  $R^2$  and  $R_{adj}^2$  through Eqs. (3-3) and (3-4), respectively (Körbahti & Rauf, 2008b).

$$R^2 = 1 - \frac{SS_{residual}}{SS_{model} + SS_{residual}} \quad (3-3)$$

$$R_{adj}^2 = 1 - \frac{SS_{residual}/DF_{residual}}{(SS_{model} + SS_{residual})/(DF_{model} + DF_{residual})} \quad (3-4)$$

Here,  $SS$  is the sum of squares,  $DF$  is the degrees of freedom.

The statistical importance of the model was checked by determining the model's adequate precision ratio using Eqs. (3-5) and (3-6), and by an  $F$ -test in the program (Körbahti & Rauf, 2009).



$$\text{Adequate Precision} = \frac{\max(Y) - \min(Y)}{\sqrt{\bar{V}(Y)}} \quad (3 - 5)$$

$$\bar{V}(Y) = \frac{1}{n} \sum_{i=1}^n \bar{V}(Y) = \frac{p\sigma^2}{n} \quad (3 - 6)$$

Here,  $Y$  is the predicted response,  $p$  is the number of model parameters,  $\sigma^2$  is the residual mean square (presented in Tables 4-1 and 4-2 for each responses), and  $n$  is the number of experiments.

The insignificant terms were eliminated after the F-test, and the final model was obtained. Three-dimensional response surfaces were presented to visualize the individual and interactive effects of the independent variables. Finally, the independent variable optimum values for maximizing the amount of studied responses were determined using the Design-Expert program 8.0.5 trial version. Additional experiments at optimum conditions were performed to verify the prediction provided by the regression model.

Table 3.2: Experimental design layout and experimental results of the responses

Run	Sample code	Coded variables			Actual variables			Responses	
		$x_1$	$x_2$	$x_3$	$X_1$ (° C)	$X_2$ (h)	$X_3$	$Y_S$ (mg/g)	$Y_D$ (wt.%)
1	OXA-600-2.5	0	0.5	1	600	2.5	OXA	28.58	93.1
2	HTA-400-2	-0.5	0	-1	400	2	HTA	24.99	95.7
3	HTA-600-2	0	0	-1	600	2	HTA	26.16	94.0
4	OXA-600-2	0	0	1	600	2	OXA	28.08	93.3
5	OXA-200-3	-1	1	1	200	3	OXA	21.81	98.1
6	HTA-600-1.5	0	-0.5	-1	600	1.5	HTA	25.6	94.5
7	HTA-1000-1	1	-1	-1	1000	1	HTA	26.05	94.1
8	OXA-600-2	0	0	1	600	2	OXA	27.95	93.4
9	HTA-600-2	0	0	-1	600	2	HTA	26.08	94.0
10	OXA-200-1	-1	-1	1	200	1	OXA	20.17	99.4
11	OXA-600-2	0	0	1	600	2	OXA	27.74	93.6
12	HTA-800-2	0.5	0	-1	800	2	HTA	27.12	92.9
13	HTA-600-2.5	0	0.5	-1	600	2.5	HTA	26.43	93.7
14	OXA-600-2	0	0	1	600	2	OXA	27.88	93.5
15	HTA-1000-3	1	1	-1	1000	3	HTA	26.31	93.5

(continued on next page)

'Table 3.2, continued'

Run	Sample code	Coded variables			Actual variables			Responses	
		$x_1$	$x_2$	$x_3$	$X_1$ (° C)	$X_2$ (h)	$X_3$	$Y_S$ (mg/g)	$Y_D$ (wt.%)
16	OXA-600-2	0	0	1	600	2	OXA	28.19	93.3
17	HTA-600-2	0	0	-1	600	2	HTA	25.84	94.2
18	HTA-200-3	-1	1	-1	200	3	HTA	22.65	97.6
19	OXA-800-2	0.5	0	1	800	2	OXA	30.04	91.9
20	OXA-1000-3	1	1	1	1000	3	OXA	28.73	92.8
21	HTA-600-2	0	0	-1	600	2	HTA	25.76	94.3
22	OXA-1000-1	1	-1	1	1000	1	OXA	28.13	93.2
23	HTA-600-2	0	0	-1	600	2	HTA	25.97	94.1
24	HTA-200-1	-1	-1	-1	200	1	HTA	21.08	98.8
25	OXA-400-2	-0.5	0	1	400	2	OXA	25.97	95.3
26	OXA-600-1.5	0	-0.5	1	600	1.5	OXA	27.26	94.0

### 3.2.4 CO<sub>2</sub> adsorption/desorption measurements

The CO<sub>2</sub> adsorption/desorption performance of the modified adsorbents was evaluated in a TGA/SDTA851 thermogravimetric analyzer (TGA) at atmospheric pressure. An isothermal CO<sub>2</sub> adsorption and desorption of the adsorbents was performed. In a typical adsorption/desorption test, approximately 10 mg of the adsorbent was placed in a small pan and heated to 105 °C at a heating rate of 2 °C min<sup>-1</sup> under a flow of pure N<sub>2</sub> (75 cm<sup>3</sup>min<sup>-1</sup>). The sample was held isothermally (30 min) until its weight became stable. The gas was then switched to pure CO<sub>2</sub> at the same flow rate. The sample was held isothermally at 105 °C under a flow of pure CO<sub>2</sub> for 90 min to achieve complete saturation. This temperature was selected because it is the expected temperature in a power plant flue gas desulfurization unit (Maroto-Valer et al., 2005; Shafeeyan, Daud, Houshmand, & Arami-Niya, 2011; Xu et al., 2002). The weight increase during this stage was taken as the CO<sub>2</sub> capture capacity of the sample at 105 °C. After adsorption, the gas was switched back to N<sub>2</sub> at the same flow rate while the temperature was maintained at 105 °C. This was done to study the desorption capacity of the adsorbents. For all of the samples, a desorption time of 30 min was selected because this is the time necessary to fully desorb CO<sub>2</sub> from untreated carbon. Cyclical adsorption and desorption were used to evaluate the stability of the adsorbent. The CO<sub>2</sub> adsorption capacity (mg-CO<sub>2</sub>/g-adsorbent) and desorption capacity (%) were calculated using the following equations:

$$\text{CO}_2 \text{ adsorption capacity (mg/g)} = \frac{m_1 - m_0}{m_0} \times 1000 \quad (3 - 7)$$

$$\text{CO}_2 \text{ desorption capacity (\%)} = \frac{m_1 - m_2}{m_1 - m_0} \times 100 \quad (3 - 8)$$

where  $m_0$ ,  $m_1$ , and  $m_2$  are the weight of the adsorbent (mg) after initial heat treatment in N<sub>2</sub>, after CO<sub>2</sub> adsorption, and after desorption in N<sub>2</sub>, respectively.

### **3.3 A semi-empirical model to predict adsorption equilibrium of carbon dioxide on ammonia modified activated carbon**

#### **3.3.1 Adsorbent materials**

Earlier, our group optimized the amination conditions of activated carbon adsorbents in an effort to maximize their CO<sub>2</sub> adsorption/desorption capacities (Shafeeyan et al., 2012). The optimal adsorbent (a pre-oxidized sample that was aminated at 425 °C for 2.12 h) exhibited promising adsorption/desorption performance during cyclical operations, making it suitable for practical applications. Therefore, in this work, the optimal adsorbent (referred to as OXA-GAC) was used as a starting material. Further details on the adsorbent preparation and modification can be found elsewhere (Shafeeyan, Daud, Houshmand, & Arami-Niya, 2011; Shafeeyan et al., 2012).

#### **3.3.2 Equilibrium CO<sub>2</sub> adsorption measurements**

CO<sub>2</sub> adsorption isotherms of the modified and untreated activated carbon samples were measured using a Micromeritics ASAP 2020 instrument, which is a static volumetric apparatus. The equilibrium experiments were conducted at temperatures of 30, 45 and 60 °C and at pressures up to 1 atm, a typical operating range in adsorption units for CO<sub>2</sub> capture from power plants. The adsorption temperature was controlled by circulating water from a thermostatic bath (Jeio Tech, model: Lab Companion RW 0525G) with an uncertainty of  $\pm 0.1$  K. Using the volumetric method with P–V–T measurements, we determined the total quantity of gas introduced into the adsorption system and the quantity that remained in the system after reaching adsorption equilibrium. Prior to the CO<sub>2</sub> adsorption measurements, known amounts of samples (e.g., 50-100 mg) were loaded into the sample tube and degassed by reducing the pressure to  $10^{-5}$  mmHg at 473 K for 15 h to dehydrate and desorb any adsorbed gases. CO<sub>2</sub> was then purged into the sample cell,

and the change in adsorption volume as a function of CO<sub>2</sub> partial pressure was recorded. The final adsorption amount at the terminal pressure and temperature was considered to be the adsorption equilibrium amount.

### 3.3.3 Adsorption isotherm equations

For each modified and untreated activated carbon adsorbent, three isotherms were measured at 30, 45, and 60 °C and at pressures up to 1 atm. To apply the adsorption equilibrium data to a specific gas-separation application, an accurate mathematical representation of the adsorption equilibrium is required (Esteves, Lopes, Nunes, & Mota, 2008). The equilibrium adsorption isotherm may provide useful insight into the adsorbate-adsorbent interactions and the surface properties and affinities of the adsorbent (Foo & Hameed, 2010). For this purpose, three different pure-species isotherm models—the Freundlich, Sips, and Toth isotherm equations—were used to correlate experimental equilibrium results. These three isotherm models are frequently used for modeling gas-separation processes.

The Freundlich isotherm can be applied to non-ideal adsorption on heterogeneous surfaces for a multilayer adsorption with a non-uniform distribution of adsorption heat. It is represented as (LeVan et al., 1999):

$$q = K_F P^{1/m_F} \quad (3-9)$$

The Sips isotherm is a combination of the Freundlich and the Langmuir isotherm models for predicting the behavior of heterogeneous adsorption systems. At low surface coverages, it reduces to the Freundlich equation, whereas, at high adsorbate concentrations, it predicts a monolayer adsorption capacity that is typical of the Langmuir isotherm. The Sips equation is given by (LeVan et al., 1999):

$$q = \frac{q_m (K_S P)^{1/m_S}}{1 + (K_S P)^{1/m_S}} \quad (3-10)$$

The Toth isotherm is a Langmuir-based isotherm derived from potential theory and is commonly used to describe heterogeneous adsorption processes. It considers a quasi-Gaussian distribution of site affinities. The Toth isotherm is written as (LeVan et al., 1999):

$$q = \frac{q_m K_T P}{\left(1 + (K_T P)^{m_T}\right)^{1/m_T}} \quad (3-11)$$

In the above mentioned equations,  $q$  represents the adsorbed concentration,  $P$  is the equilibrium pressure,  $q_m$  is the maximum loading capacity,  $K_i$  is the equilibrium constant ( $K_F$ ) or the affinity parameter ( $K_S$  and  $K_T$ ), and  $m_i$  ( $m_F$ ,  $m_S$ , and  $m_T$ ) is the parameter that refers to the system heterogeneity.

The next step is to fit the experimental equilibrium adsorption data to the aforementioned isotherm models and adjust each set of isotherm parameters. Because of the inherent bias associated with transforming non-linear isotherm equations into linear forms, several authors have proposed using a non-linear regression procedure (Ho, Porter, & McKay, 2002; Porter, McKay, & Choy, 1999). Accordingly, in the current study, the parameters of the isotherm equations for each temperature were obtained by non-linear regression analysis using the Marquardt-Levenberg algorithm implemented in SigmaPlot software version 12.0 (Systat Software Inc., USA), with a user-defined equation added to the Regression Wizard. To quantify and compare the goodness of fit of the above isotherm models to the experimental data and adjust each set of isotherm constants, two different error functions, the average relative error (ARE) and nonlinear regression coefficient ( $R^2$ ), were evaluated. The average relative error, which measures the deviation between the

experimental equilibrium data and the fitted model values, was calculated according to the following equation (Foo & Hameed, 2010):

$$ARE(\%) = \frac{100}{n} \sum_{i=1}^n \left| \frac{q_{meas} - q_{cal}}{q_{meas}} \right|_i \quad (3-12)$$

where  $n$  is the number of data points at a given temperature, and subscripts “*meas*” and “*cal*” refer to the measured and calculated values of  $q$ , respectively.

### **3.4 Modeling of carbon dioxide adsorption onto ammonia-modified activated carbon: Kinetic analysis and breakthrough behavior**

#### **3.4.1 Adsorbent materials**

Commercial granular palm shell-based activated carbon (referred to as GAC) was used as the starting material for this study. The GAC was enriched with nitrogen using oxidation followed by amination at 425 °C for 2.12 h (referred to as OXA-GAC). The selected modification condition was optimum to provide the adsorbent with promising adsorption/desorption capacity and stability during cyclical operations (Shafeeyan et al., 2012). Further details on the adsorbent preparation and modification can be found elsewhere (Shafeeyan, Daud, Houshmand, & Arami-Niya, 2011; Shafeeyan et al., 2012).

#### **3.4.2 Kinetic adsorption measurements**

The kinetics of CO<sub>2</sub> adsorption on the GAC and OXA-GAC adsorbents were studied using a TGA/SDTA851 thermogravimetric analyzer at atmospheric pressure. Before each kinetic measurement, the adsorbent sample (approximately 10 mg) was pretreated under a 100 ml min<sup>-1</sup> flow of pure nitrogen at 110 °C for 1 h to guarantee removal of moisture and other dissolved gases. The temperature was decreased to the desired temperature (selected temperatures ranging from 30 to 60 °C) and the nitrogen gas was then changed to pure CO<sub>2</sub> at the same flow rate. The sample was maintained at the final temperature



under a constant flow of CO<sub>2</sub> until the rate of the measured mass change of the sample approached zero, implying that thermodynamic equilibrium was attained. The adsorption capacity of the adsorbent is expressed in mol CO<sub>2</sub>/kg adsorbent and is determined from the weight change of the sample after the introduction of CO<sub>2</sub>.

### **3.4.3 Fixed-bed adsorption experiments**

The experimental breakthrough apparatus shown in Fig. 3.2 consists of a stainless steel column 0.2 m in length and 0.01 m in internal diameter packed with the adsorbent sample. Two fine meshes were placed at the bottom and top of the column to ensure a uniform gas distribution and to retain the adsorbent particles in the bed. The CO<sub>2</sub> and N<sub>2</sub> flow rates were regulated using two digital mass-flow controllers (Aalborg ® GFC17) with an accuracy and repeatability of 1% and 0.1% full scale, respectively. To achieve the desired inlet composition of the feed gas (15% CO<sub>2</sub>/N<sub>2</sub>, v/v), the gas flow rates of CO<sub>2</sub> and N<sub>2</sub> were adjusted by mass flow controllers before entering the column to attain a constant total flow of 50 ml min<sup>-1</sup> (flow rates: CO<sub>2</sub> = 7.5 ml min<sup>-1</sup> and N<sub>2</sub> = 42.5 ml min<sup>-1</sup>) and 100 ml min<sup>-1</sup> (flow rates: CO<sub>2</sub> = 15 ml min<sup>-1</sup> and N<sub>2</sub> = 85 ml min<sup>-1</sup>) of feed gas for the first and second series of experiments, respectively. Continuous monitoring of the CO<sub>2</sub> concentration at the bed exit (after every 20 s) was performed using a CO<sub>2</sub> analyzer (Bacharach Inc., IEQ Chek-Indoor Air Quality Monitor) equipped with a thermal conductivity detector that was connected to a data recording system. The temperature was measured using a K-type thermocouple with an accuracy of ±1 K located inside of the solids bed at a height of 0.05 m above the exit end of the column. The thermocouple was connected to a temperature data logger to monitor the temperature during the experiment. The column was placed inside of a tubular furnace with a programmable temperature controller.

In a typical experiment, a sample of ca. 5.5 g of adsorbent was packed into the column. At the beginning of the experiments, the adsorbent bed was pretreated by purging with a 300 ml min<sup>-1</sup> flow of N<sub>2</sub> at 130 °C and atmospheric pressure for at least 3 h to ensure complete desorption of volatile compounds and pre-adsorbed gases. Subsequently, the bed was cooled to the desired adsorption temperature, and the nitrogen flow rate was reduced to the predefined value according to the experimental conditions (i.e., 42.5 and 85 ml min<sup>-1</sup>). The CO<sub>2</sub> was then introduced at flow rates of 7.5 and 15 ml min<sup>-1</sup>, resulting in a feed gas mixture containing 15 vol % CO<sub>2</sub> in N<sub>2</sub>. The feed gas was fed to the column through a three-way valve in an upward flow pattern at the predefined flow rates. The adsorption breakthrough experiments were performed at the temperatures of 30, 45, and 60 °C while changing the feed gas flow rate from 50 to 100 ml min<sup>-1</sup> under 1 atm total pressure. The column adsorption temperatures and feed gas concentration were selected based on the fact that a typical post-combustion flue gas contains mostly N<sub>2</sub> and CO<sub>2</sub> (approximately 10–15% CO<sub>2</sub>) at a total pressure of 1 bar and over a temperature range of 40-60 °C (Auta & Hameed, 2014; Mason, Sumida, Herm, Krishna, & Long, 2011). The experiment continued until the effluent concentration was equal to the feed concentration, i.e.,  $c_t/c_0 = 1$ . Table 3.3 lists some of the physical properties of the adsorbent and characteristics of the adsorption bed along with the operating conditions used for the fixed-bed experiments. Given that the ammonia modification yielded material with very similar physical properties compared with the parent carbon (Shafeeyan, Wan Daud, Houshmand, & Arami-Niya, 2012), it is reasonable to assume that the difference in the amount of the presented characteristics of the modified and untreated adsorbents is negligible.

Table 3.3: Physical properties of the adsorbent and characteristics of the adsorption bed along with the operating conditions used for the fixed-bed experiments

Parameter	Unit	Values
Particle apparent density ( $\rho_s$ )	kg m <sup>-3</sup>	800
Average particle diameter ( $d_p$ )	m	$0.65 \times 10^{-3}$
Bed height ( $L$ )	m	0.2
Bed diameter ( $d$ )	m	0.01
Bed weight ( $m$ )	kg	$5.5 \times 10^{-3}$
Bed voidage ( $\epsilon_b$ )	-	0.56
Feed flowrate ( $Q$ )	ml min <sup>-1</sup>	50 and 100
Feed composition ( $c_0$ )	vol %	15% CO <sub>2</sub> in N <sub>2</sub>
Total pressure (P)	atm	1
Adsorption temperature ( $T$ )	°C	30, 45, and 60

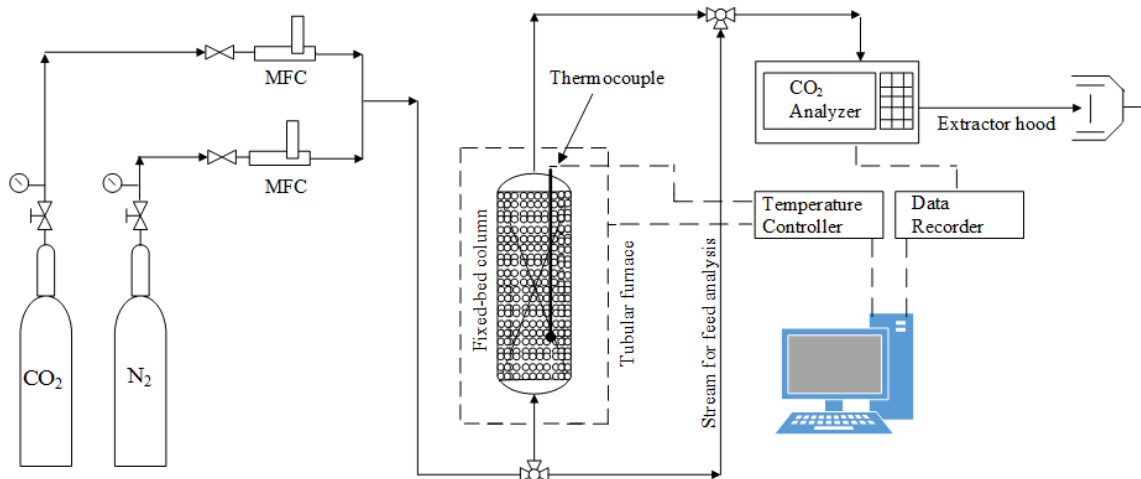


Figure 3.2: Schematic of the experimental system used for the column breakthrough measurements

### 3.4.4 Model description and solution methodology

#### 3.4.4.1 Kinetic models

Among the key characteristics required for the design, simulation, and development of a CO<sub>2</sub> removal system, adsorption kinetic data are important because the residence time required for completion of an adsorption process, the adsorption bed size and, consequently, the unit capital costs are significantly influenced by the kinetic

considerations (Loganathan, Tikmani, Edubilli, Mishra, & Ghoshal, 2014; Monazam, Spenik, & Shadle, 2013). A wide variety of kinetic models with different degrees of complexity have been developed to quantitatively describe the adsorption processes and to identify the adsorption mechanism. Due to the complexities associated with the exact description of kinetic parameters, a common approach involves fitting the experimental results to a number of conventional kinetic models and selecting the model with the best fit (Loganathan et al., 2014; Serna-Guerrero & Sayari, 2010). Accordingly, three of the most common theoretical kinetic models (pseudo-first-order, pseudo-second-order, and Avrami models) that have been previously applied to describe the adsorbent–adsorbate interactions and adsorption rate behavior were employed in this study.

The pseudo-first-order kinetic model assumes reversible interactions with an equilibrium established between the gas and solid surfaces. The model states that the rate of change of a species is directly proportional to the difference between the saturation concentration of that species and its mean concentration within the particle. This model is represented by the following equation (Shokrollahi, Alizadeh, Malekhosseini, & Ranjbar, 2011):

$$\frac{dq_t}{dt} = k_F (q_e - q_t) \quad (3-13)$$

where  $k_F$  ( $s^{-1}$ ) represents the pseudo-first-order kinetic rate constant, and  $q_e$  and  $q_t$  ( $\text{mol kg}^{-1}$ ) denote the equilibrium uptake and the amount adsorbed at time  $t$ (s), respectively.

Integration of Eq. (3-13) with the boundary conditions of  $q_t = 0$  at  $t = 0$  and  $q_t = q_e$  at  $t = t_\infty$  gives the following equation:

$$q_t = q_e (1 - e^{-k_F t}) \quad (3-14)$$

The pseudo-second-order kinetic model is based on the assumption that the chemical interactions control the overall adsorption kinetics. The model assumes a linear relationship between the uptake rate and the square of the number of unoccupied

adsorption sites. This model is expressed according to the following equation (Borah, Sarma, & Mahiuddin, 2011):

$$\frac{dq_t}{dt} = k_S (q_e - q_t)^2 \quad (3-15)$$

where  $k_S$  ( $\text{mol kg}^{-1}\text{s}^{-1}$ ) is the pseudo-second-order kinetic rate constant.

Integration of Eq. (3-15) with the boundary conditions of  $q_t = 0$  at  $t = 0$  and  $q_t = q_e$  at  $t = t_\infty$  leads to the following equation:

$$q_t = \frac{q_e^2 k_S t}{1 + q_e k_S t} \quad (3-16)$$

The Avrami model was originally developed to model phase transitions and crystal growth of materials and has recently been applied to the prediction of the adsorption kinetics of  $\text{CO}_2$  on amine-functionalized adsorbents (Stevens et al., 2013; Wang, Stevens, Drage, & Wood, 2012). The adsorption rate of the Avrami equation is described as follows:

$$\frac{dq_t}{dt} = k_A^n t^{n-1} (q_e - q_t) \quad (3-17)$$

where  $n$  is the Avrami exponent and  $k_A$  ( $\text{s}^{-1}$ ) is the Avrami kinetic constant.

The integrated form of Eq. (3-17) can be written as follows:

$$\frac{q_t}{q_e} = 1 - e^{-(k_A t)^n} \quad (3-18)$$

To establish a complete kinetic model, the equilibrium adsorption capacity,  $q_e$ , must be determined. Accordingly, in this study, the adsorption equilibrium was described using a semi-empirical Toth isotherm. This model was previously developed by our group to consider the simultaneous occurrence of two independent chemical and physical adsorption mechanisms for  $\text{CO}_2$  adsorption. The model offers the advantage of differentiating the contributions of physical and chemical adsorption to the total  $\text{CO}_2$  uptake, enabling its application for the description of the adsorption equilibria of  $\text{CO}_2$  on

untreated and modified adsorbents. The proposed equilibrium model can be written as follows:

$$q_e = \left[ \frac{q_m K_T P}{\left(1 + (K_T P)^{m_T}\right)^{1/m_T}} \right]_{phys} + \left[ \frac{q_m K_T P}{\left(1 + (K_T P)^{m_T}\right)^{1/m_T}} \right]_{chem} \quad (3-19)$$

To express the temperature dependence of the Toth isotherm parameters, the parameters  $K_T$ ,  $q_m$ , and  $m_T$  were described by the following equations (Li & Tezel, 2008):

$$K_T = K_{T_0} \exp \left[ -\frac{\Delta H}{RT_0} \left( \frac{T_0 - T}{T} \right) \right] \quad (3-20)$$

$$q_m = q_{m_0} \exp \left[ \eta \left( \frac{T_0 - T}{T_0} \right) \right] \quad (3-21)$$

$$m_T = m_{T_0} + \alpha \left( \frac{T - T_0}{T} \right) \quad (3-22)$$

where  $T$  is the absolute temperature (K),  $T_0$  is the reference temperature,  $K_{T_0}$  and  $m_{T_0}$  are the affinity and heterogeneity parameters at the reference temperature, respectively,  $\alpha$  and  $\eta$  are constant parameters,  $(-\Delta H)$  is the isosteric heat of adsorption at zero coverage (kJ mol<sup>-1</sup>), and  $R$  is the gas-law constant (J mol<sup>-1</sup> K<sup>-1</sup>).

The optimal values of the isotherm parameters are summarized in Table 3.4, using 30 °C as a reference temperature.

Table 3.4: Optimal values of the proposed Toth equilibrium isotherm parameters

	$q_m$ (mol kg <sup>-1</sup> )	$K_T$ (atm <sup>-1</sup> )	$m_T$ (dimensionless)	$\alpha$ (dimensionless)	$\eta$ (dimensionless)	$(-\Delta H)$ (kJ mol <sup>-1</sup> )
<i>Physical adsorption</i>	5.01	7.1×10 <sup>-1</sup>	0.59	0.96	13.43	23.05
<i>Chemical adsorption</i>	0.54	1.05×10 <sup>5</sup>	0.29	0.25	1.67	68.11

To determine each set of kinetic model parameters, the experimental data were then fitted to the previously mentioned kinetic models. The transformation of non-linear kinetic equations into linear forms is generally associated with the error distribution, depending on the method used to linearize the kinetic equations (Kumar & Sivanesan, 2006). Therefore, to rigorously estimate the kinetic parameter sets from the original form of each kinetic model, a non-linear regression analysis using the Marquardt-Levenberg algorithm implemented in SigmaPlot software version 12.0 (Systat Software Inc., USA) was employed in this study. To quantitatively compare the goodness of fit of the kinetic models with the experimental results, two different error functions, the nonlinear regression coefficient ( $R^2$ ) and the normalized standard deviation ( $\Delta q$ ), were evaluated. The regression coefficient, which determines how well the data points fit the model, was calculated as follows (Stevens et al., 2013):

$$R^2 = 1 - \left( \frac{\sum_{i=1}^n (q_{t(mes)} - q_{t(mod)})^2}{\sum_{i=1}^n (q_{t(mes)} - \overline{q_{t(mes)}})^2} \right) \cdot \left( \frac{n-1}{n-p} \right) \quad (3-23)$$

The normalized standard deviation, which reflects the deviation between the experimental results and the values predicted by the kinetic models, can be represented using the following equation (Vargas, Cazetta, Kunita, Silva, & Almeida, 2011):

$$\Delta q (\%) = 100 \times \sqrt{\frac{\sum [(q_{t(mes)} - q_{t(mod)}) / q_{t(mes)}]^2}{n-1}} \quad (3-24)$$

where  $n$  is the number of experimental adsorption points of the kinetic curves, the subscripts “*mod*” and “*mes*” refer to the model predicted and measured values of the amount adsorbed, respectively,  $\overline{q_{mes}}$  is the average of the experimental data, and  $p$  is the number of parameters of the model.

#### **3.4.4.2 Modeling dynamic column breakthrough experiments**

A basic study on the dynamics behavior of an adsorption column system is required to obtain a deeper understanding of the behavior of new adsorbents during the adsorption/desorption cycles and for process design and optimization purposes (Shafeeyan, Wan Daud, & Shamiri, 2014). To predict the breakthrough behavior of CO<sub>2</sub> adsorption in a fixed-bed packed with GAC and OXA-GAC adsorbents, the following model was proposed based on the mass balance concept combined with an Avrami model for the representation of the adsorption kinetics and a semi-empirical Toth model for the description of the adsorption equilibrium. To develop the fixed-bed model, we assumed the following:

(1) The gas phase behaves as an ideal gas. (2) An axially dispersed plug-flow model is adopted. (3) The radial gradient of concentration is negligible (given that the ratio of the particle to the column radius is less than 10) (Monazam et al., 2013). (4) The fixed bed is assumed to operate isothermally. (5) The feed contains a low concentration of CO<sub>2</sub>; thus, the pressure drop throughout the column is negligible, and the linear velocity remains constant along the bed (Dantas et al., 2009). (6) The effect of nitrogen adsorption is negligible. (7) The effect of external mass transfer (i.e., macropore diffusion and film mass transfer) is considered negligible. (8) The rate of adsorption is described using an Avrami kinetic rate expression, which is explained in Section 4.4.1. (9) The adsorption equilibrium is expressed by a semi-empirical Toth model, as will be described in Section 3.1. Most of these assumptions are commonly accepted for a modeling PSA operation (Ruthven, 1984) and are clearly a compromise between accuracy and effort of parameter determination and model solution (Bonnot, Tondeur, & Luo, 2006). The correlations used for the estimation of the model parameters are summarized in Table 3.5.



Based on these assumptions, the transient gas-phase mass balance for a differential control volume of the adsorption column can be described by the following equation (Ruthven, 1984):

$$-D_L \frac{\partial^2 c}{\partial z^2} + u \frac{\partial c}{\partial z} + \frac{\partial c}{\partial t} + \left( \frac{1 - \varepsilon_b}{\varepsilon_b} \right) \rho_p \frac{\partial q}{\partial t} = 0 \quad (3-25)$$

where  $D_L$  is the effective axial dispersion coefficient,  $z$  represents the length in the axial direction,  $c$  denotes the CO<sub>2</sub> concentration in the gas phase,  $\varepsilon_b$  is the bed voidage,  $u$  is the superficial velocity,  $t$  represents time,  $\rho_p$  is the particle density,  $q$  represents the volume-averaged concentration in the adsorbed phase that may constitute a connection between the solid and gas phase mass balances, and the term  $\partial q / \partial t$  expresses the adsorption rate, which is determined from an Avrami kinetic model, as described in Section 4.4.1.

In Eq. (3-25), the first term is the axial dispersion term, the second term is the convective flow term, and the third and fourth terms represent the accumulation in the fluid and solid phases, respectively. The equation is applied to describe the gas composition distribution in the bed. Ignoring the radial dependence of concentration in the gas and adsorbed phases,  $c$  and  $q$  are expressed as functions of  $z$  and  $t$ , respectively. In addition, applying the ideal gas law, the concentration  $c$  can be correlated with the partial pressure as  $c = yP/RT$ , where  $P$  is the total pressure,  $y$  denotes the CO<sub>2</sub> mole fraction in the feed gas,  $R$  is the universal gas constant, and  $T$  expresses the feed gas temperature.

The following initial and boundary conditions are assumed (Khalighi et al., 2012):

$$I.C.: \quad c(z, t = 0) = 0; \quad q(z, t = 0) = 0 \quad (3-26)$$

$$B.C.: \quad D_L \left. \frac{\partial c}{\partial z} \right|_{z=0} = -u(c_0 - c) \quad (3-27)$$

$$\left. \frac{\partial c}{\partial z} \right|_{z=L} = 0 \quad (3-28)$$

Table 3.5: Correlations used for estimation of the model parameters

Molecular diffusivity ( $D_m$ )	$D_{i,j} = \frac{T^{1.5}}{P\sigma_{i,j}^2\Omega_D} \left( \frac{1}{M_i} + \frac{1}{M_j} \right)^{0.5} \left( 0.0027 - 0.0005 \left( \frac{1}{M_i} + \frac{1}{M_j} \right)^{0.5} \right)$
(Bird et al., 2002; Perry, Green, & Maloney, 1997)	<p>where,</p> $\Omega_D = \frac{1.06036}{T^{*0.15610}} + \frac{0.19300}{\exp(0.47635T^*)} + \frac{1.03587}{\exp(1.52996T^*)} + \frac{1.76474}{\exp(3.89411T^*)};$ $\sigma_{i,j} = (\sigma_i + \sigma_j) / 2; T^* = kT / \varepsilon_{i,j};$ $\varepsilon_{i,j} = (\varepsilon_i \varepsilon_j)^{0.5}; \varepsilon / k = 0.77T_c; \sigma = 2.44(T_c / P_c)^{1/3}$
Axial dispersion coefficient ( $D_L$ )	$\varepsilon_b \frac{D_L}{D_m} = 20 + 0.5ScRe; Sc = \frac{\mu}{\rho_g D_m}; Re = \frac{\rho_g u \varepsilon_b d_p}{\mu}$
(Ruthven, 1984)	<p>where <math>D_m</math> (<math>\text{m}^2 \text{s}^{-1}</math>) is the molecular diffusivity and <math>Sc</math> and <math>Re</math> are the Schmidt and Reynolds numbers, respectively.</p>
Pure gas viscosity ( $\mu$ )	$\mu = 2.6693 \times 10^{-5} \frac{\sqrt{MT}}{\sigma^2 \Omega_\mu}$
(Bird et al., 2002)	<p>where <math>\mu</math> is in <math>\text{g cm}^{-1} \text{s}^{-1}</math> and</p> $\Omega_\mu = \frac{1.16145}{T^{*0.14874}} + \frac{0.52487}{\exp(0.77320T^*)} + \frac{2.16178}{\exp(2.43787T^*)}$
Viscosity of gas mixture ( $\mu_{\text{mix}}$ )	$\mu_{\text{mix}} = \frac{\sum_{i=1}^n y_i \mu_i}{\sum_{i=1}^n y_i \Phi_{i,j}}; \Phi_{i,j} = \frac{1}{\sqrt{8}} \left( 1 + \frac{M_i}{M_j} \right)^{-0.5} \left[ 1 + \left( \frac{\mu_i}{\mu_j} \right)^{0.5} \left( \frac{M_j}{M_i} \right)^{0.25} \right]^2$
(Bird et al., 2002)	
Density of gas mixture ( $\rho_g$ )	$\rho_g = \sum_{i=1}^n y_i M_i \times \frac{P}{P_0} \times \frac{T_0}{T} \times \frac{1}{V_m}$
	<p>where <math>\rho_g</math> (<math>\text{kg m}^{-3}</math>) is the density; <math>T_0</math> and <math>P_0</math> are the temperature and pressure at STP conditions; and <math>V_m</math> is <math>22.4 \text{ L mol}^{-1}</math>.</p>

$\sigma$  ( $\text{\AA}$ ) and  $\varepsilon/k$  (K) are the Lennard- Jones length and energy parameters;  $T$  (K) is the temperature;  $P$  (atm) is the total pressure;  $M_i$  ( $\text{g mol}^{-1}$ ) is the component molecular weight;  $T_c$  (K) and  $P_c$  (atm) are the critical temperature and pressure;  $y_i$  is the component mole fraction.

#### **3.4.4.3 Solution methodology**

The simultaneous solution of a set of coupled nonlinear partial differential equations constructed from mass conservation along with ordinary differential and algebraic equations representing kinetic and equilibrium equations yields the predicted adsorption breakthrough curve. The resultant system of differential and algebraic equations (Eqs. 3-25, 3-17, and 3-19) which are coupled with one another, together with the corresponding initial and boundary conditions (Eqs. 3-26 to 3-28) detailed in section 3.5.2 are solved numerically using a chemical reaction engineering module implemented in COMSOL Multiphysics version 4.4 (Burlington, MA, USA), which uses the finite element method for the numerical solution of differential equations.

## CHAPTER 4: RESULTS AND DISCUSSION

### 4.1 Introduction

Growing environmental concern regarding the adverse effects of anthropogenic carbon dioxide (CO<sub>2</sub>) emissions on global warming and climate change have motivated research into the capture of CO<sub>2</sub> from large emission point sources and the mitigation of the unfettered release of this major greenhouse gas into the atmosphere (Delgado et al., 2006; Samanta, Zhao, Shimizu, Sarkar, & Gupta, 2011). Fossil fuel-fired power plants account for approximately one-third of global CO<sub>2</sub> emissions due to the combustion of fossil fuels such as petroleum, coal, and natural gas (Dantas et al., 2011; Monazam et al., 2013). Therefore, remarkable growth in research activity related to the development, improvement, and optimization of efficient separation techniques for removing CO<sub>2</sub> from power-plant flue gas has occurred over the past three decades (Agarwal et al., 2010a). Currently, amine-based chemical absorption processes are the most mature methods for removing CO<sub>2</sub> from industrial gas streams (Delgado et al., 2006; Serna-Guerrero, Belmabkhout, & Sayari, 2010b). Unfortunately, the absorption process is highly energy-intensive because of the high energy requirements for regeneration. A low CO<sub>2</sub> loading capacity, extensive corrosion of the process equipment and toxicity are additional disadvantages associated with the amine absorption process (Gray et al., 2005; Rinker et al., 2000). A promising alternative procedure for separating CO<sub>2</sub> from flue gases is adsorption using solid physical adsorbents, which could reduce the costs associated with the capture step (Ho et al., 2008; Radosz et al., 2008). Other advantages of these solid physical adsorption processes over traditional aqueous amine processes include greater capacity, higher selectivity, smaller regeneration energy requirements, and easier handling (Garcés et al., 2013; Samanta et al., 2011). Many literature reports have investigated CO<sub>2</sub> capture from flue gas streams using pressure swing adsorption (PSA)

(Ho et al., 2008; Ko et al., 2003; Reynolds et al., 2005; Xiao et al., 2008). However, the success of a PSA process depends on the selection of an adsorbent with sufficient adsorption capacity, selectivity, and durability (Su et al., 2010). Accordingly, in recent years, various adsorbents, including zeolites, carbon molecular sieves, metal organic frameworks, silicas, and activated carbon, have been extensively investigated for their application in removing CO<sub>2</sub> from flue-gas streams (Loganathan et al., 2014; Sevilla & Fuertes, 2011).

Activated carbon has the advantages of low energy requirements for regeneration, an inherent affinity for CO<sub>2</sub>, stability at higher temperatures, low cost, a large surface area and high micropore volume, hydrophobicity, and the possibility of tailoring its surface chemistry and structural properties (Bezerra et al., 2011; Garcés et al., 2013; Sjostrom & Krutka, 2010). Notably, however, most of the conventional adsorbents based on physisorption suffer from the disadvantage of poor adsorption capacities at relatively low CO<sub>2</sub> concentrations and high adsorption temperatures (i.e., the operating conditions characteristic of the separation of CO<sub>2</sub> from a typical flue gas mixture), which may represent a serious drawback for flue gas CO<sub>2</sub> removal using gas adsorption (Bezerra et al., 2011; Samanta et al., 2011). To improve CO<sub>2</sub> adsorption capacity, modifications of adsorbent surface chemical properties by the incorporation of nitrogen surface groups have gained much attention in the past few years (Drage et al., 2007; Knowles et al., 2006; Maroto-Valer et al., 2005; Plaza et al., 2007). CO<sub>2</sub> is a weak Lewis acid that can interact with electron donors; therefore, the presence of basic nitrogen-containing surface groups is thought to provide adsorbents capable of interacting strongly with CO<sub>2</sub> (Plaza et al., 2011; Zhijuan Zhang, Xu, et al., 2010). Przepiórski et al. demonstrated that the CO<sub>2</sub> adsorption capacity on an ammonia-treated CWZ-35 activated carbon was 76 mg g<sup>-1</sup> at 309.15 K and 102.5 kPa (Przepiórski et al., 2004). Hao et al. observed a maximum CO<sub>2</sub> uptake of 3.13 mmol g<sup>-1</sup> at 25 °C and 1 atm for synthesized nitrogen-doped porous carbon

monolith samples (Hao, Li, Qian, & Lu, 2010), and Wahby et al. reported a CO<sub>2</sub> uptake of 4.7 mmol g<sup>-1</sup> by chemically activated petroleum pitch at 25 °C and 1 atm (Wahby et al., 2010). In this study, a commercial granular activated carbon (GAC) adsorbent was modified through an oxidation–amination process in an effort to increase its surface basicity and consequently enhance its CO<sub>2</sub> adsorption capacity. The promising characteristics of the optimal adsorbent (OXA-GAC) in terms of adsorption capacity (exhibiting an increase of 44% in capacity compared with the capacity of the original AC at 1 atm and 105 °C) and multicycle durability make it suitable for practical applications. For the design and simulation of separation processes, the study of the adsorption equilibria is essential in supplying the basic information required for developing and validating models that represent the nature of the adsorption processes (Cavenati et al., 2004; Grande & Rodrigues, 2004). Although reliable experimental equilibrium data for some adsorbates on carbon adsorbents are extensively available in the literature (An, Feng, & Su, 2009; Garcés et al., 2013), as far as we know, very few data have been reported for CO<sub>2</sub> adsorption over ammonia-modified activated carbons under the conditions used here. Furthermore, no studies have been conducted to analyze the CO<sub>2</sub> adsorption isotherms over such adsorbents to fit to a proper isotherm model. Therefore, in the present study, the adsorption equilibria of carbon dioxide over the parent GAC and its ammonia-modified counterpart (OXA-GAC) at various operating conditions were obtained and used to fit to an appropriate semi-empirical isotherm model.

Despite the notable increase in the practical applications of adsorption for separation and purification, due to the inherent complexity associated with such systems, the industrial design and optimization of adsorptive gas-separation processes has largely remained an experimental effort (Bastos-Neto et al., 2011). The main disadvantages of the empirical design of an adsorption column are the high costs and operational effort required (Siahpoosh et al., 2009). Therefore, to develop, evaluate, and optimize an appropriate

adsorption process, several researchers have proposed the application of a mathematical model capable of describing the combined effect of equilibrium and kinetics on a fixed bed with the selected adsorbent (Agarwal et al., 2010a; Dantas et al., 2011; Shivaji Sircar, 2006). Shafeeyan et al. provided a comprehensive review of previous studies on the mathematical modeling of packed columns to capture CO<sub>2</sub> from various flue-gas streams for a variety of adsorption systems (Shafeeyan et al., 2014). A predictive model using independently established equilibrium and kinetic parameters may, in principle, provide a method of estimating the column dynamic capacity without extensive experimentation. Moreover, such models are capable of estimating the concentration profile for a certain constituent in the bulk gas at all locations within the packed column (Shafeeyan et al., 2014). Accordingly, in this study, the experimental kinetics data of CO<sub>2</sub> adsorption at different temperatures were fitted to three different kinetic models (i.e., pseudo-first order, pseudo-second order, and Avrami models), and the corresponding kinetic rate constants were estimated from the model providing the best fit. To the best of our knowledge, no studies have been conducted to develop a kinetic model for CO<sub>2</sub> capture over ammonia-modified activated carbon. Furthermore, using the best fitted kinetic model and an appropriate equilibrium equation, a simple dynamic model was developed. The proposed model was constructed based on the mass balance concept and used to describe the breakthrough behavior of the CO<sub>2</sub> adsorption in a fixed-bed reactor packed with ammonia-modified and untreated adsorbents. Finally, the model predictions were verified by comparing the simulations with the experimental results.

In this chapter the results are presented in three parts. Part 1 investigates the application of response surface methodology in predicting and optimizing the amination conditions of activated carbon adsorbent toward CO<sub>2</sub> adsorption. Part 2 studies the adsorption equilibrium of carbon dioxide onto the GAC and OXA-GAC adsorbents and develops a

semi-empirical equilibrium model able to distinguish the contributions of physical and chemical adsorption to the total CO<sub>2</sub> uptake. Part 3 studies the kinetics of CO<sub>2</sub> adsorption on the GAC and OXA-GAC adsorbents. To predict the breakthrough behavior of the fixed-bed adsorption of CO<sub>2</sub>, the focus of Part 3 is to develop a dynamic model that consists of an Avrami equation to describe the kinetics of adsorption and a semi-empirical Toth equation to represent the gas–solid equilibrium isotherm. In addition, a comprehensive discussions and explanations on experimental results are presented.

## **4.2 The application of response surface methodology to optimize the amination of activated carbon for the preparation of carbon dioxide adsorbents**

### **4.2.1 Evaluation of CO<sub>2</sub> adsorption and desorption capacity**

The experimental points (in coded and actual values) together with the values of both responses are represented in Table 3.2. As can be seen from the table, adsorbents O9 and O5 displayed the highest and lowest CO<sub>2</sub> adsorption capacities of 30.04 and 20.17 mg/g at 105 °C, respectively. On the contrary, sorbent O5 exhibited the highest and sorbent O9 showed the lowest CO<sub>2</sub> desorption capacities of 99.4 %, and 91.9 %, respectively. Inspection of the data presented in Table 3.2 reveals that the sorbent preparation variables have a significant effect on the CO<sub>2</sub> adsorption/desorption capacity. The relationship between the responses and independent variables was analyzed using response surface methodology (RSM). When multiple regression analysis is applied to the design matrix and the obtained response values, a fitted quadratic polynomial equation is generated. This equation can be used to optimize the amination conditions. For both responses, the quadratic model was selected as suggested by the software. The models were attained based on the highest order polynomials where the additional terms were significant and the models were not aliased. The general response models in terms of coded factors



include all numerical and categorical parameters (i.e.,  $x_1, x_2$  and  $x_3$ ). The predictive models in coded terms (i.e.,  $Y_S$  and  $Y_D$ ) are presented in Tables 4.1 and 4.2, respectively. On the contrary, the final equations in actual form are defined for each type of categorical factor separately. The final empirical equation obtained for CO<sub>2</sub> sorption capacity ( $Y_S$ ) of the adsorbents prepared from HTA and OXA (symbolized by  $Y_{S-1}$  and  $Y_{S+1}$ , respectively) are given in Eqs. (4-1) and (4-2) respectively. For CO<sub>2</sub> desorption capacity ( $Y_D$ ) of the adsorbents prepared from HTA and OXA (symbolized by  $Y_{D-1}$  and  $Y_{D+1}$ , respectively), the final equations are given in Eqs. (4-3) and (4-4), respectively.

$$Y_{S-1} = +12.48480 + 0.016138X_1 + 6.89030X_2 - 7.7356 \times 10^{-6}X_1^2 - 1.48770X_2^2 - 7.34375 \times 10^{-4}X_1X_2 \quad (4-1)$$

$$Y_{S+1} = +11.36317 + 0.020149X_1 + 7.03586X_2 - 7.7356 \times 10^{-6}X_1^2 - 1.4877X_2^2 - 7.34375 \times 10^{-4}X_1X_2 \quad (4-2)$$

$$Y_{D-1} = +105.39959 - 0.016811X_1 - 4.21352X_2 + 8.50528 \times 10^{-6}X_1^2 + 0.86084X_2^2 + 4.6875 \times 10^{-4}X_1X_2 \quad (4-3)$$

$$Y_{D+1} = +105.87736 - 0.018477X_1 - 4.20241X_2 + 8.50528 \times 10^{-6}X_1^2 + 0.86084X_2^2 + 4.6875 \times 10^{-4}X_1X_2 \quad (4-4)$$

Table 4.1: Analysis of variance (ANOVA) for the CO<sub>2</sub> adsorption capacity

Source	Sum of squares	Degree of freedom	Mean square	F-value	p-value (Prob>F)	
Model	141.51	8	17.69	85.09	<0.0001,	Significant
$X_1$	78.68	1	78.68	378.46	<0.0001	
$X_2$	2.94	1	2.94	14.15	0.0016	
$X_3$	16.15	1	16.15	77.67	<0.0001	
$X_1^2$	0.75	1	0.75	3.59	0.0751	
$X_2^2$	1.08	1	1.08	5.19	0.0359	
$X_1X_2$	0.69	1	0.69	3.32	0.0861	
$X_1X_3$	5.79	1	5.79	27.86	<0.0001	
$X_2X_3$	0.048	1	0.048	0.23	0.6381	
Residual	3.53	17	0.21	-	-	

Final equation in terms of coded factors after excluding the insignificant terms:

$$Y_S = +27.12 + 2.96x_1 + 0.57x_2 + 0.79x_3 - 1.24x_1^2 - 1.49x_2^2 - 0.29x_1x_2 + 0.8x_1x_3 + 0.073x_2x_3$$

$R^2 = 0.9756$ ; Adjusted- $R^2 = 0.9642$ ; Predicted-  $R^2 = 0.8229$ ; Adequate precision= 33.522

Checking the adequacy of the model is one of the most important parts of the data analysis procedure, as the model functions would give poor or misleading results if the fit were inadequate (Körbahti, 2007; Körbahti & Rauf, 2008a; Myer & Montgomery, 2002; Yetilmezsoy et al., 2009). An analysis of variance (ANOVA) was carried out for each response to assess the significance and fitness of the model. The results are presented in Tables 4.1 and 4.2.

Table 4.2: Analysis of variance (ANOVA) for the CO<sub>2</sub> desorption capacity

Source	Sum of squares	Degree of freedom	Mean square	F-value	p-value (Prob>F)	
Model	90.61	8	11.33	171.31	<0.0001,	Significant
$X_1$	60.84	1	60.84	920.26	<0.0001	
$X_2$	2.1	1	2.10	31.80	<0.0001	
$X_3$	1.63	1	1.63	24.58	0.0001	
$X_1^2$	0.9	1	0.90	13.66	0.0018	
$X_2^2$	0.36	1	0.36	5.47	0.0318	
$X_1X_2$	0.28	1	0.28	4.25	0.0548	
$X_1X_3$	1.00	1	1.00	15.13	0.0012	
$X_2X_3$	0.0002	1	0.0002	0.0042	0.9491	
Residual	1.12	17	0.066	-	-	

Final equation in terms of coded factors after excluding the insignificant terms:  
 $Y_s = +93.7 - 2.6x_1 - 0.48x_2 - 0.25x_3 + 1.36x_1^2 + 0.86x_2^2 + 0.19x_1x_2 - 0.33x_1x_3 + 5.556 \times 10^{-3}x_2x_3$   
 $R^2 = 0.9877$ ; Adjusted- $R^2 = 0.9820$ ; Predicted-  $R^2 = 0.9342$ ; Adequate precision= 45.921

ANOVA is a statistical technique that subdivides the total variation in a set of data into component parts associated with specific sources of variation; this allows one to test hypotheses based on the parameters of the model (Gönen & Aksu, 2008). Table 4.3 and 4.4 illustrate the reduced quadratic models in terms of coded factors and also show other statistical parameters for both of the studied responses. Based on the ANOVA results presented in these tables, it can be concluded that the models were significant for both responses with p-values less than 0.0001(model and term p-value <0.05 indicates the model and the term are significant for 95% confidence intervals) to predict the response values (Azargohar & Dalai, 2005). In this case, amination temperature ( $X_1$ ), amination time ( $X_2$ ), type of starting material ( $X_3$ ),  $X_1X_3$ , and  $X_2^2$  were significant model terms for both the CO<sub>2</sub> adsorption and desorption capacities with p-values less than 0.05. In

addition, the interaction between the  $X_2$  and  $X_3$  variables ( $X_2X_3$ ) was insignificant to the responses (term p-value  $>0.100$  indicates the model terms are not significant) which could be manually removed from the model to improve the regression model and optimization results.

The fit of model to the empirical data was tested by calculating the regression coefficient  $R^2$  and  $R_{adj}^2$ . The  $R_{adj}^2$  values of 0.9642 and 0.9820 were obtained for the  $CO_2$  adsorption ( $Y_S$ ) and desorption ( $Y_D$ ) capacity, respectively. This indicated that 96.42 and 98.20% of the total variation in the  $CO_2$  adsorption and desorption capacity, respectively, could be explained by the quadratic model. The high  $R^2$  value (i.e. close to unity) and reasonable agreement between the predicted and adjusted  $R^2$  observed for both responses implies that the developed model can satisfactorily account for the experimental data (Azargohar & Dalai, 2005; Can et al., 2006; Garg, Kaur, Garg, & Sud, 2008; Yetilmezsoy et al., 2009). Adequate precision measures the signal-to-noise ratio and compares the range of the predicted values at the design points to the average prediction error. The adequate precision ratios of 33.5 and 45.9, derived for the  $CO_2$  adsorption and desorption capacity, respectively, are much greater than 4 and indicate adequate model discrimination (Ölmez, 2009). It is worth noting that despite the lack-of-fit was significant, due to the reasonable agreement between the predicted and adjusted  $R^2$ , the model suggested here can be used to navigate into design space to find an optimum.

It is known that the  $CO_2$  capture capacity of activated carbons is a combination of both physical and chemical adsorption (is governed by porous structure and is influenced by the surface chemistry) (Arenillas, Drage, Smith, & Snape, 2005; Drage et al., 2007). Our previous study showed that ammonia modification did not significantly alter the pore structure of the studied adsorbents (less than 15%) (Shafeeyan et al., 2011). Therefore, the behavior of these materials in carbon dioxide adsorption may be primarily attributed

to the change in their chemical surface properties. The best way of expressing the effect of amination parameters on the CO<sub>2</sub> adsorption/desorption within the experimental range was to generate response surface plots of the equation. The linear, quadratic and cross terms in the second-order polynomial model were used to generate a three-dimensional (3D) response surface graph and a two-dimensional contour plot. Based on the ANOVA results presented in Tables 4.3 and 4.4, amination time ( $X_2$ ), type of starting material ( $X_3$ ), and  $X_2^2$  were found to have significant effects, but amination temperature ( $X_1$ ) has the largest effect on both the CO<sub>2</sub> adsorption and desorption capacities (due to the highest  $F$ -values). Furthermore, among the interaction terms,  $X_1X_3$  was found to significantly affect the studied responses whereas the effect of interaction between  $X_2$  and  $X_3$  ( $X_2X_3$ ) was not statistically significant.

#### **4.2.1.1 Effect of amination variables on the CO<sub>2</sub> adsorption capacity**

Three-dimensional (3D) response surface plots of the predictive quadratic model for the CO<sub>2</sub> adsorption capacity of pre-heat treated and pre-oxidized carbons are presented in Fig. 4.1 (a) and (b), respectively. The response surfaces were generated based on Eqs. (4-1) and (4-2). For both type of adsorbents, CO<sub>2</sub> capture capacity increases as the temperature and time of the ammonia treatment increases. In addition, the positive sign in front of the ( $X_1$ ) and ( $X_2$ ) terms in Eqs. (4-1) and (4-2) also implies a favorable or synergistic effect of these terms on capture capacity. It has been reported that the CO<sub>2</sub> adsorption performance of modified adsorbents is strongly influenced by the types of nitrogen functionalities introduced on the carbon surface (Drage et al., 2007; Maroto-Valer et al., 2005; Pevida, Plaza, et al., 2008; Plaza, Rubiera, et al., 2010; Shafeeyan et al., 2011). However, the nature of the incorporated nitrogen functionalities differed with the temperature of ammonia treatment (Mangun, Benak, Economy, & Foster, 2001). Therefore, the synergistic effect of  $X_1$  and  $X_2$  factors on the  $Y_s$  response may be related

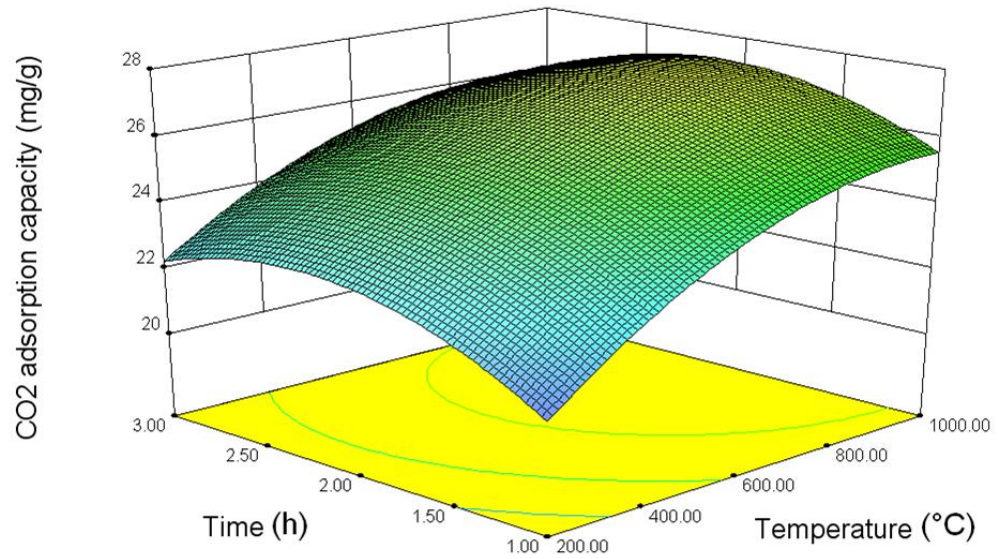
to the formation of more N-containing functionalities particularly in the form of pyrrole and pyridinic-like functionalities which are appeared during high temperature ( $>600\text{ }^{\circ}\text{C}$ ) amination (suitable surface chemistry) (Jansen & van Bekkum, 1994; Maroto-Valer et al., 2005; Pevida, Plaza, et al., 2008; M. G. Plaza et al., 2009; Plaza, Rubiera, et al., 2010). In addition, a partial gasification of the adsorbents with free radicals that were generated during the decomposition of ammonia would lead to pore enlargement, which may contribute to the enhancement of  $\text{CO}_2$  uptake (favorable textural properties) (Boehm, Mair, Stoehr, De Rincón, & Tereczki, 1984; Bota & Abotsi, 1994; Pevida, Plaza, et al., 2008; Plaza, Pevida, et al., 2010). This is in accordance with our previous findings, in which the surface chemistry and porous texture of the modified sorbent became more favorable as the amination temperature increased (Shafeeyan et al., 2011).

As can be seen in Table 3.2 and Fig. 4.1, in comparison with the pre heat-treated aminated samples, the pre-oxidized carbon displayed an enhanced ability to adsorb  $\text{CO}_2$ . The greatest experimental  $\text{CO}_2$  adsorption capacity (Table 3.2),  $30.04\text{ mg/g}$ , was obtained for the pre-oxidized sample that had been modified with ammonia at  $800\text{ }^{\circ}\text{C}$  for 2 h (O9). The increased  $\text{CO}_2$  capture capacity observed for pre-oxidized adsorbents indicates that the presence of oxygen functionalities on the carbon surface prior to ammonia treatment plays an important role in improving the  $\text{CO}_2$  capture performance of the modified samples. When the oxidized carbon is treated with ammonia at elevated temperatures, free radicals such as  $\text{NH}_2$ ,  $\text{NH}$ , and atomic hydrogen, which are created during ammonia decomposition, may attack the surface oxides and active sites present on the carbon surface and form N-containing functional groups (Bota & Abotsi, 1994; Jansen & van Bekkum, 1995; Stöhr, Boehm, & Schlögl, 1991; Vinke, van der Eijk, Verbree, Voskamp, & van Bekkum, 1994). As a consequence of the improved surface chemistry, stronger interactions between the acidic gaseous  $\text{CO}_2$  and the basic nitrogen groups would take place and lead to a higher  $\text{CO}_2$  capture. Dastgheib et al. (Dastgheib, Karanfil, & Cheng,

2004) modified granular activated carbons (GACs) with dry ammonia and demonstrated that the presence of a threshold number of oxygen-containing acidic functionalities on the carbon surface is a prerequisite for effective ammonia treatment. Mangun et al. (2001) reported that the reactivity of ammonia gas with carbon surfaces and the consequent formation of nitrogen surface groups increase with the oxygen content of the carbon precursor. The authors suggested that using a post-oxidation ammonia treatment may enlarge the carbon pores while increasing the surface basicity (number of N-containing functionalities). These changes in the carbon pore structure and surface chemistry are desirable because they enhance CO<sub>2</sub> uptake.

In the case of the amination temperature factor ( $X_1$ ), the trend of enhanced CO<sub>2</sub> uptake is limited to mid-range temperatures (near 800 °C). As can be observed from Fig. 4.1, when the amination temperature goes beyond a certain limit (over 800 °C), there is a decrease in the amount of CO<sub>2</sub> uptake for both type of adsorbent. The observed decrease in CO<sub>2</sub> uptake may be, in part, a consequence of the thermal decomposition of nitrogen surface groups during the high temperature treatment, which would decrease chemisorption (Drage et al., 2007). However, decreased CO<sub>2</sub> uptake can also be associated with the collapse of adjacent pore walls during the pre-heating stage, which leads to diminished textural properties (i.e., a decrease in physisorption contributions) (Maroto-Valer et al., 2005). Furthermore, lowered CO<sub>2</sub> capture capacities of activated carbons treated with ammonia at higher temperatures have been reported for commercial activated carbons. This is likely a result of micropores being closed and blocked by N-containing groups (Przepiórski et al., 2004). The clear maximum values observed in the response plots (Fig. 4.1) imply that the optimum conditions for maximum capture capacity are highly dependent on the amination time and temperature in the design space.

a)



b)

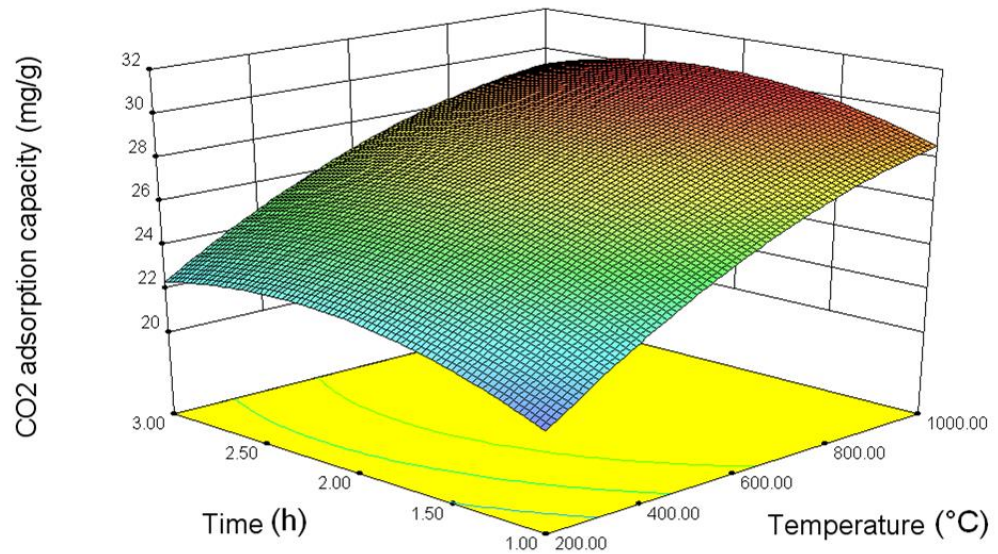


Figure 4.1: Response surface plot of CO<sub>2</sub> adsorption capacity for (a) pre-heat treated, and (b) pre-oxidized adsorbent.

#### 4.2.1.2 Effect of amination variables on the CO<sub>2</sub> desorption capacity

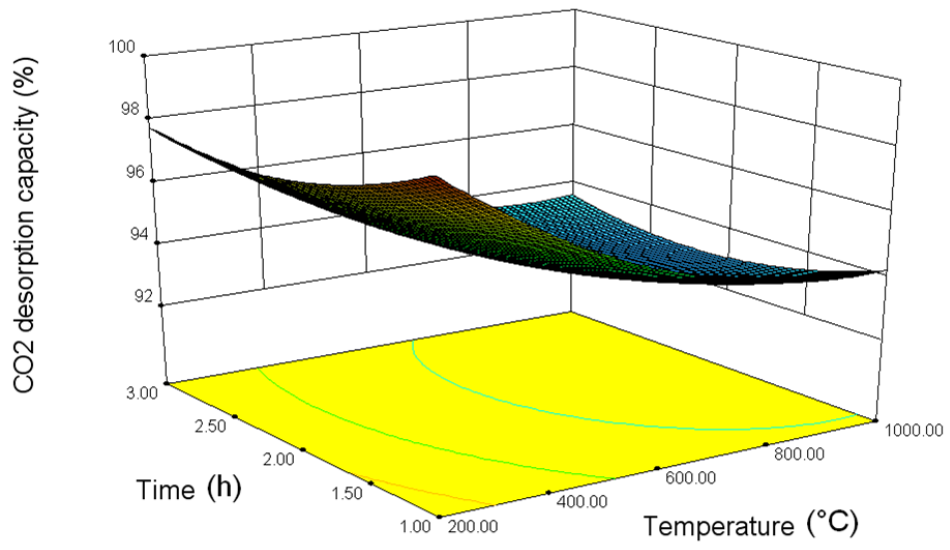
All of the studied samples were regenerated by changing the reactive gas, CO<sub>2</sub>, to a non-reactive gas, N<sub>2</sub>, at 105 °C. Fig. 4.2 a and b represents the 3D response surfaces that were constructed to show the variables' effectiveness on the CO<sub>2</sub> desorption capacity of the modified adsorbents. The response surfaces were generated based on Eqs. (4-3) and (4-

4). A decrease in desorption capacity with an increase in amination temperature can be observed for both types of adsorbents. Furthermore, the negative sign in front of the ( $X_1$ ) and ( $X_2$ ) terms in Eqs. (4-3) and (4-4) also indicates their unfavorable or antagonistic effect on the desorption performance. One possible reason for this observation is that for high temperature adsorption (e.g., over 100 °C), CO<sub>2</sub> uptake is mainly controlled by chemical adsorption (Plaza, Rubiera, et al., 2010; Shafeeyan et al., 2011). In samples with favorable surface chemistries, the stronger interactions between acidic, gaseous CO<sub>2</sub> and the incorporated basic N-functionalities lead to the formation of stronger chemical bonds that hinder regeneration. Accordingly, the sample with the highest CO<sub>2</sub> adsorption capacity (O9), demonstrated the lowest desorption capacity (91.9%). In contrast, as can be seen in Table 3-2 and Fig. 4.2, the sample with the lowest capture capacity (O5) had the highest desorption capacity (99.4%), which may be the result of either weak chemical interactions between the CO<sub>2</sub> and N-functionalities or its poor textural properties compared to the other adsorbents. The aforementioned conclusion was based on the chemical and textural characterization results reported from our group (Shafeeyan et al., 2011).

It should be noted that higher temperature of amination (over 800 °C) did not result in additional decreases in the regeneration potential of either type of adsorbent. The results presented in Table 3.2 demonstrates that the samples treated with ammonia at temperatures above 800 °C showed a slight increase in the CO<sub>2</sub> desorption capacity. As has been previously discussed, this may be attributed to either the elimination of basic N functionalities suitable for CO<sub>2</sub> adsorption or poorly developed textural properties that appear during high temperature treatments. Consequently, the adsorbed gas on the surface of the activated carbon becomes unstable, which results in more desorption of adsorbed CO<sub>2</sub> molecules.



a)



b)

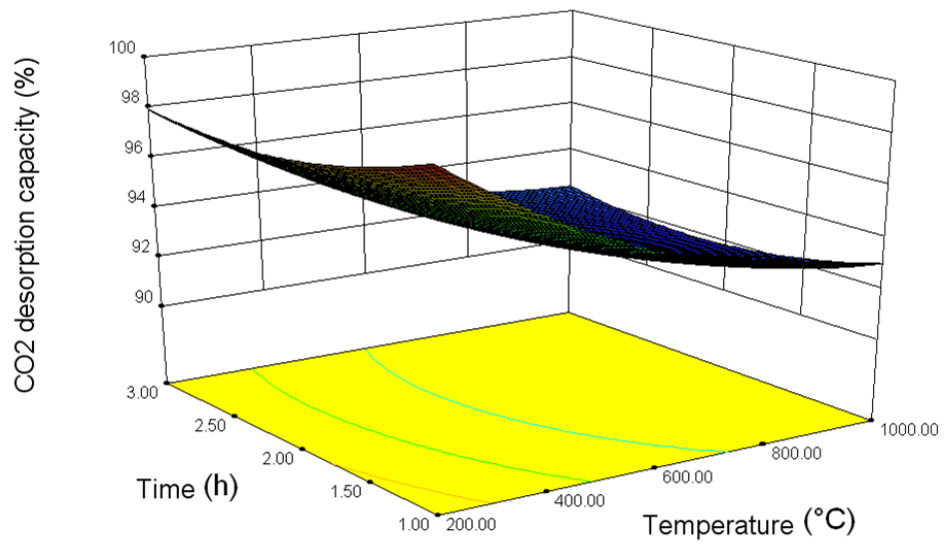


Figure 4.2: Response surface plot of CO<sub>2</sub> desorption capacity for (a) pre-heat treated, and (b) pre-oxidized adsorbent.

#### 4.2.2 Investigation of the optimum amination conditions

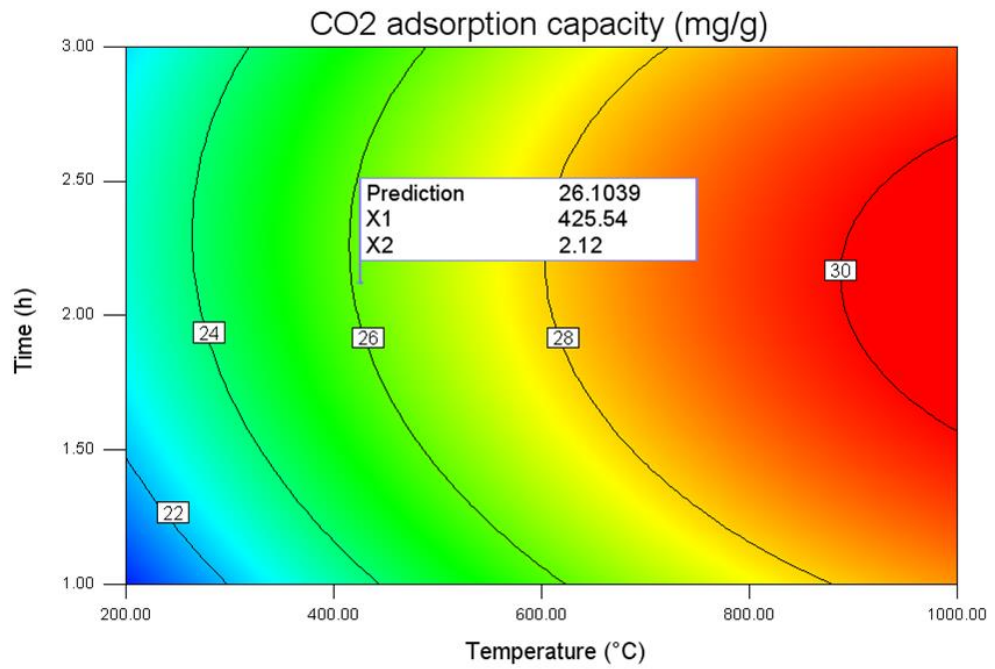
In the production of efficient CO<sub>2</sub> adsorbents, relatively high capture capacities are necessary for production to be economically feasible. For practical applications, the modified adsorbents should not only possess high adsorption capacities but also show high desorption capacities for economical viability. However, the CO<sub>2</sub> adsorption ( $Y_S$ ) and desorption ( $Y_D$ ) capacities are compensatory (i.e., when  $Y_S$  increases,  $Y_D$  decreases and vice versa). Thus, it is difficult to find a balance between high adsorption and desorption capacities. The determination of the optimum amination conditions for maximizing the amounts of  $Y_S$  and  $Y_D$  within the studied experimental range was carried out using the point prediction function in the Design-Expert software. In addition, the optimization was also used to determine whether the use of HTA or OXA is more favorable to the production of adsorbents with higher CO<sub>2</sub> adsorption/desorption capacities.

Multiple response optimizations could be generated from the contour plots of the second order model for each response in the experimental ranges of each factor (Fig. 4.3a and b). Furthermore, the optimum conditions could be graphically visualized by superimposing the contours of the response surfaces in an overlay plot (Fig. 4.4). The shaded area in the overlay plot of the responses (Fig. 4.4) corresponds to the optimum variable ranges for the production of an adsorbent with a high CO<sub>2</sub> adsorption ( $\geq 26$  mg/g) and desorption capacity ( $\geq 94\%$ ). To identify the optimum conditions, the targeted criteria were set as maximum values for the responses (CO<sub>2</sub> adsorption and desorption capacity), whereas the values of the numerical variables (amination temperature and amination time) were set in the ranges studied for both HTA and OXA adsorbents. The amination conditions that showed the highest desirability were experimentally verified (desirability is an objective function that ranges from zero outside of the limits to one at the goal; the program seeks to maximize this function (Amini et al., 2008)). The optimal point indicated

by numerical optimization corresponds to a pre-oxidized adsorbent that has been aminated at 425 °C for 2.1 h, as indicated in Fig. 4.3. Fig. 4.3a and b shows the contour plots for predicting the maximum CO<sub>2</sub> adsorption and desorption capacities, respectively, under the determined optimum conditions for pre-oxidized adsorbents. It was predicted that maximum CO<sub>2</sub> adsorption and desorption capacities of 26.1 mg/g and 94.9%, respectively, could be obtained for the activated carbon adsorbent. From the aforementioned optimization results, the application of post-oxidation ammonia treatment (preparation method) at 425 °C for 2.12 h (experimental conditions) was found to produce a high adsorption/ desorption capacity activated carbon for carbon dioxide adsorption.

To evaluate the accuracy of the second order equations, three additional CO<sub>2</sub> adsorption/desorption experiments were carried out using adsorbents that were prepared under the RSM-predicted optimum conditions. The average values of the repeated experiments and predicted results are presented in Table 4.3. As can be seen in this table, the deviation errors between the experimental and predicted (by regression model) values of CO<sub>2</sub> adsorption and desorption capacity were 1.41% and 0.61%, respectively. The close agreement between the experimental values and those predicted from the CCD (regression) model suggests that the developed model can correlate the amination variables to CO<sub>2</sub> adsorption and desorption capacities with a high degree of accuracy. It is expected that the optimization results presented in this paper may provide background information for detailed process improvement research.

a)



b)

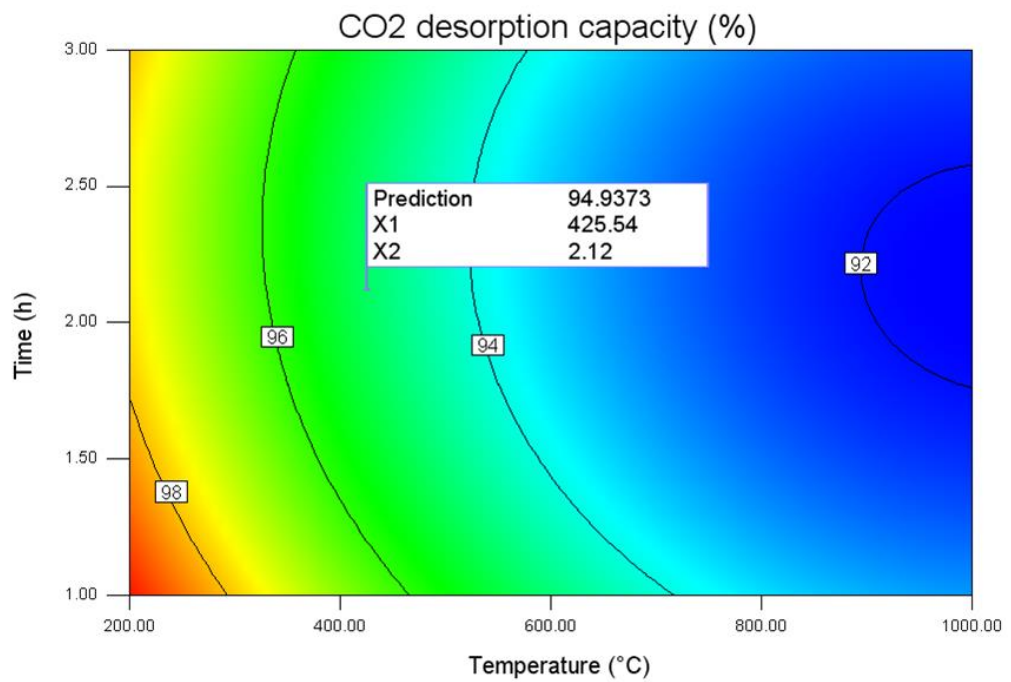


Figure 4.3: Contour plot of (a) CO<sub>2</sub> adsorption capacity and (b) CO<sub>2</sub> desorption capacity as a function of amination temperature and time for pre-oxidized adsorbents.

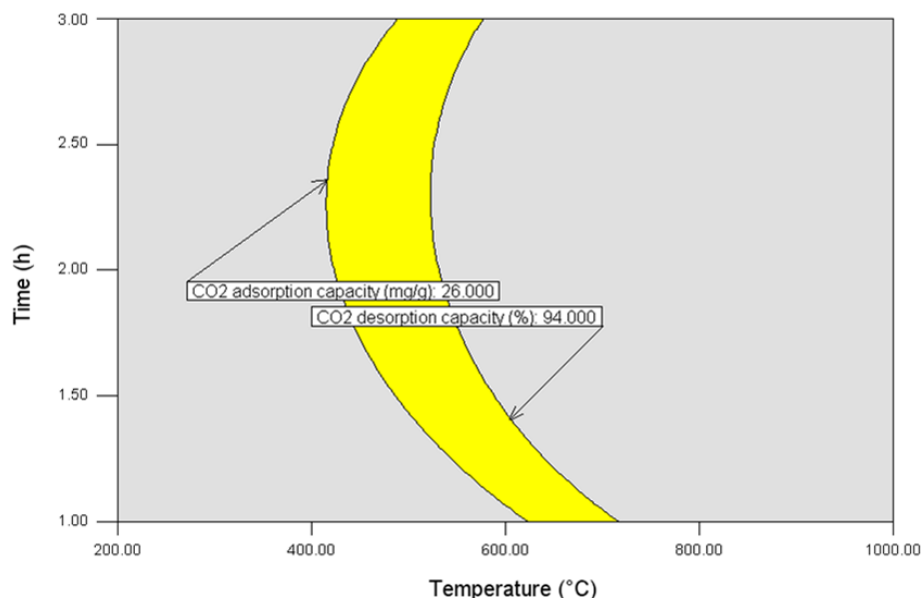


Figure 4.4: Overlay plot of the optimal region for pre-oxidized adsorbents.

Table 4.3: Predicted and experimental values of the studied responses obtained at optimum conditions.

Response	Experimental results <sup>a</sup>	Predicted value	Error (%)
CO <sub>2</sub> adsorption capacity (mg/g)	26.47	26.10	1.41
CO <sub>2</sub> desorption capacity (%)	95.4	94.93	0.61

<sup>a</sup> Represents the average values of the repeated experiments.

#### 4.2.3 Reusability of the sorbent prepared under optimum conditions

Though having high CO<sub>2</sub> adsorption and desorption capacities is essential for practical application of the adsorbents, stable adsorption/ desorption performance is also a crucial issue. To evaluate the reusability of the optimal activated carbon adsorbent (OXA sorbent that was aminated at 425 °C for 2.12 h) in cyclic processes, four consecutive adsorption/regeneration experiments at 105 °C were carried out, and the results are presented in Fig. 4.5. The desorption capacities presented here were calculated based on the time necessary to fully desorb CO<sub>2</sub> from untreated carbon. As can be seen in the figure, the adsorption performance and the desorption capacity show slight changes after first

regeneration (less than 4%). However, the alterations in these capacities after next regenerations are almost negligible (i.e., remain more or less unchanged). The regeneration potential of this adsorbent and its stability under the investigated conditions would be promising characteristics for further study toward practical applications.

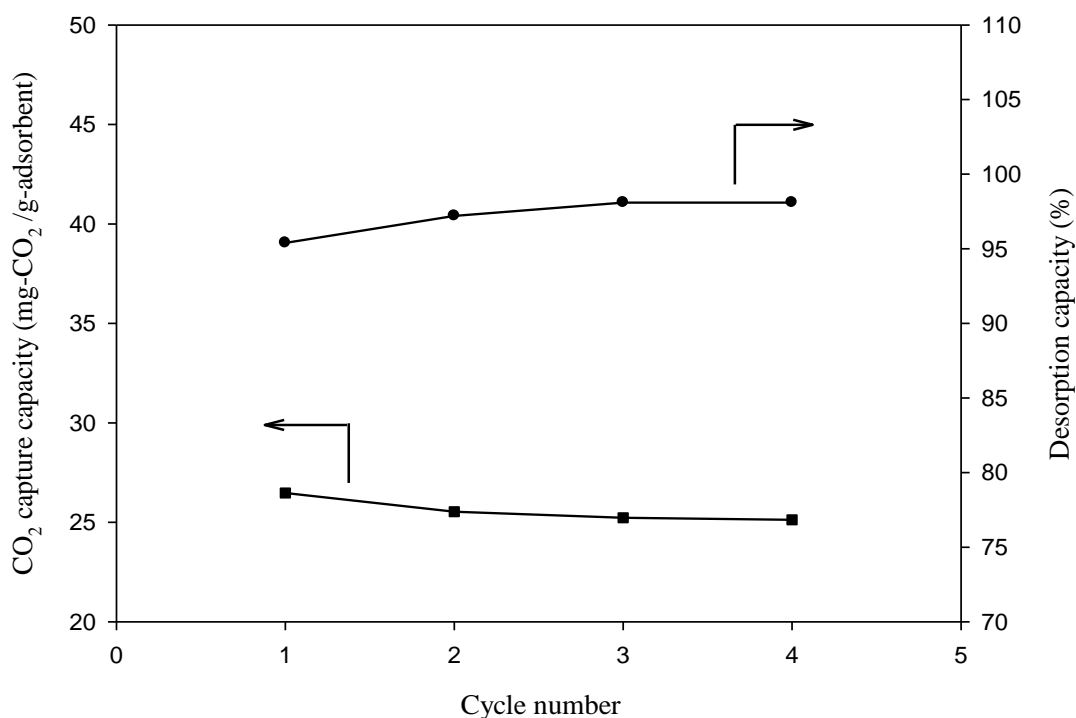


Figure 4.5: Cyclical adsorption and desorption of CO<sub>2</sub> at 105 °C by the optimal activated carbon adsorbent.

### 4.3 A semi-empirical model to predict adsorption equilibrium of carbon dioxide on ammonia modified activated carbon

#### 4.3.1 Adsorption equilibrium study

The volumetric method of measuring adsorption involves measuring the pressure change in a known volume of gas introduced to an adsorbent sample. As the gas is adsorbed and allowed to reach equilibrium, the measured decrease in the closed-system pressure yields the amount of gas adsorbed under the given conditions (Li & Tezel, 2008). Adsorption

isotherms obtained at temperatures of 30, 45 and 60 °C and at pressures up to 1 atm for the ammonia-modified and untreated carbon are graphically represented in Figs. 4.6a and b, respectively. The ranges for temperature and pressure were chosen on the basis that a typical post-combustion flue gas contains approximately 10–15% CO<sub>2</sub> at a total pressure of 1 bar and a temperature range of 40-60 °C (Mason et al., 2011). As evident in these figures, for both modified and unmodified adsorbent, the concentration of adsorbed CO<sub>2</sub> increases with increasing pressure. At a given temperature, the shape of the function  $M = f(P)$  (where  $M$  is the uptake at equilibrium pressure  $P$ ) corresponded to a type I isotherm (i.e., a monotonically concave isotherm) according to the International Union of Pure and Applied Chemistry (IUPAC) classification scheme. A type I isotherm is typically characteristic of a microporous adsorbent.

The adsorption of CO<sub>2</sub> is well established to possibly result from physical and/or chemical factors both influencing the adsorbent performance (Drage et al., 2007; Maroto-Valer et al., 2005; Pevida, Drage, & Snape, 2008). For the unmodified adsorbent, CO<sub>2</sub> capture with a pure physisorption process was proposed as a controlling mechanism. As evident in Figs. 4.6a and b, in comparison with the unmodified adsorbent, OXA-GAC exhibited a higher CO<sub>2</sub> uptake, particularly at low partial pressures, as reflected by the steep initial slope of the isotherms. This enhanced uptake stems from adsorption by the nitrogen functional groups in addition to CO<sub>2</sub> capture by physical adsorption (Belmabkhout & Sayari, 2009). As the CO<sub>2</sub> partial pressure increases, the slopes of the OXA-GAC adsorption isotherms decrease steeply compared with the slopes of the GAC adsorption isotherms, possibly in response to a decrease of CO<sub>2</sub>–nitrogen surface-group interactions. At low CO<sub>2</sub> partial pressures, the contribution of chemisorption to the total CO<sub>2</sub> uptake is more pronounced, whereas physisorption within the pores becomes significant at higher concentrations (Serna-Guerrero et al., 2010b). Nevertheless, the general trend for both adsorption isotherms was a steady increase in CO<sub>2</sub> uptake with increasing CO<sub>2</sub> pressure.

As evident in the figures, the CO<sub>2</sub> adsorption was strongly dependent on the nitrogen functionalities: OXA-GAC exhibited a higher uptake than GAC over the whole pressure range studied. Notably, the reported values for the amount of carbon dioxide adsorbed were also in good agreement with the data from the cited literature for various ammonia-modified activated carbons (Pevida, Plaza, et al., 2008; Plaza et al., 2011; M. G. Plaza et al., 2009; Przepiórski et al., 2004).

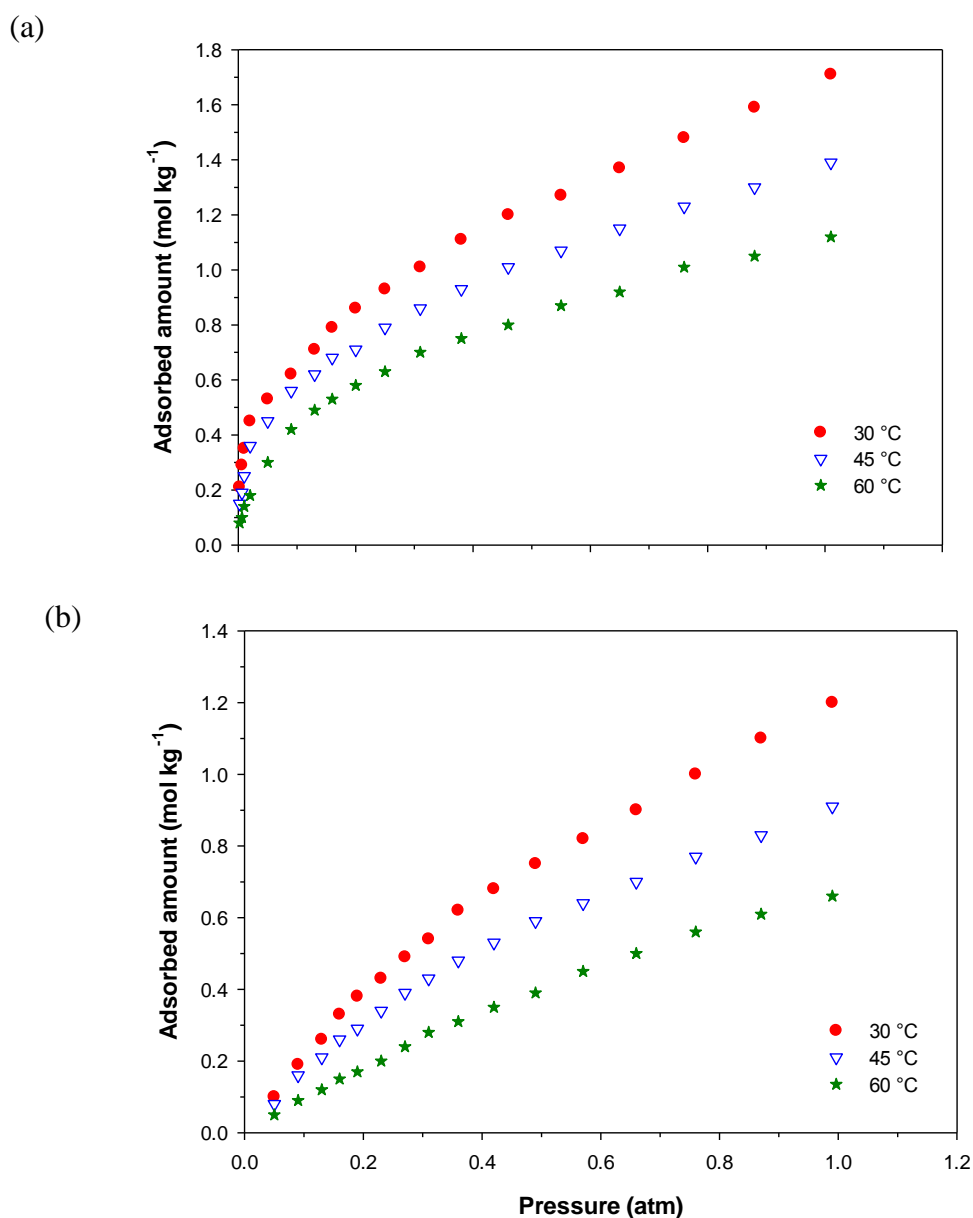


Figure 4.6: Experimental adsorption isotherms of CO<sub>2</sub> on (a) modified and (b) untreated activated carbon measured at 30, 45 and 60 °C.



Moreover, as shown in Figs. 4.6a and b, both of the adsorbents adsorbed less CO<sub>2</sub> at 45 and 60 °C than at 30 °C. The observed decrease in CO<sub>2</sub> uptakes at higher temperatures is attributed to the exothermic nature of the adsorption process, where both the molecular diffusion rate and the surface adsorption energy increase with increasing temperature (Maroto-Valer et al., 2005; Shafeeyan et al., 2011). According to the isothermal data, at 30 °C and atmospheric feed pressure, the amount of CO<sub>2</sub> adsorbed by OXA-GAC was approximately 1.71 mol kg<sup>-1</sup>, whereas only approximately 1.12 mol of CO<sub>2</sub>/kg of the adsorbent was adsorbed at 60 °C. However, interestingly, the results at 40 °C and especially at 60 °C indicate that, compared to the unmodified adsorbent, OXA-GAC exhibited a smaller decrease in the amount adsorbed with increasing temperature. The modified adsorbent did exhibit a decrease in the amount adsorbed with increasing temperature; however, this decrease was not as pronounced as the uptake reduction observed for GAC, where physisorption is the only retention phenomenon. Because in the high-temperature adsorption, the contribution of chemisorption to the total adsorption is more significant; a possible explanation for this observation is the occurrence of strong chemical reactions between CO<sub>2</sub> and incorporated nitrogen-functionalities on the surface. These observations are consistent with the studies performed by Do et al. (1998) and Na et al. (2001), who reported a decrease in the amount of CO<sub>2</sub> adsorbed onto commercial and Ajax-activated carbon from 3.2 to 1.6 mmol g<sup>-1</sup> and from 0.75 to 0.11 mmol g<sup>-1</sup> when the temperature was increased from 288 to 328 K and from 298 to 373 K, respectively, at 1 atm.

### **4.3.2 Equilibrium isotherms modeling**

Isotherm data analysis is generally a prerequisite to establish an equation that accurately predicts adsorption and that can be used to designing an adsorption separation process (Ho, 2004). As previously suggested, the overall CO<sub>2</sub> adsorption on the ammonia-

modified activated carbon could be the result of both physical adsorption within the pores and chemical adsorption onto the nitrogen surface groups (Shafeeyan et al., 2011; Shafeeyan et al., 2012). Distinguishing between these two mechanisms is useful in identifying the factors that may affect the rate of the adsorption process (Lu, Bai, Wu, Su, & Hwang, 2008; Su et al., 2010). Therefore, in the analysis of the adsorption equilibrium in the present study, we implemented an approach that takes into account the physical adsorption as well as the enhanced adsorption due to chemical interactions. A semi-empirical model that considers the simultaneous occurrence of two independent chemical and physical adsorption mechanisms for CO<sub>2</sub> adsorption can be expressed as the following equation:

$$q = q_{chem} + q_{phys} \quad (4-5)$$

where  $q$  is the overall adsorption of CO<sub>2</sub> on ammonia-modified activated carbon,  $q_{chem}$  represents the CO<sub>2</sub> uptake by nitrogen functionalities and  $q_{phys}$  denotes the physical adsorption onto the porous structure.

To differentiate the contribution of each independent mechanism to the total adsorption capacity of the modified adsorbent, a procedure was used to calculate  $q_{phys}$  on the basis of the CO<sub>2</sub> adsorption data for the untreated activated carbon adsorbent. In our previous study, we demonstrated that, under the conditions used for the modification of the adsorbent, the ammonia treatment did not significantly alter the pore structure of the studied adsorbent. In fact, the ammonia modification yielded a material with textural characteristics very similar to those of the parent carbon (Shafeeyan et al., 2012). Given that the amount of physical adsorption is proportional to the adsorbent textural properties, the difference in the amount of CO<sub>2</sub> physisorbed onto both modified and untreated activated carbon under the same operating conditions is reasonably assumed to be almost

negligible. Therefore, the contribution from chemical adsorption ( $q_{chem}$ ) to the total CO<sub>2</sub> uptake is estimated by subtracting the amount of  $q_{phys}$  for the untreated adsorbent from the overall adsorption uptake ( $q$ ), measured experimentally for the modified sample. The same approach was applied successfully by Serna-Guerrero et al. to differentiate the contributions of each independent mechanism of CO<sub>2</sub> adsorption on amine-grafted mesoporous silica (Serna-Guerrero et al., 2010b). They also provided further evidence of the applicability of the assumption used in the present study and extended it to other adsorption processes that combine the contribution of physisorption and chemisorption mechanisms.

Accordingly, using the equilibrium adsorption data for GAC, and subtracting the measured contribution of physisorption from the overall uptake, the corresponding values of  $q_{chem}$  for OXA-GAC at different temperatures were calculated; the results are represented in Fig. 4.7. As evident in this figure, the amount of CO<sub>2</sub> chemisorbed by the nitrogen functional groups corresponds to a type I isotherm in the IUPAC classification scheme, consistent with adsorption due to chemical interactions.

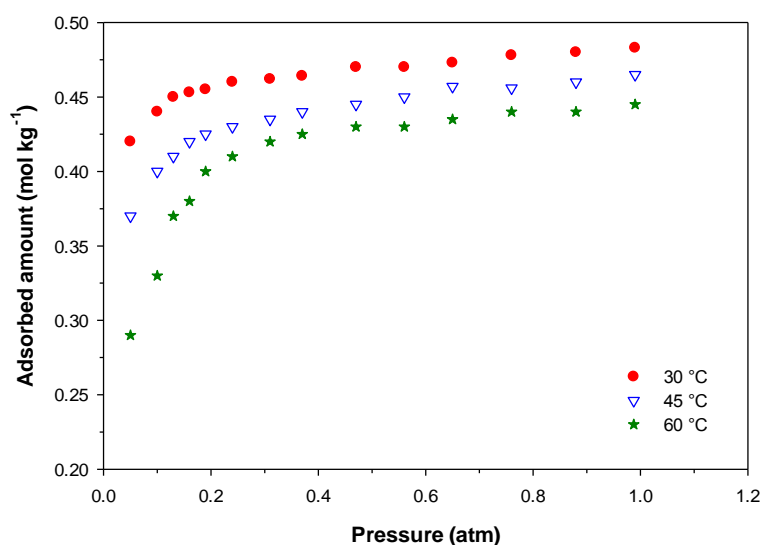


Figure 4.7: Calculated adsorption isotherms for CO<sub>2</sub> chemisorption onto the modified adsorbent at 30, 45 and 60 °C.

After the contributions of the two independent physisorption and chemisorption mechanisms were distinguished, different equilibrium isotherm equations could potentially be used to correlate equilibrium data. Applying various conventional isotherm models, we can express the terms on the right side of Eq. (4-5) in different forms to describe each of the mechanisms with a proper isotherm model. The main distinguishing feature for selecting an appropriate isotherm model arises from the accuracy as well as simplicity of the equations. Non-idealities in the isotherms mainly stem from the heterogeneity of the adsorbent surface, and such heterogeneities often occur in the case of activated carbon (Malek & Farooq, 1996). From this point of view, three of the most common pure-species isotherm models (i.e., Freundlich, Sips and Toth) that have been previously applied to describe adsorption equilibria on heterogeneous adsorbents were employed in this work.

For each temperature and mechanism, a non-linear regression method was applied to independently determine the parameters corresponding to the aforementioned isotherm models. The optimal values of the Freundlich, Sips and Toth isotherm parameters are summarized in Tables 4.4-4.6, respectively. To quantitatively compare the quality of the nonlinear regressions for these three models, the average relative error (ARE) and nonlinear regression coefficient ( $R^2$ ) were calculated; the results are included in Tables 4.4-4.6. As evident in these tables, the parameters of each isotherm model varied when the adsorption mechanism and temperature were changed. In the Freundlich model, the  $K_F$  parameter refers to the adsorption capacity and represents the adsorption quantity per unit equilibrium concentration, whereas the exponent  $1/m_F$  is a measure of the adsorbent-adsorbate binding energy and expresses both the adsorption intensity and the surface heterogeneity (Ferraro, Cruz, Jorge, Pintado, & Castro, 2013). The higher values of  $K_F$  obtained for the physisorption mechanism indicated greater adsorption compared

to chemisorption, whereas the higher values of  $m_F$  observed for chemisorption denoted a more favorable adsorption and a stronger bond between CO<sub>2</sub> and the modified adsorbent ( $5 < m_F < 25$ ). The heterogeneity of the adsorbent surface can also be described with the exponent  $m_i$  in the Sips and Toth isotherm equations (Esteves et al., 2008). When the surface is homogeneous,  $m_i$  is equal to unity and the isotherm expressions reduce to the Langmuir equation. In agreement with the Freundlich model, the obtained values of the surface heterogeneity parameter in the Toth ( $m_T < 1$ ) and Sips ( $m_S > 1$ ) equations showed a higher degree of heterogeneous adsorption for CO<sub>2</sub> chemisorption. From Tables 4.5 and 4.6, the values of the saturation capacity parameter ( $q_m$ ), which indicate the maximum amount that can possibly be adsorbed, decreased with increasing temperature. The observed decrease is associated with the exothermicity of the adsorption process (Ning et al., 2012). Because  $\eta$  is the parameter that reflects the temperature dependence of  $q_m$  in the Toth isotherm (Table 4), the lower values of  $\eta$  obtained for the chemisorption compared to the physisorption imply that, within the temperature range studied, the chemical adsorption mechanism exhibited a greater tendency to remain the same with changes in temperature. Furthermore, compared with physical adsorption, the chemisorption mechanism presented larger values of  $K_i$  (for instance,  $q_{chem}$  ( $1.05 \times 10^5$  atm<sup>-1</sup>) compared to  $q_{phys}$  ( $7.1 \times 10^{-1}$  atm<sup>-1</sup>) at 303 K), which is attributed to the strength of the adsorbate–adsorbent interactions for the chemisorption mechanism (Do, 1998).

Table 4.4: Freundlich isotherm parameters with  $R^2$  and ARE for each independent mechanism at temperatures of 303, 318, and 333 K

	Temperatures		
	303 K	318 K	333 K
<i>Physical adsorption</i>			
$K_F$ ( $mol\ kg^{-1}\ atm^{-1/m_F}$ )	1.22	0.93	0.68
$m_F$ (dimensionless)	1.40	1.45	1.24
$R^2$	0.996	0.995	0.996
ARE (%)	5.56	5.95	5.02
<i>Chemical adsorption</i>			
$K_F$ ( $mol\ kg^{-1}\ atm^{-1/m_F}$ )	0.48	0.47	0.46
$m_F$ (dimensionless)	24.57	14.75	8.41
$R^2$	0.962	0.965	0.865
ARE (%)	0.86	0.79	5.16

Table 4.5: Sips isotherm parameters with  $R^2$  and ARE for each independent mechanism at temperatures of 303, 318, and 333 K

	Temperatures		
	303 K	318 K	333 K
<i>Physical adsorption</i>			
$q_m$ ( $mol\ kg^{-1}$ )	3.43	2.12	1.76
$K_S$ ( $atm^{-1}$ )	0.69	0.39	0.23
$m_S$ (dimensionless)	1.11	1.08	0.98
$R^2$	0.998	0.998	0.999
ARE (%)	2.93	2.08	1.71
<i>Chemical adsorption</i>			
$q_m$ ( $mol\ kg^{-1}$ )	0.53	0.48	0.44
$K_S$ ( $atm^{-1}$ )	$8.73 \times 10^2$	$1.96 \times 10^2$	50.76
$m_S$ (dimensionless)	2.12	2.02	1.83
$R^2$	0.970	0.981	0.991
ARE (%)	0.54	0.67	0.99

Table 4.6: Toth isotherm parameters with  $R^2$  and ARE for each independent mechanism at temperatures of 303, 318, and 333 K

	Temperatures		
	303 K	318 K	333 K
<i>Physical adsorption</i>			
$q_m$ ( $mol\ kg^{-1}$ )	5.01	2.58	1.32
$K_T$ ( $atm^{-1}$ )	0.71	1.09	1.50
$m_T$ (dimensionless)	0.59	0.63	0.68
$R^2$	0.999	0.999	0.999
ARE (%)	2.65	2.01	1.65
<i>Chemical adsorption</i>			
$q_m$ ( $mol\ kg^{-1}$ )	0.54	0.49	0.46
$K_T$ ( $atm^{-1}$ )	$1.05 \times 10^5$	$3.76 \times 10^5$	$1.20 \times 10^6$
$m_T$ (dimensionless)	0.29	0.30	0.31
$R^2$	0.971	0.982	0.992
ARE (%)	0.52	0.64	0.93

On the basis of the calculated values of ARE and  $R^2$  tabulated in Tables 4.4-4.6, both the Sips and Toth isotherms were capable of fitting the equilibrium data over a broad range of experimental conditions. However, the Toth equation, which involves a symmetrical quasi-Gaussian distribution of adsorption sites, provided a slightly better fit. The low values obtained for the ARE (in no case greater than 3%), as well as the high values of the nonlinear regression coefficient (very near unity,  $R^2 \geq 0.97$ ), indicate the goodness of the fit. Therefore, compared to the Freundlich and Sips models, the Toth equation is more accurate and more capable of describing the CO<sub>2</sub> adsorption isotherms over the ammonia-modified adsorbent. Thus, only the Toth model was used here to illustrate the quality of its fit to the experimental equilibrium data (Fig. 4.8). The complete form of the proposed semi-empirical model is expressed as follows:

$$q = \left[ \frac{q_m K_T P}{\left(1 + (K_T P)^{m_T}\right)^{1/m_T}} \right]_{phys} + \left[ \frac{q_m K_T P}{\left(1 + (K_T P)^{m_T}\right)^{1/m_T}} \right]_{chem} \quad (4-6)$$

where the subscripts “*phys*” and “*chem*” indicate the contributions of each independent mechanism to the total CO<sub>2</sub> uptake.

To express the temperature dependence of the Toth isotherm parameters for the purpose of interpolating or extrapolating the equilibrium data to various temperatures, as well as determining the isosteric enthalpy of adsorption, the parameters,  $K_i$ ,  $q_m$  and  $m_i$  are described by the following equations (Li & Tezel, 2008):

$$K_r = K_{r_0} \exp \left[ -\frac{\Delta H}{RT_0} \left( \frac{T_0 - T}{T} \right) \right] \quad (4-7)$$

$$q_m = q_{m_0} \exp \left[ \eta \left( \frac{T_0 - T}{T_0} \right) \right] \quad (4-8)$$

$$m_r = m_{r_0} + \alpha \left( \frac{T - T_0}{T} \right) \quad (4-9)$$

Where  $T$  is the absolute temperature (K),  $T_0$  is the reference temperature and was taken as 303 K,  $K_{i0}$  and  $m_{i0}$  are the affinity and heterogeneity parameters at the reference temperature, respectively,  $\alpha$  and  $\eta$  are constant parameters,  $(-\Delta H)$  is the isosteric heat of adsorption at zero coverage (kJ mol<sup>-1</sup>), and  $R$  is the gas-law constant (J mol<sup>-1</sup> K<sup>-1</sup>). The optimal parameter values for both the chemical and physical adsorption mechanisms were obtained by nonlinear regression; the results are presented in Table 4.7. The surface obtained from the global fitting of the aforementioned model to the experimental data (Fig. 4.8) shows that the equilibrium data are described well for all temperatures when the adsorption isotherm plotted according to the proposed Toth equation is used.

Table 4.7: Optimal values of the proposed Toth temperature-dependent parameters

	$\alpha$ (dimensionless)	$\eta$ (dimensionless)	$(-\Delta H)$ (kJ mol <sup>-1</sup> )
<i>Physical adsorption</i>	0.96	13.43	23.05
<i>Chemical adsorption</i>	0.25	1.67	68.11



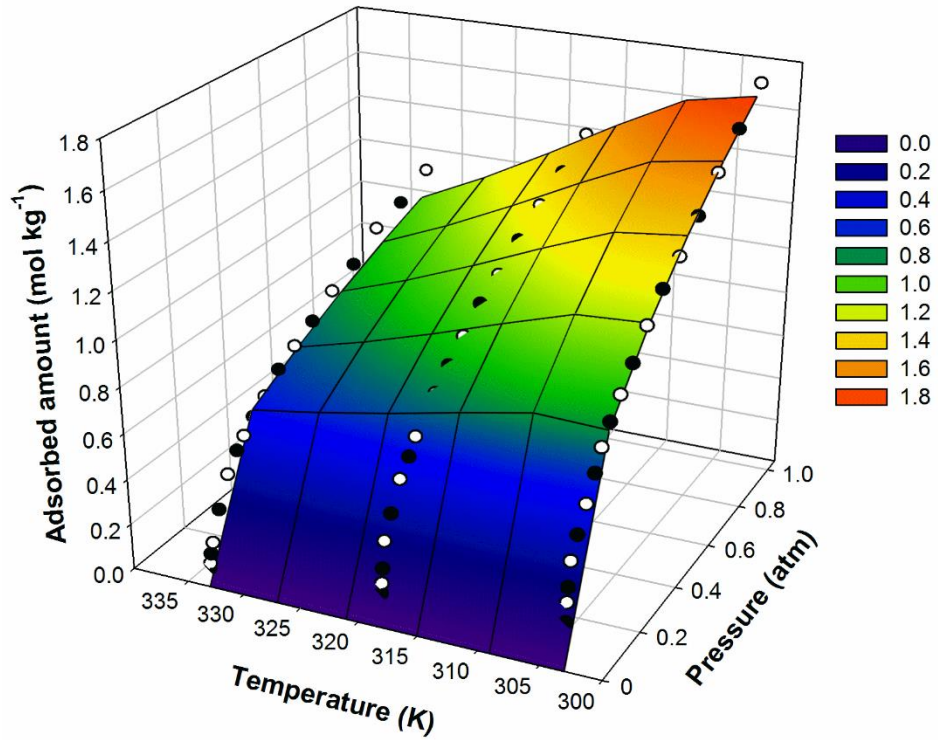


Figure 4.8: Graphical evaluation of the fit of the experimental equilibrium data to the proposed model for the modified adsorbent, whose parameters are presented in Tables 4.6 and 4.7. The surface is the global isotherm model, and the black and white circles show the experimental data at 303, 318 and 333 K.

### 4.3.3 Isotheric heat of adsorption

The isosteric heat of adsorption is a critical parameter for designing and operating an adsorption-based separation process such as PSA. It is a measure of the interaction between the adsorbate molecules and the surface of the adsorbent, and it can be obtained from the temperature dependence of the adsorption isotherm (Esteves et al., 2008; Ning et al., 2012). The isosteric heat of adsorption,  $Q_{st}$ , also denoted as  $-\Delta H$  ( $\text{kJ mol}^{-1}$ ), at a specific adsorbate loading can be estimated using the Clausius–Clapeyron equation as follows (Park, Lee, Choi, Lee, & Kim, 2002):

$$-\frac{Q_{st}}{R} = \left( \frac{\partial \ln P}{\partial 1/T} \right)_{q^a} \quad (4-10)$$

where  $q^a$  is a specific surface loading ( $\text{mol kg}^{-1}$ ).

Integration of Eq. (4-10) enables the calculation of  $Q_{st}$  by knowing the differential partial pressure change as a function of a differential change in system temperature for a given adsorbed amount:

$$Q_{st} = R \left[ \frac{\ln P_1 - \ln P_2}{1/T_2 - 1/T_1} \right]_{q^a} \quad (4-11)$$

Therefore, the isosteric heats are obtained from the slopes of the lines in the plots of  $\ln P$  vs.  $1/T$  for the same adsorption amount for the different isotherms. In the present study, the experimental isotherms at the three temperatures of 303, 318, and 333 K for a given adsorption amount (from 0.2-1.2 mol kg<sup>-1</sup> in 0.2 mol kg<sup>-1</sup> increments) were used to measure the isosteric enthalpies of adsorption for OXA-GAC and GAC adsorbents (see Figs. 4.9a and b).

The observed linear behavior is based on the assumption that, over the temperature range investigated, the isosteric heat of adsorption is independent of temperature and depends only on the surface coverage. In practice, the assumption of temperature independence of the heat of adsorption was shown to be valid for the pressure and loading estimations (Berlier & Frère, 1996; Esteves et al., 2008). Notably, consistent with the exothermic character of the adsorption process, negative  $Q_{st}$  values were attained at 303-333 K, indicating that the entropy was reduced in the system.

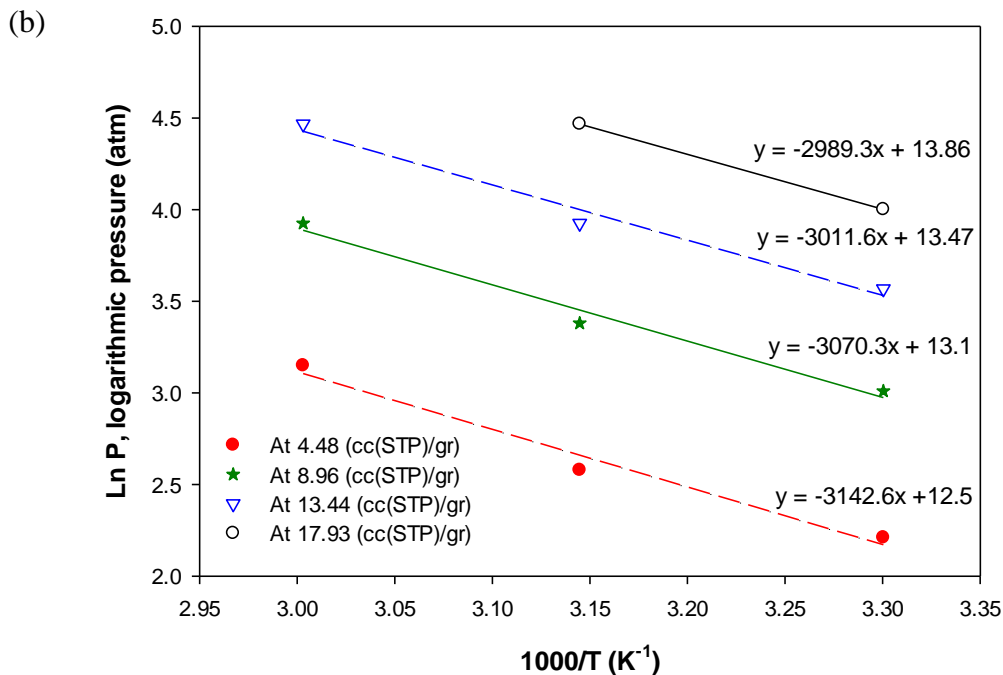
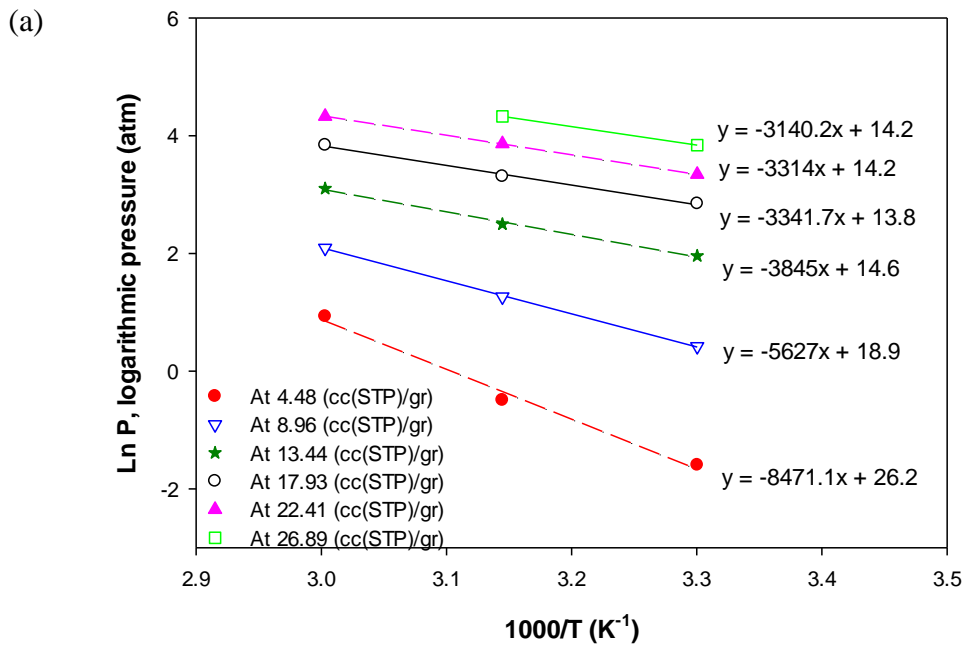


Figure 4.9: Adsorption isotherms of CO<sub>2</sub> for (a) modified and (b) untreated adsorbent in the temperature range from 303 to 333 K. The points were calculated by numerical interpolation, and the lines represent the linear fit. All of the isotherms are marked with the corresponding amount of CO<sub>2</sub> adsorbed in units of (cm<sup>3</sup> STP/g).

The isosteric enthalpy changes accompanying adsorption can be used to examine the molecular-scale interactions between the adsorbate molecules and the adsorbent. Moreover, information regarding the magnitude of the adsorption enthalpy and its surface coverage dependence can be used as criteria for determining the energetic heterogeneity of a solid surface (Belmabkhout & Sayari, 2009; Park et al., 2002). The isosteric heat is independent of the surface coverage when no interaction occurs between adsorbed molecules, and the surface is energetically homogeneous. However, a variation of the isosteric heats with the surface loading indicates the existence of different levels of surface energy and heterogeneity of the adsorbent surface (Ning et al., 2012). Figure 4.10 depicts the variation of  $Q_{st}$  (calculated using the Clausius–Clapeyron equation) as a function of the amount of CO<sub>2</sub> adsorbed for the OXA-GAC and GAC adsorbents. As evident in the figure, the unmodified adsorbent exhibited approximately constant values of  $Q_{st}$  for different CO<sub>2</sub> loadings, indicating the uniform nature of the adsorbent surface. Notably, the obtained initial heat of adsorption for GAC (25 kJ mol<sup>-1</sup>) corresponds closely to the value of  $-\Delta H$  (23 kJ mol<sup>-1</sup>) calculated from the temperature-dependent parameters of the proposed model for  $q_{phys}$  and is also of the same order of magnitude as the typical values for commercial activated carbon reported in the literature (Chue et al., 1995; Esteves et al., 2008; Garcés et al., 2013; Himeno, Komatsu, & Fujita, 2005; Van Der Vaart, Huiskes, Bosch, & Reith, 2000). In contrast, OXA-GAC exhibited rather high values of  $Q_{st}$  at the low range of loading, which reflects the relatively strong chemical interactions between CO<sub>2</sub> and the basic nitrogen functionalities.

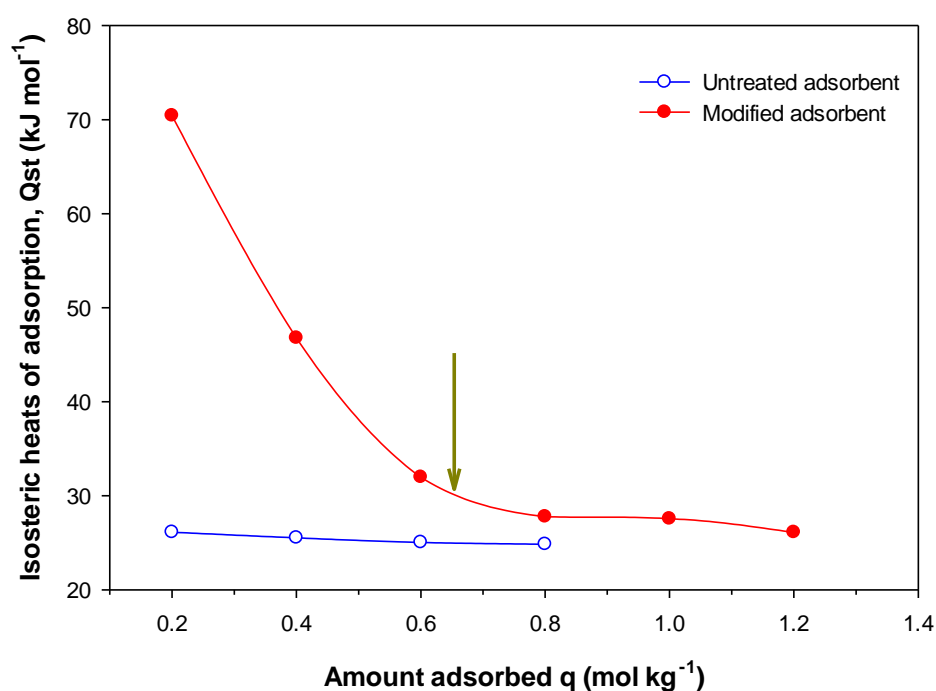


Figure 4.10: Concentration dependence of the isosteric enthalpy for CO<sub>2</sub> adsorption on the GAC and the OXA-GAC

The isosteric enthalpy of adsorption over OXA-GAC decreases with increasing CO<sub>2</sub> surface loading until it approaches values similar to those of the untreated carbon adsorbent. The observed decrease with increasing loading is attributed to the high degree of heterogeneity of the adsorbent surface (Belmabkhout & Sayari, 2009). At the beginning of the adsorption process, only the most active adsorption sites are filled, the activation energy is low and the heat of adsorption is high. With increasing surface coverage, less-active adsorption sites start to be occupied, thereby increasing the activation energy and decreasing the heat of adsorption (Himeno, Tomita, Suzuki, & Yoshida, 2007; Ning et al., 2012; Zhao, Xu, Sun, Zhang, & Liu, 2009). The observed heats of adsorption for the ammonia-modified adsorbent clearly demonstrate the strong and weak interactions of the nitrogen surface groups with CO<sub>2</sub> at low and high coverages, respectively. Notably, the  $Q_{st}$  value obtained at low coverage (70.4 kJ mol<sup>-1</sup>) is consistent with the value calculated from the proposed Toth parameter  $K_i$  for  $q_{chem}$  (68.1 kJ mol<sup>-1</sup>)

at zero loading and is in the range of values for typical cases of CO<sub>2</sub> chemisorption (60 to 90 kJ mol<sup>-1</sup>) (Samanta et al., 2011).

Indeed, this value is higher than that for a physical interaction but lower than that for a strong chemical interaction. In addition, in agreement with the observed inflection in the isotherms for CO<sub>2</sub> adsorption over the OXA-GAC adsorbent (see Fig. 4.6a), a corresponding curvature in the plot of the isosteric heat vs. coverage was detected, coinciding with the saturation of the most active adsorption sites (indicated by an arrow in Fig. 4.10). The observed variation of the slope of the  $Q_{st}$  vs. CO<sub>2</sub> loading curve clearly reflects the occurrence of two independent adsorption mechanisms.

#### **4.4 Modeling of carbon dioxide adsorption onto ammonia-modified activated carbon: Kinetic analysis and breakthrough behavior**

##### **4.4.1 Adsorption kinetics**

Fig. 4.11 displays the experimental data of CO<sub>2</sub> uptake as a function of time over the ammonia-modified and untreated adsorbents at 30, 45, and 60 °C determined using the gravimetric uptake method. As shown in Fig. 4.11, the adsorption kinetics over OXA-GAC were faster than the untreated carbon, particularly at high temperatures, and the uptake capacity increased rapidly during the first minutes of the process. For example, at 60 °C, OXA-GAC reached approximately 90% of its maximum capacity within the first 70 seconds of CO<sub>2</sub> exposure (Fig. 4.11c). However, the CO<sub>2</sub> uptake rate then decelerates, and approximately 1,200 seconds are required to reach a constant equilibrium value. The obtained experimental kinetic data for CO<sub>2</sub> adsorption were fitted to three different kinetic models (i.e., pseudo-first-order, pseudo-second-order, and Avrami models), and the corresponding predicted kinetic curves are presented in Fig. 4.11. These three kinetic models are frequently used for the mass transfer coefficient determination of various

gases on different adsorbents, including activated carbon (Heydari-Gorji & Sayari, 2011; Loganathan et al., 2014; Serna-Guerrero & Sayari, 2010; Stevens et al., 2013). A non-linear regression method was used to determine the parameters corresponding to the mentioned kinetic models; the values obtained are summarized in Tables 4.8 and 4.9. To quantify and compare the quality of the nonlinear regressions for these three models, the associated coefficients of determination ( $R^2$ ) and the normalized standard deviation ( $\Delta q$ ) were calculated using Eqs. 3.23 and 3.24; the results are presented in Tables 4.8-4.9. These tables reveal that the parameters of each kinetic model varied when the adsorption temperature and type of adsorbent were changed.

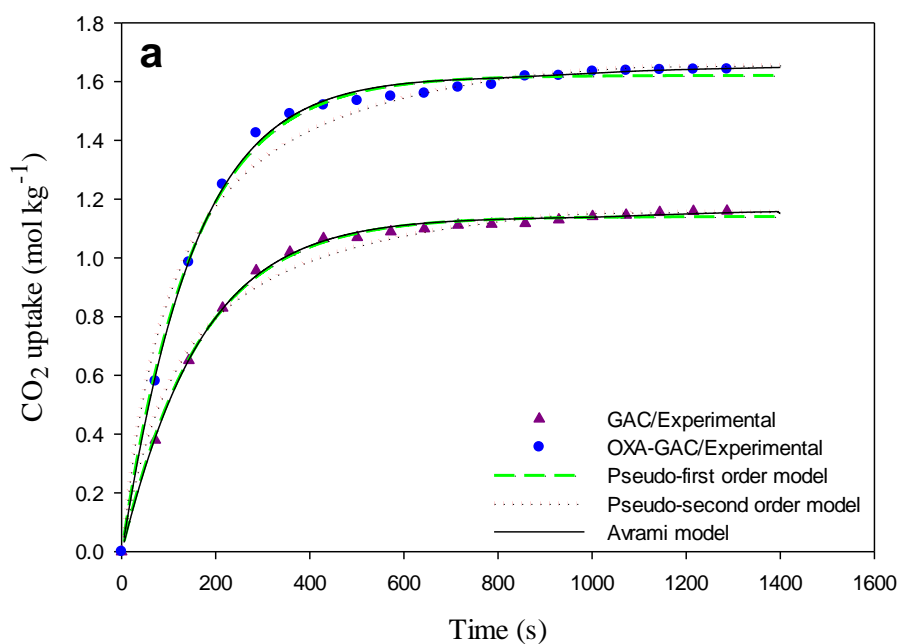
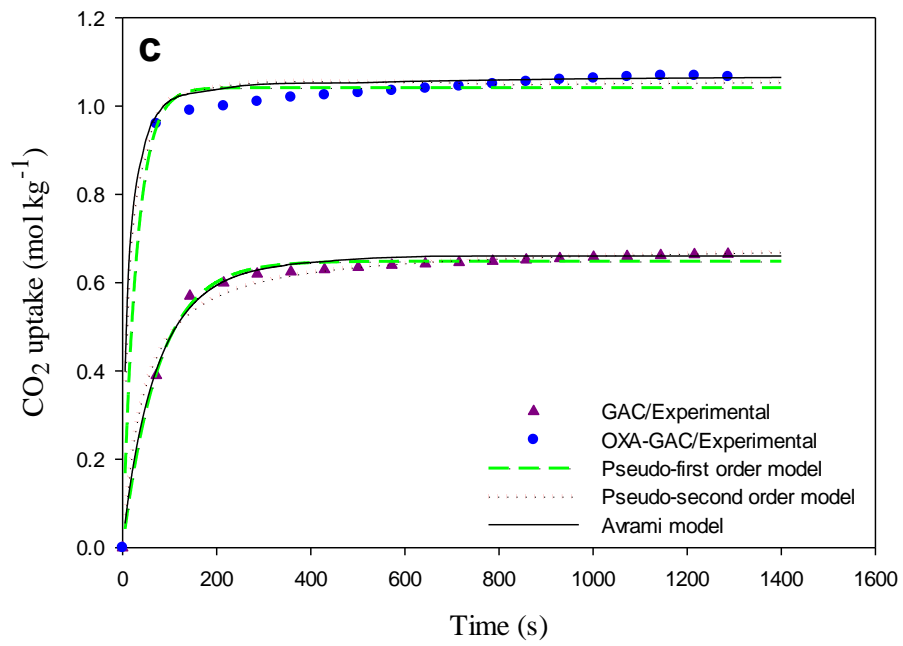
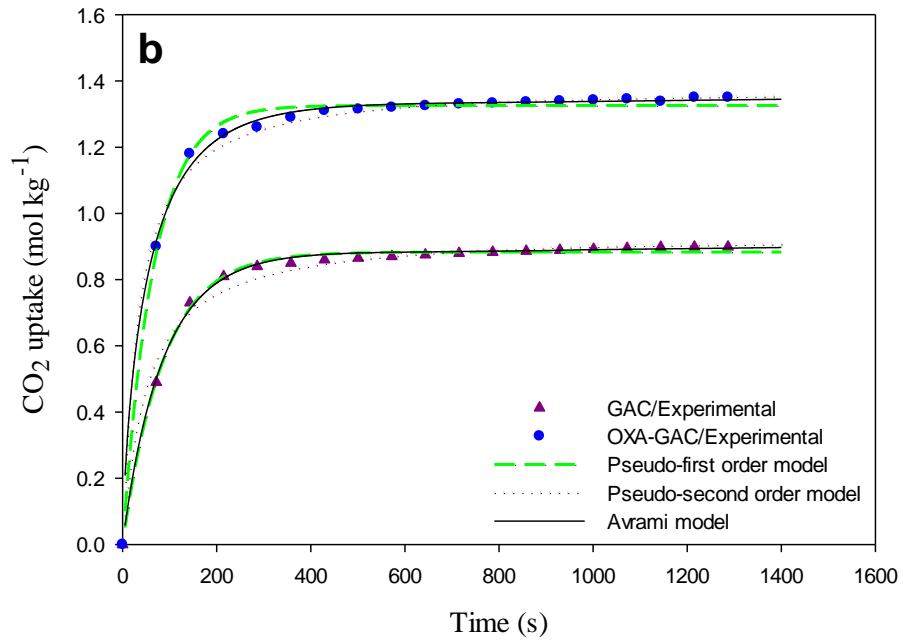


Figure 4.11: Experimental CO<sub>2</sub> adsorption onto modified and untreated adsorbents at (a) 30 °C, (b) 45 °C, and (c) 60 °C along with the corresponding fit to kinetic models.

'Figure 4.11, continued'





Although because of the exothermic nature of the adsorption process, the CO<sub>2</sub> uptake decreased with increasing temperature, as evident in Tables 4.8 and 4.9, for each adsorbent, the rate constants ( $k_F$ ,  $k_S$ , and  $k_A$ ) obtained using the kinetic models increased when the higher adsorption temperatures were applied. The favorable adsorption kinetics observed at higher temperatures can be attributed to the faster migration of CO<sub>2</sub> molecules inside of the pores due to the increase in their kinetic energy, which results in an increase in the diffusion rate (Loganathan et al., 2014). The increase in the mass transfer coefficient with the rise in temperature is reflected in the faster kinetics of adsorption and the significantly steeper kinetic curves. For example, at 30 °C, the time required for GAC to reach approximately 85% of its equilibrium capacity was ( $\sim <350$  s), whereas this time was reduced to ( $\sim <140$  s) when the temperature was increased to 60 °C (Fig. 2a and c). The trend observed agrees well with the data presented in the literature in which the  $k$  values were reported to increase with an increasing adsorption temperature (Loganathan et al., 2014; Serna-Guerrero & Sayari, 2010; Stevens et al., 2013; Zhijuan Zhang, Zhang, Chen, Xia, & Li, 2010). In addition, consistent with the previous observation that the kinetic behavior of the modified sample was comparatively faster than that of untreated adsorbent, the calculated values of the rate constants ( $k_F$ ,  $k_S$ , and  $k_A$ ) for OXA-GAC were higher than those for GAC. As shown in Tables 4-5, GAC exhibited a  $k_A$  of  $1.14 \times 10^{-2}$  at 60 °C, whereas it increased to  $4.01 \times 10^{-2}$  for the modified sample under the same conditions. In addition, the estimated values of parameter  $n$  in the Avrami model for untreated adsorbent were lower compared with the values for its modified counterpart. A variation in the value of this parameter, which describes how fast the adsorption process occurs, suggests a change in the adsorption mechanism (Cestari, Vieira, Vieira, & Almeida, 2006; Wang et al., 2012). This result may be attributed to the occurrence of chemical reactions between the CO<sub>2</sub> and nitrogen functionalities incorporated onto the adsorbent surface, in addition to CO<sub>2</sub> capture by physical adsorption. Notably, the

calculated values of the kinetic rate constants for the untreated and modified adsorbents ( $\sim 8 \times 10^{-3} < k < \sim 4 \times 10^{-2}$ ) were consistent with the typical values reported in the literature for various activated carbons (Do & Wang, 1998; Dreisbach, Staudt, & Keller, 1999).

Fig. 4.11 shows that for both of the adsorbents, the pseudo-first-order kinetic model reasonably fit the experimental kinetic curves of CO<sub>2</sub> adsorption at all of the studied temperatures. However, a slight deviation was observed at high surface coverage (underestimation of the CO<sub>2</sub> uptake) because as previously reported by other authors (Ho, 2006; Loganathan et al., 2014; Serna-Guerrero & Sayari, 2010), the most accurate range for the pseudo-first-order model to fit the kinetic curves occurs in the early stages of adsorption. Moreover, in the case of adsorption onto OXA-GAC, the observed deviation may also be due to the simultaneous occurrence of physisorption and chemisorption in which the assumption that the uptake rate is proportional to the linear difference between the equilibrium and the actual concentration is no longer satisfactory (Stevens et al., 2013). However, the estimated values of  $\Delta q$  for the pseudo-first-order kinetic model varied by less than 3% for the temperature range studied, suggesting that the model can be applied with a reasonable degree of confidence to describe the CO<sub>2</sub> capture kinetics of both of the adsorbents. The advantage of using the pseudo-first-order kinetic model is the mathematical simplicity of its expression. Using this expression of the adsorption rate, which does not involve the spatial coordinates, the partial differential equation describing mass conservation for gas penetrating pores can transform into a significantly simpler ordinary differential equation; thus, the solutions are mathematically simpler and faster than the solution of the diffusional models (Shafeeyan et al., 2014). Yang and Lee have demonstrated that although this adsorption rate model is relatively simple, it can predict the experimental data with satisfactory accuracy (Yang & Lee, 1998). Consequently, this approximation has found widespread application in modeling fixed-bed and cyclic CO<sub>2</sub> adsorption processes.

In contrast, as shown in Fig. 4.11, the pseudo-second-order model significantly deviates from the experimental results at the beginning of the process (low surface coverage) and only appears to fit the kinetic data when the adsorbate loadings become sufficiently high. Based on the calculated values of  $R^2$  and  $\Delta q$  (%) presented in Tables 4-5 for both of the studied adsorbents, the Avrami model provided the best fit to the experimental kinetic data over the range of temperatures considered. The high values obtained for the nonlinear regression coefficient (close to unity,  $R^2 \geq 0.99$ ) and the low values of the  $\Delta q$  (%) (in no case greater than 2%) indicate the goodness of fit over the range of the recorded data. Therefore, compared with the pseudo-first-order and pseudo-second-order kinetic models, the Avrami equation is more accurate and more capable of describing CO<sub>2</sub> adsorption kinetics over the studied adsorbents. The excellent quality of the fit of the Avrami model to the experimental kinetic data at the low and high surface coverages is most likely associated with its potential to account for the occurrence of complex reaction pathways (Cestari et al., 2006; Lopes, dos Anjos, Vieira, & Cestari, 2003; Serna-Guerrero & Sayari, 2010; Wang et al., 2012). The findings are in good agreement with previous studies, which have demonstrated that the pseudo-first-order and Avrami kinetic models successfully described the adsorption kinetics of CO<sub>2</sub> on activated carbon (Zhijuan Zhang, Zhang, et al., 2010) and MCM-41 adsorbents (Berenguer-Murcia et al., 2003) (physical adsorbents) and functionalized pore-expanded mesoporous silica (physicochemical adsorbent) (Loganathan et al., 2014), respectively. Because the Avrami model provided the best experimental simulation fit, we employed this equation for the modeling of the fixed bed CO<sub>2</sub> adsorption.

Table 4-8: The calculated parameters of the kinetic models and associated  $R^2$  and  $\Delta q$  (%) for the CO<sub>2</sub> adsorption onto GAC at different temperatures.

Adsorption temperature (°C)		30	45	60
Pseudo-first order model	$K_F$ (s <sup>-1</sup> )	$7.99 \times 10^{-3}$	$1.01 \times 10^{-2}$	$1.13 \times 10^{-2}$
	$R^2$	0.9970	0.9961	0.9942
	$\Delta q$ (%)	1.71	1.84	1.96
Pseudo-second order model	$K_S$ (mol kg <sup>-1</sup> s <sup>-1</sup> )	$8.01 \times 10^{-3}$	$9.97 \times 10^{-3}$	$1.16 \times 10^{-2}$
	$R^2$	0.9860	0.9885	0.9897
	$\Delta q$ (%)	6.61	3.94	3.46
Avrami model	$K_A$ (s <sup>-1</sup> )	$7.97 \times 10^{-3}$	$1.01 \times 10^{-2}$	$1.14 \times 10^{-2}$
	$n$	1.03	0.96	0.91
	$R^2$	0.9979	0.9981	0.9994
	$\Delta q$ (%)	1.40	1.39	1.01

Table 4-9: The calculated parameters of the kinetic models and associated  $R^2$  and  $\Delta q$  (%) for the CO<sub>2</sub> adsorption onto OXA-GAC at different temperatures.

Adsorption temperature (°C)		30	45	60
Pseudo-first order model	$K_F$ (s <sup>-1</sup> )	$3.15 \times 10^{-2}$	$3.68 \times 10^{-2}$	$3.97 \times 10^{-2}$
	$R^2$	0.9961	0.9947	0.9909
	$\Delta q$ (%)	2.08	2.68	3.09
Pseudo-second order model	$K_S$ (mol kg <sup>-1</sup> s <sup>-1</sup> )	$2.78 \times 10^{-2}$	$3.29 \times 10^{-2}$	$4.02 \times 10^{-2}$
	$R^2$	0.9841	0.9958	0.9942
	$\Delta q$ (%)	6.72	1.94	2.27
Avrami model	$K_A$ (s <sup>-1</sup> )	$3.11 \times 10^{-2}$	$3.53 \times 10^{-2}$	$4.01 \times 10^{-2}$
	$n$	1.74	1.53	1.38
	$R^2$	0.9970	0.9981	0.9943
	$\Delta q$ (%)	1.63	1.48	2.03

To describe the temperature dependence of the rate constants, the following Arrhenius-type equation was employed:

$$k = k_0 \exp(-E_a / RT) \quad (4-12)$$

where  $k_0$  is the pre-exponential factor,  $R$  denotes the universal gas constant,  $E_a$  is the apparent activation energy, and  $T$  expresses the absolute temperature.

Because the fit statistics of the Avrami kinetic model were adequate, its corresponding  $k$  constants at 30, 45, and 60 °C were used to estimate the parameters of the Arrhenius equation (Fig. 4.12). From the slope and the intercept of the straight line of the plot of the natural logarithm of  $k_A$  against the inverse of the absolute temperature,  $E_a$  values of 7.11 and 10.06 kJ mol<sup>-1</sup> and  $k_0$  values of  $5.21 \times 10^{-1}$  and  $4.38 \times 10^{-1}$  (s<sup>-1</sup>) were determined for the OXA-GAC and GAC adsorbents, respectively. The lower value of  $E_a$  on the OXA-GAC sample compared with the untreated adsorbent indicates the stronger adsorbate-adsorbent interaction potential of the modified adsorbent compared with the GAC sample. The plots of  $\ln k_A$  vs  $1/T$  were linearly fitted, with coefficients of determination ( $R^2$ ) greater than 0.97, indicating a good linearity between  $\ln k_A$  and  $1/T$ .

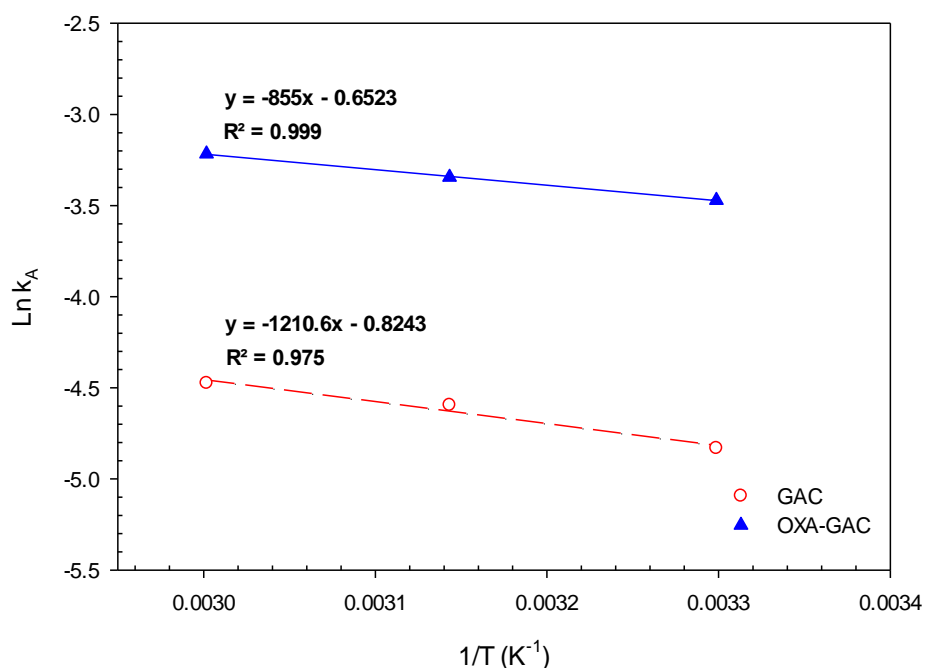


Figure 4.12: Arrhenius plots for the estimation of the CO<sub>2</sub> adsorption activation energies on the GAC and OXA-GAC adsorbents.

#### 4.4.2 Column breakthrough experiments and model validation

Breakthrough adsorption experiments for the ammonia-modified and untreated adsorbents were performed at different adsorption temperatures and feed flow rates. Fig. 4.13 represents the effluent CO<sub>2</sub> concentration as a function of time (breakthrough curve) for each sample at 30, 45, and 60 °C with varying CO<sub>2</sub> flow rates from 50 to 100 ml min<sup>-1</sup> in the feed gas. To describe the breakthrough behavior of the CO<sub>2</sub> adsorption, the characteristic parameters of the breakthrough time,  $t_b$ , saturation time,  $t_s$ , length of the mass transfer zone,  $L_{MTZ}$ , and the dynamic adsorption capacity,  $q$ , were determined. The obtained results for each experimental breakthrough curve are tabulated in Table 4.10. The breakthrough and saturation times were considered as the required times to reach 10% and 90% of the inlet CO<sub>2</sub> concentration at the column outlet, whereas the equilibrium adsorption capacity was taken as the loading amount until the point at which the effluent CO<sub>2</sub> concentration was equal to the feed concentration. Assuming a constant pattern profile, the length of the mass transfer zone, which is the active part of the fixed bed where adsorption occurs, was estimated using the following correlation (Zhao, Shen, Bai, & Ni, 2012):

$$L_{MTZ} = L \left[ \frac{t_s - t_b}{t_s - 0.5(t_s - t_b)} \right] \quad (4-13)$$

where  $L$  is the bed height (cm).

The equilibrium dynamic adsorption capacity of the bed was determined as a function of the feed concentration applying a mass balance to the bed, as shown in Eq. (4-14):

$$q = \frac{Q_F c_0 t_q}{m_S} \times \frac{T_0}{T} \times \frac{1}{V_m} \quad (4-14)$$

where  $q$  (mol kg<sup>-1</sup>) is the calculated CO<sub>2</sub> loading at a certain time,  $m_S$  (kg) denotes the mass of adsorbent loaded in the column,  $Q_F$  (ml min<sup>-1</sup>) is the volumetric flow rate of the

feed gas,  $c_0$  is the inlet CO<sub>2</sub> concentration (vol.% or mol%),  $T$  (K) expresses the gas temperature,  $T_0$  is 273.15 (K),  $V_m$  is ( $22.4 \times 10^3$  ml mol<sup>-1</sup>), and  $t_q$  is the time equivalent to the CO<sub>2</sub> stoichiometric adsorption capacity of the bed and is calculated from the area between the breakthrough profile and a line at  $c_t/c_0 = 1.0$ , as described in Eq. (20) (Liu et al., 2010; Y. Liu et al., 2011; Monazam et al., 2013; Serna-Guerrero & Sayari, 2010):

$$t_q = \int_0^{\infty} \left(1 - \frac{c_t}{c_0}\right) dt \quad (4-15)$$

where  $c_t$  (vol %) is the concentration of CO<sub>2</sub> at time  $t$ .

The efficiency of the column ( $\Phi$ ) was calculated based on the conventional concept of the length of unused bed (LUB) (Beaver, Caram, & Sircar, 2009):

$$\frac{LUB}{L} = 1 - \frac{t_b}{t^*} = 1 - \Phi \quad (4-16)$$

where  $t^*$  is the stoichiometric breakthrough time and can be determined by extending a vertical line on the breakthrough profile at a point at which the adsorbed quantity of adsorbate is equal to its unadsorbed quantity in the effluent. Assuming a symmetric breakthrough curve,  $t^*$  can also be estimated as  $t^* = (t_s + t_b)/2$  (Monazam et al., 2013). Based on the above definition, in Eq. 4-16,  $\Phi$  is the portion of the bed capacity used for CO<sub>2</sub> capture when incipient breakthrough occurs at the column effluent ( $t=t_b$ ) (Beaver et al., 2009; García et al., 2011).

Table 4-10: Breakthrough curve characteristic parameters under different operating conditions

ID	T	Q	$t_{b(exp)}$	$t_{b(sim)}$	$t_{s(exp)}$	$t_{s(sim)}$	$L_{MTZ}$	$\Phi$	$q_{exp}$	$q_{sim}$
	(°C)	(ml min <sup>-1</sup> )	(min)	(min)	(min)	(min)	(cm)	-	(mol kg <sup>-1</sup> )	(mol kg <sup>-1</sup> )
GAC	30	50	3.3	3.3	7.0	6.9	14.37	0.64	0.28	0.28
GAC	45	50	2.7	2.7	5.6	5.5	13.97	0.65	0.21	0.21
GAC	60	50	1.6	1.6	3.2	3.1	13.33	0.67	0.12	0.12
GAC	30	100	1.5	1.5	3.4	3.5	15.51	0.61	0.26	0.27
GAC	45	100	1.1	1.1	2.4	2.5	14.86	0.63	0.19	0.20
GAC	60	100	0.7	0.7	1.5	1.5	14.54	0.64	0.11	0.11
OXA-GAC	30	50	10.9	10.8	13.5	13.3	4.26	0.89	0.67	0.63
OXA-GAC	45	50	9.7	9.6	11.9	11.8	4.07	0.90	0.57	0.55
OXA-GAC	60	50	8.3	8.2	10.0	9.9	3.72	0.91	0.46	0.45
OXA-GAC	30	100	4.4	4.4	6.4	6.4	7.40	0.81	0.60	0.60
OXA-GAC	45	100	3.9	4.0	5.6	5.7	7.16	0.82	0.51	0.52
OXA-GAC	60	100	3.3	3.3	4.7	4.8	7.00	0.83	0.40	0.41

#### 4.4.2.1 Effect of temperature on the breakthrough profile of CO<sub>2</sub> adsorption

The effect of temperature on the breakthrough curves of CO<sub>2</sub> adsorption on both of the studied adsorbents at feed rates of 50 and 100 ml min<sup>-1</sup> is illustrated in Fig. 4.13 As shown in this figure (and in Table 4.10), for both of the adsorbents and flow rates investigated, the CO<sub>2</sub> breakthrough times and dynamic adsorption capacities significantly decreased with increasing adsorption temperature due to the exothermic nature of the adsorption process (Auta & Hameed, 2014; Lua & Yang, 2009; Mulgundmath et al., 2012; Y. Zhao et al., 2012). However, the results indicated that compared with OXA-GAC, the breakthrough curves obtained by GAC shows a shorter breakthrough time with increasing temperature. The OXA-GAC exhibited a decrease in the breakthrough time with increasing temperature but not as pronounced as the time reduction observed for GAC in which the physisorption is the dominant feature. For example, under a feed rate of 50 ml



$\text{min}^{-1}$  (Fig. 4.13b), the breakthrough time by OXA-GAC exhibited a 25% decrease (from 10.9 s to 8.2 min) for an increase in temperature from 30 to 60 °C, whereas a decrease of 51% (from 3.3 s to 1.6 min) was observed for the GAC over the 30–60 °C temperature range (Fig. 4.13a). Similarly, compared with the GAC, the modified adsorbent exhibited a lower decrease in the equilibrium dynamic capacity with a rising temperature from 30 to 60 °C (31% decrease vs 57% decrease at 50  $\text{ml min}^{-1}$  and 33% decrease vs 58% decrease at 100  $\text{ml min}^{-1}$ ). A plausible interpretation of this observation is that in contrast to the expected reduction in the physisorption capacity of both of the adsorbents with increasing temperature, chemisorption through the nitrogen functionalities incorporated onto the surface of OXA-GAC aid the retention of the adsorption capacity at higher temperatures.

The findings are in accordance with the studies of García et al. and Thote et al. reporting that the breakthrough time and the dynamic  $\text{CO}_2$  adsorption capacity of a nitrogen-enriched carbon and a commercial activated carbon decreased with increasing temperature (García et al., 2011; Thote et al., 2010).

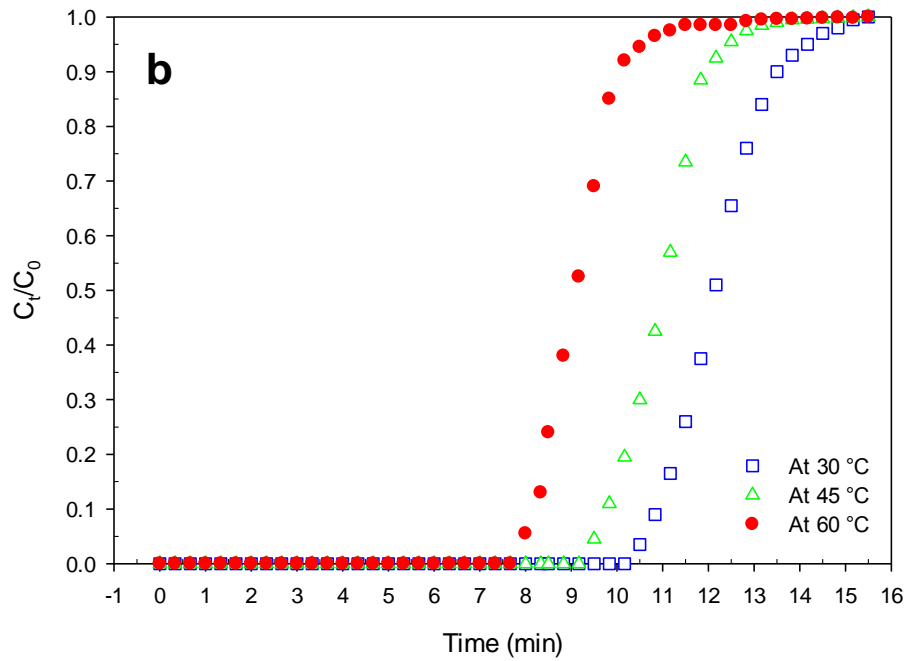
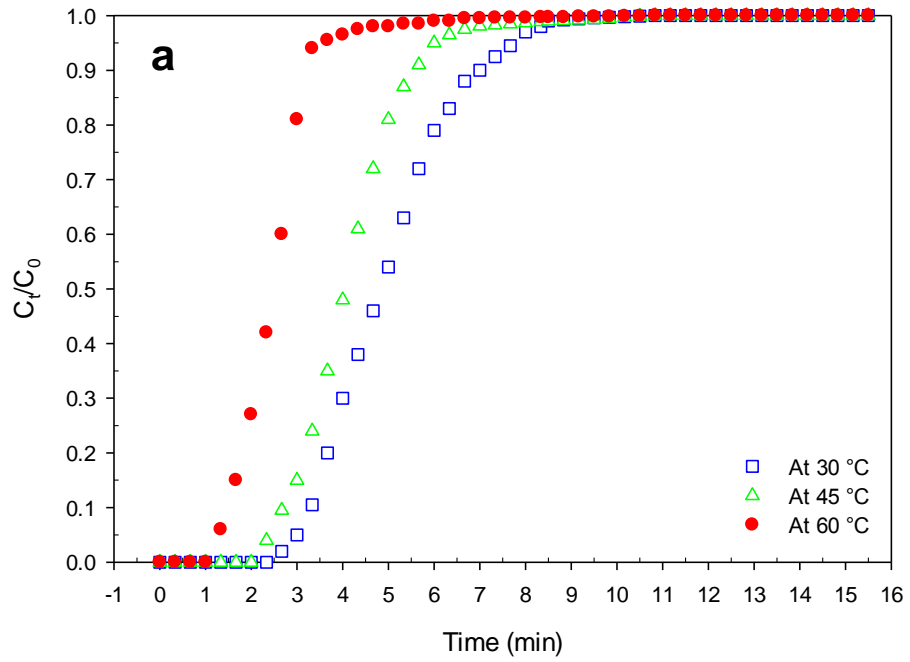
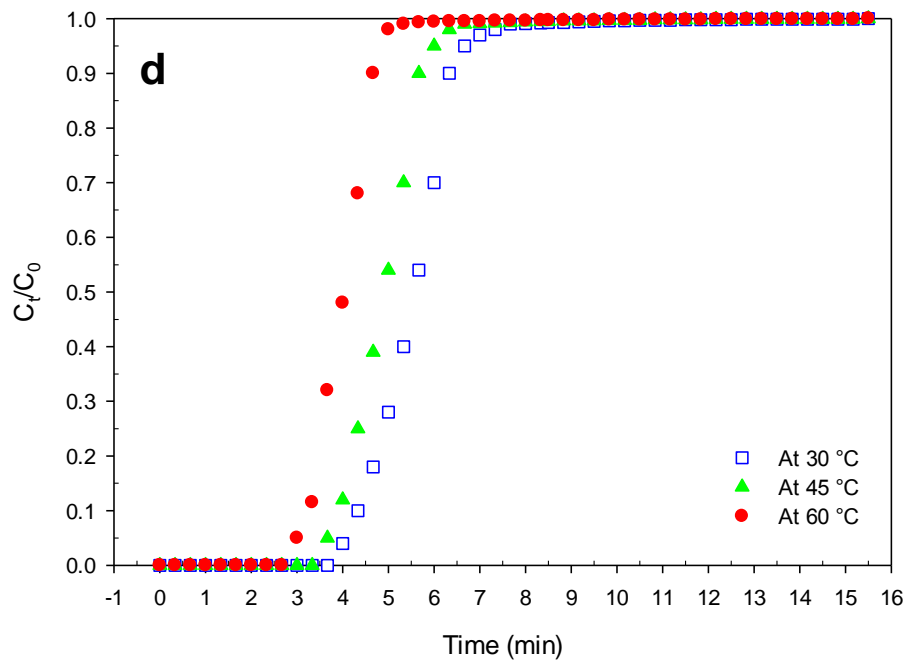
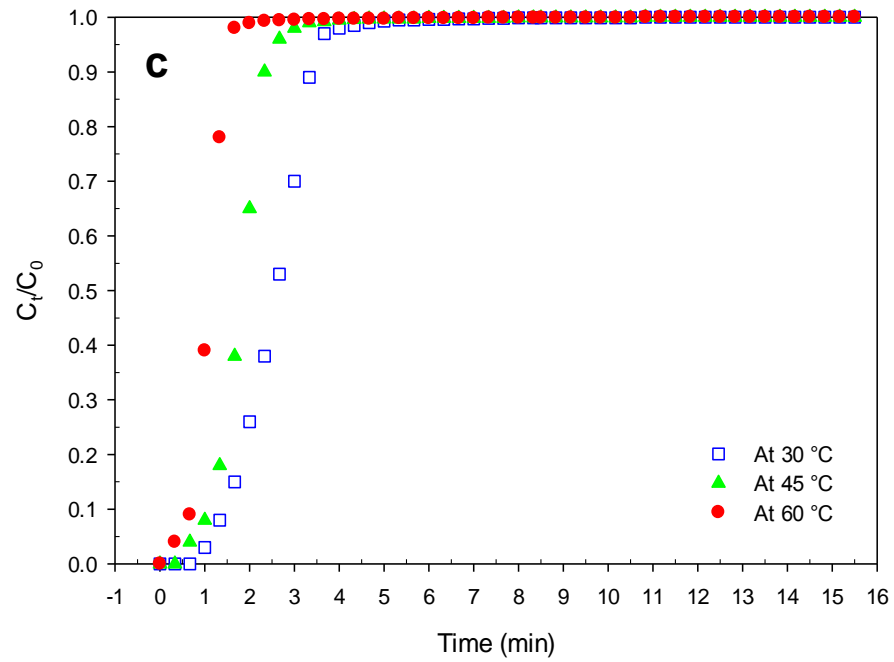


Figure 4.13: Effect of temperature on breakthrough curves of CO<sub>2</sub> adsorption onto (a) GAC and (b) OXA-GAC adsorbents at a 50 ml min<sup>-1</sup> feed flow rate and (c) GAC and (d) OXA-GAC at a 100 ml min<sup>-1</sup> feed flow rate.

'Figure 4.13, continued'



Moreover, for a given adsorbent sample and the feed flow rate studied, a lower adsorption temperature leads to longer saturation times. For example, at a feed flow rate of 100 ml  $\text{min}^{-1}$  when the temperature decreased from 60 to 30 °C, the time required to reach the saturation level increased from 1.5 to 3.4 min and from 4.7 to 6.4 min for the GAC and

the OXA-GAC adsorbents, respectively (Fig. 4.13 c and d). Notably, the slope of the OXA-GAC breakthrough curves was steeper than that obtained for the untreated sample. In addition, the breakthrough profile became steeper as the temperature increased. Therefore, the use of modified adsorbent and increasing temperatures favor mass transfer and decrease the mass transfer zone ( $L_{MTZ}$ ), consequently increasing the column efficiency ( $\Phi$ ) (Fig. 4.14). For example, the efficiency of the column packed with GAC adsorbent under a  $50 \text{ ml min}^{-1}$  feed flow rate at  $30 \text{ }^\circ\text{C}$  increased from 0.64 to 0.67 when the temperature increased to  $60 \text{ }^\circ\text{C}$ , whereas it increased to 0.89 when the OXA-GAC adsorbent was at  $30 \text{ }^\circ\text{C}$  and the same feed flow rate was used (Table 4.10). This observation is consistent with the results presented in section 4.4.1 in which the rate constants increased with increasing adsorption temperature and/or the use of a modified sample.

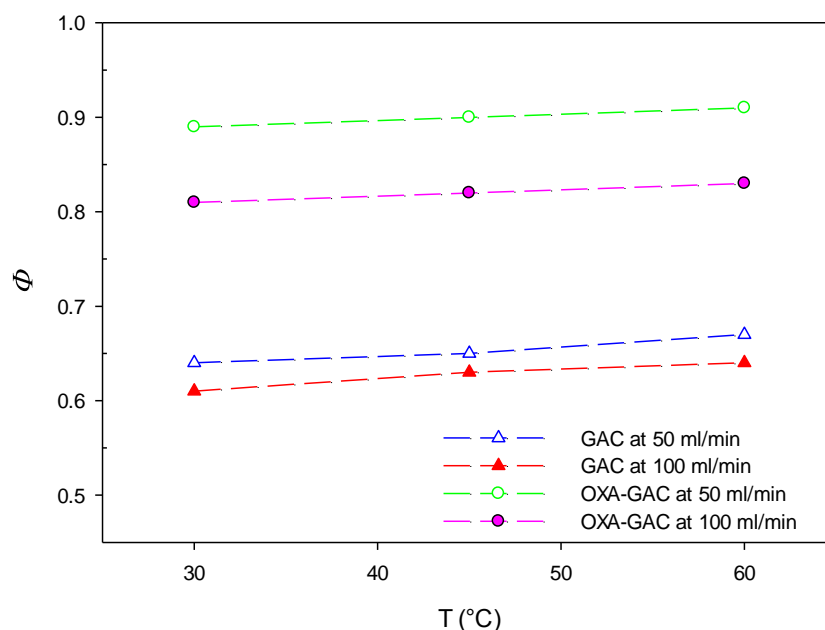


Figure 4.14: The efficiency of the adsorption bed for the breakthrough experiments with GAC and OXA-GAC adsorbents at varying adsorption temperatures and feed flowrates.

#### 4.4.2.2 Effect of feed flow rate on the breakthrough curve for the adsorption of CO<sub>2</sub>

Fig. 4.15 shows the effect of the feed flow rate on the breakthrough curves obtained at 30, 45, and 60 °C for both of the studied adsorbents. This figure and Table 4.10 show that for both of the adsorbents over the temperature range studied, a considerably shorter breakthrough and saturation time and a relatively steeper breakthrough curve were achieved as the flow rate increased. This result was obtained because with an increasing flow rate, the degree of turbulence and mixing increases, and breakthrough occurs faster with more adsorbate entering the bed per unit time (Lua & Yang, 2009; Monazam et al., 2013; Mulgundmath et al., 2012). A faster feed flow rate results in a higher Reynolds number and may cause the mass transfer zone to move faster, leading to a reduction in the column efficiency (Fig. 4.14). Conversely, the lower flow rate of the feed gas was accompanied by the slower transport of the adsorbate molecules, leading to a prolonged breakthrough time, thereby increasing the diffusion coefficient (Auta & Hameed, 2014). In line with this finding, for both of the adsorbents over the temperature range studied, the calculated values of the dynamic adsorption capacity decreased as the feed flow rate varied from 50 to 100 ml min<sup>-1</sup>. These observations are in accordance with those reported elsewhere (Ahmed, Mohammed, & Kadhum, 2011; Auta & Hameed, 2014; K.-S. Hwang et al., 2010; Sabouni, Kazemian, & Rohani, 2013). The use of OXA-GAC adsorbent at 60 °C (Table 6) resulted in the most significant decrease in the measured breakthrough time (from 8.3 s to approximately 3.3 min) and dynamic adsorption capacity (from 0.46 to approximately 0.4 mol kg<sup>-1</sup>) when the flow rate was increased from 50 to 100 ml min<sup>-1</sup>. Note that the enhanced adsorption capacity of the OXA-GAC adsorbent compared with the GAC sample at higher adsorption temperatures is primarily attributed to chemisorption with the attached nitrogen surface groups. Therefore, with an increasing flow rate and a decreasing residence time of the adsorbate in the bed, the observed chemisorption significantly decreases because the contact time for the CO<sub>2</sub> molecules to

react with the incorporated N-functionalities decreases. The results also indicated that at the tail-end part of the experimental breakthrough curves in which the  $c_t/c_0$  ratio reaches 1, the higher feed flow rates led to the slower approach of the ratio to unity compared with the lower flow rates (Fig. 4.15).

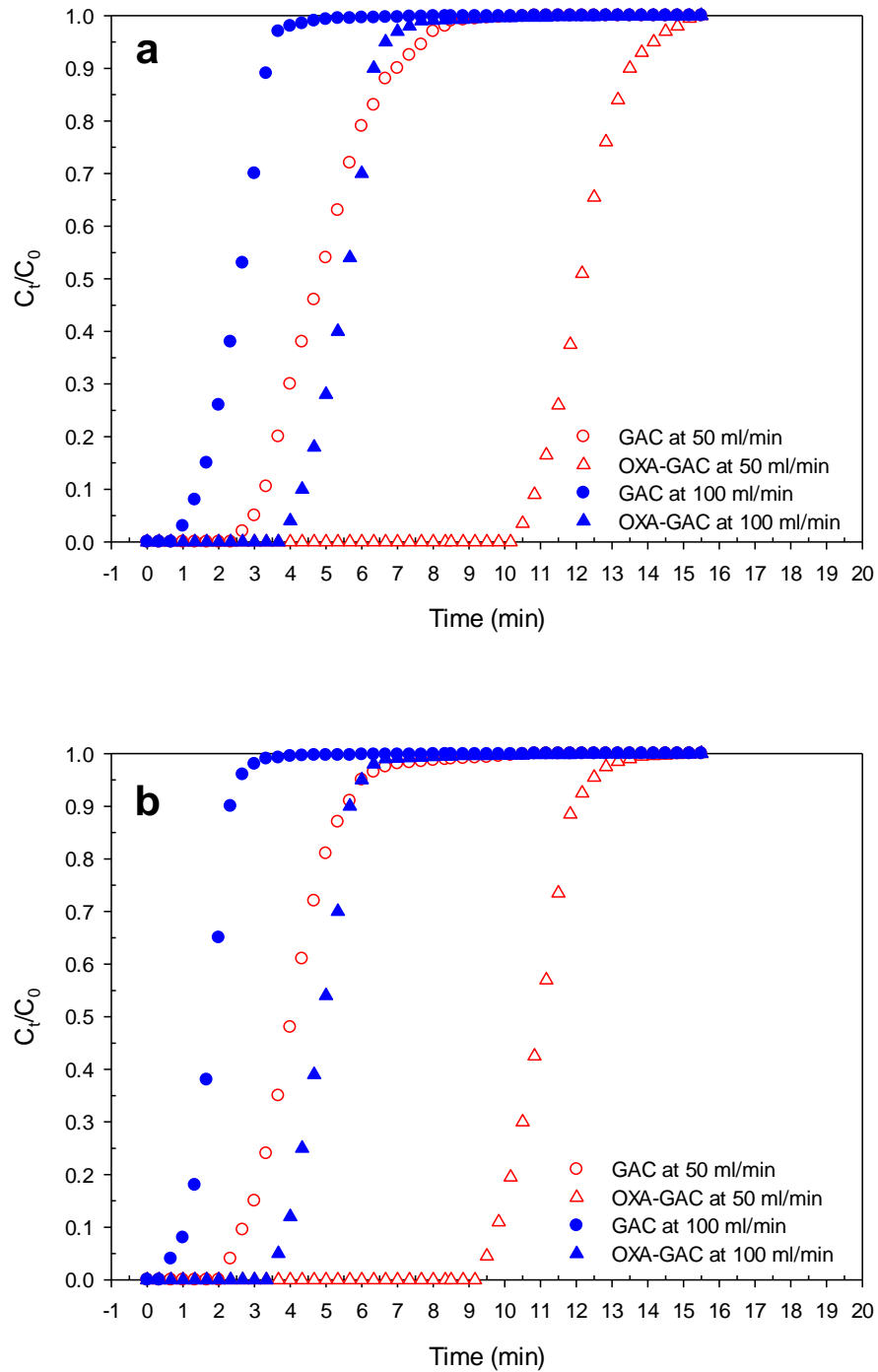
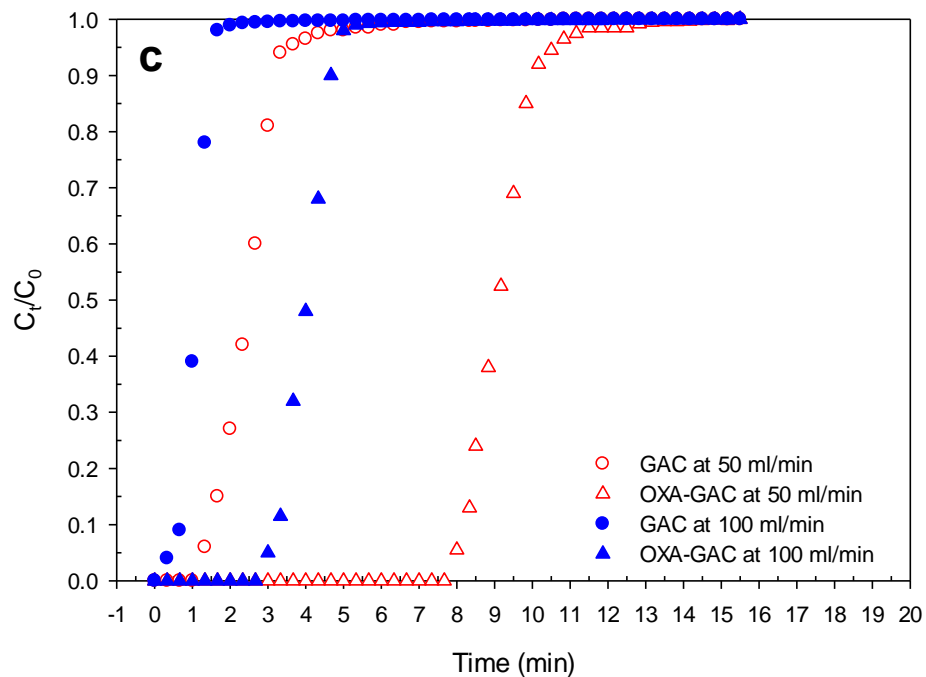


Figure 4.15: Effect of feed flow rate on breakthrough curves of CO<sub>2</sub> adsorption onto GAC and OXA-GAC adsorbents at (a) 30 °C (b) 45 °C and (c) 60 °C.

‘Figure 4.15, continued’



#### 4.4.2.3 Validation of the proposed model

The breakthrough curves were simulated using the adsorption bed characteristics and the model parameters presented in Tables 3.3 and 3.5, respectively. To test the validity of the proposed mathematical model, a series of experimental breakthrough profiles was compared with the theoretical breakthroughs for different adsorption temperatures, flow rates, and types of adsorbents. Fig. 4.16 illustrates the representative experimental data (discrete symbols) and the corresponding simulations (solid lines) under different operating conditions. An evaluation of the three verification cases demonstrates a reasonable agreement between the measured and simulated breakthrough curves over the entire  $c_t/c_0$  time. This result indicates that the estimated parameters and the hypothesis on which the model is based are valid for the system studied. However, a slight discrepancy was detected between the predicted and experimental breakthrough curves, which can be attributed to the experimental errors. The simulated values of the breakthrough time,

$t_{b(sim)}$ , exhibited relative error deviations of less than 2% from the experimental data,  $t_{b(exp)}$ , whereas relative error deviations of up to ca. 4% and 6% were observed in the estimation of the saturation time,  $t_{s(sim)}$ , and the maximum sorption capacity,  $q_{sim}$ , respectively (Table 4.10). Therefore, considering the level of accuracy achieved, it is deduced that the use of the proposed model based on the semi-empirical Toth equation for the adsorption equilibrium and the Avrami model for adsorption kinetics was suitable to describe the dynamics of CO<sub>2</sub> adsorption in a fixed bed packed with GAC and OXA-GAC adsorbents.

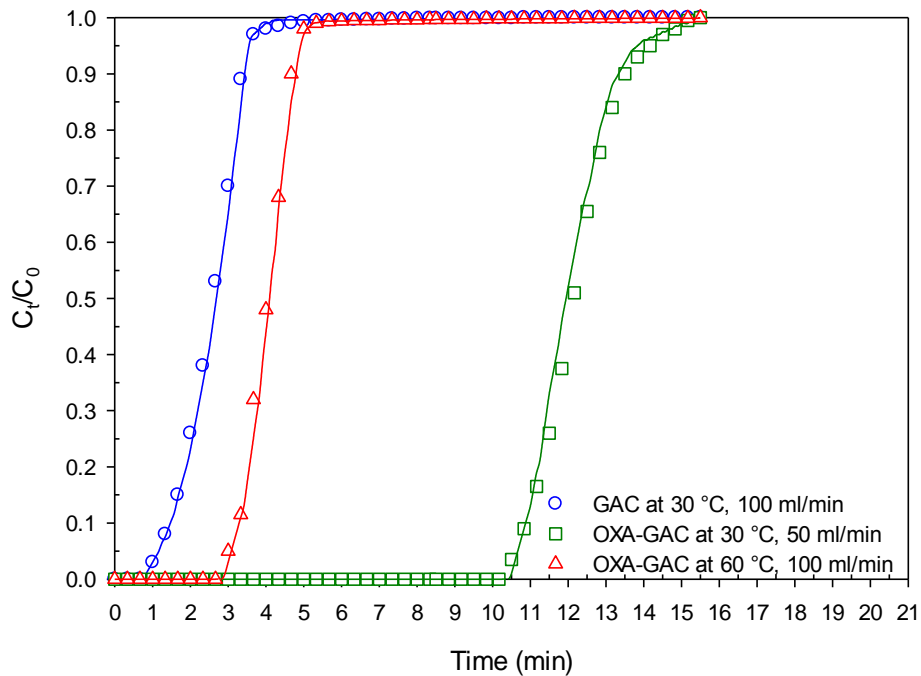


Figure 4.16: Verification of the proposed model with experimental breakthrough curves at three representative operating conditions. Discrete symbols are experimental data, and solid lines are predictions by the model.



## CHAPTER 5: CONCLUSION AND RECOMMENDATIONS

### 5.1 Conclusion

The first objective of this study was to optimize the amination conditions of activated carbon adsorbents in an effort to maximize their CO<sub>2</sub> adsorption/desorption capacities. The effects of amination temperature, amination time, and the type of starting materials (variables) on the CO<sub>2</sub> adsorption/desorption capacities of modified adsorbents (responses) were investigated using a central composite design. Among the process parameters studied, the temperature of ammonia treatment was found to have the most significant positive and negative influence on the CO<sub>2</sub> adsorption and desorption capacity, respectively. The use of a pre-oxidized sorbent as a starting material and amination at 425 °C for 2.1 h were found to be the optimum conditions for obtaining an efficient carbon dioxide adsorbent. This material exhibited CO<sub>2</sub> adsorption and desorption capacity values of 26.47 mg/g and 95.4%, respectively. The experimental values of the responses were found to agree satisfactorily with the values predicted by the models. This indicates that the second-order response surface models were suitable and sufficient to predict CO<sub>2</sub> adsorption/desorption capacities within the investigated range of chosen variables. The adsorption performance of the optimal adsorbent, as well as its desorption capacity under the investigated condition, remained essentially unchanged during cyclic adsorption/desorption operations.

The adsorption equilibria of carbon dioxide on an untreated GAC and its ammonia-modified counterpart were investigated over the temperature range of 303–333 K and up to pressures of 1 atm. Compared to untreated carbon, the OXA-GAC adsorbent exhibited a higher CO<sub>2</sub> uptake, particularly at low partial pressures. To distinguish the contribution of chemisorption and physisorption mechanisms to the overall CO<sub>2</sub> adsorption, we developed a semi-empirical equilibrium model. A non-linear regression method was

employed to estimate the best fitting parameters corresponding to the isotherm model. An analysis of the calculated statistical parameters indicated that the proposed model successfully fit the experimental data over the entire analyzed ranges of temperature and pressure. The initial isosteric enthalpy of adsorption calculated using the Clausius–Clapeyron equation indicated a sharp increase in CO<sub>2</sub>–adsorbent interaction after ammonia modification of the untreated adsorbent, consistent with a dramatic uptake of CO<sub>2</sub> at low partial pressures. The heats of adsorption calculated using the temperature-dependent parameters of the proposed model for physisorption and chemisorption of CO<sub>2</sub> onto the modified adsorbent were in excellent agreement with the heats of adsorption obtained from the experimental data.

The kinetics of CO<sub>2</sub> adsorption on ammonia-modified and untreated activated carbon adsorbents over the temperature range of 30–60 °C were studied using the pseudo-first-order, pseudo-second-order, and Avrami kinetic models. The best fit with the experimental kinetic data for both of the studied adsorbents was obtained by applying the Avrami kinetic model, with average relative errors of less than 2%. The kinetic rate constants of CO<sub>2</sub> capture on both of the adsorbents increased with increasing adsorption temperature. Fixed-bed breakthrough experiments for CO<sub>2</sub> adsorption onto the GAC and OXA-GAC adsorbents were performed by changing the adsorption temperature over the range of 30 to 60 °C and the feed flow rate from 50 to 100 ml min<sup>-1</sup>. An investigation of the effect of the column adsorption temperature, feed flow rate, and type of adsorbent revealed that using OXA-GAC adsorbent under the operating conditions of 30 °C under a 50 ml min<sup>-1</sup> feed flow resulted in the longest breakthrough time (10.9 min) and the highest breakthrough adsorption capacity (0.67 mol kg<sup>-1</sup>). In addition, to predict the breakthrough behavior of CO<sub>2</sub> adsorption in the fixed-bed column, a simple model was developed, including the Toth and Avrami equations to describe the equilibrium and kinetics of adsorption, respectively. The set of coupled differential equations was solved

using the finite element method implemented in computational fluid dynamics software. The validity of the model predictions was evaluated by a comparison with the experimental data. The results showed that the simulated breakthrough profiles reproduce the experimental breakthrough curves reasonably well under the different operating conditions examined.

## **5.2 Recommendations**

Based on the findings of this research, the following recommendations can be utilized for the development of future studies:

1. One of the typical variables in the design of an ammonia-modified adsorbent is the type of nitrogen containing functional groups. Considering the established role of the amine groups and pyridine-like functionalities on the high-temperature CO<sub>2</sub> adsorption performance of activated carbon, it could be of interest to explore other nitrogen-related modification techniques, which may produce adsorbents with interesting properties after optimization of synthesis conditions.
2. Although the concentration breakthrough curves were predicted very well by the proposed isothermal model, efforts could be placed to develop a non-isothermal model with the inclusion of the radial bed gradients. Since the energy and mass balances are tightly coupled, the radial temperature gradients created by a non-isothermal operation could have a significant effect on the concentration breakthrough curve.
3. For the flue gas separation, moisture is a bulk component which was not included in this study. Ternary mixture separations including moisture have to be incorporated in the experiments. The possibility of using layered adsorbent beds to target specific gas components should be investigated.

## REFERENCES

- Afzal, S., Rahimi, A., Ehsani, M. R., & Tavakoli, H. (2010). Modeling hydrogen fluoride adsorption by sodium fluoride. *Journal of Industrial and Engineering Chemistry*, 16(6), 978-985.
- Agarwal, A., Biegler, L. T., & Zitney, S. E. (2010a). Superstructure-Based Optimal Synthesis of Pressure Swing Adsorption Cycles for Precombustion CO<sub>2</sub> Capture. *Industrial & Engineering Chemistry Research*, 49(11), 5066-5079.
- Agarwal, A., Biegler, L. T., & Zitney, S. E. (2010b). A superstructure-based optimal synthesis of PSA cycles for post-combustion CO<sub>2</sub> capture. *AIChE Journal*, 56(7), 1813-1828.
- Ahmed, M., Mohammed, A. K., & Kadhum, A. (2011). Modeling of Breakthrough Curves for Adsorption of Propane, n-Butane, and Iso-Butane Mixture on 5A Molecular Sieve Zeolite. *Transport in Porous Media*, 86(1), 215-228.
- Ahn, H., Lee, C.-H., Seo, B., Yang, J., & Baek, K. (1999). Backfill Cycle of a Layered Bed H<sub>2</sub> PSA Process. *Adsorption*, 5(4), 419-433.
- Ahn, H., Yang, J., & Lee, C.-H. (2001). Effects of Feed Composition of Coke Oven Gas on a Layered Bed H<sub>2</sub> PSA Process. *Adsorption*, 7(4), 339-356.
- Aksu, Z., & Gönen, F. (2006). Binary biosorption of phenol and chromium(VI) onto immobilized activated sludge in a packed bed: Prediction of kinetic parameters and breakthrough curves. *Separation and Purification Technology*, 49(3), 205-216.
- Alpay, E., Kenney, C. N., & Scott, D. M. (1993). Simulation of rapid pressure swing adsorption and reaction processes. *Chemical Engineering Science*, 48(18), 3173-3186.
- Amini, M., Younesi, H., & Bahramifar, N. (2009). Biosorption of nickel(II) from aqueous solution by *Aspergillus niger*: Response surface methodology and isotherm study. *Chemosphere*, 75(11), 1483-1491.
- Amini, M., Younesi, H., Bahramifar, N., Lorestani, A. A. Z., Ghorbani, F., Daneshi, A., & Sharifzadeh, M. (2008). Application of response surface methodology for optimization of lead biosorption in an aqueous solution by *Aspergillus niger*. *Journal of Hazardous Materials*, 154(1-3), 694-702.
- An, H., Feng, B., & Su, S. (2009). CO<sub>2</sub> capture capacities of activated carbon fibre-phenolic resin composites. *Carbon*, 47(10), 2396-2405.
- Arenillas, A., Drage, T. C., Smith, K., & Snape, C. E. (2005). CO<sub>2</sub> removal potential of carbons prepared by co-pyrolysis of sugar and nitrogen containing compounds. *Journal of Analytical and Applied Pyrolysis*, 74(1-2), 298-306.

- Arenillas, A., Smith, K. M., Drage, T. C., & Snape, C. E. (2005). CO<sub>2</sub> capture using some fly ash-derived carbon materials. *Fuel*, 84(17), 2204-2210.
- Auta, M., & Hameed, B. H. (2014). Adsorption of carbon dioxide by diethanolamine activated alumina beads in a fixed bed. *Chemical Engineering Journal*, 253, 350-355.
- Azargohar, R., & Dalai, A. K. (2005). Production of activated carbon from Luscar char: Experimental and modeling studies. *Microporous and Mesoporous Materials*, 85(3), 219-225.
- Banik, R. M., Santhiagu, A., & Upadhyay, S. N. (2007). Optimization of nutrients for gellan gum production by *Sphingomonas paucimobilis* ATCC-31461 in molasses based medium using response surface methodology. *Bioresource Technology*, 98(4), 792-797.
- Bastos-Neto, M., Moeller, A., Staudt, R., Bohm, J., & Glaser, R. (2011). Dynamic bed measurements of CO adsorption on microporous adsorbents at high pressures for hydrogen purification processes. *Separation and Purification Technology*, 77(2), 251-260.
- Beaver, M. G., Caram, H. S., & Sircar, S. (2009). Selection of CO<sub>2</sub> chemisorbent for fuel-cell grade H<sub>2</sub> production by sorption-enhanced water gas shift reaction. *International Journal of Hydrogen Energy*, 34(7), 2972-2978.
- Belmabkhout, Y., & Sayari, A. (2009). Effect of pore expansion and amine functionalization of mesoporous silica on CO<sub>2</sub> adsorption over a wide range of conditions. *Adsorption*, 15(3), 318-328.
- Berenguer-Murcia, Á., Fletcher, A. J., García-Martínez, J., Cazorla-Amorós, D., Linares-Solano, Á., & Thomas, K. M. (2003). Probe Molecule Kinetic Studies of Adsorption on MCM-41. *The Journal of Physical Chemistry B*, 107(4), 1012-1020.
- Berlier, K., & Frère, M. (1996). Adsorption of CO<sub>2</sub> on Activated Carbon: Simultaneous Determination of Integral Heat and Isotherm of Adsorption. *Journal of Chemical & Engineering Data*, 41(5), 1144-1148.
- Bezerra, D., Oliveira, R., Vieira, R., Cavalcante, C., Jr., & Azevedo, D. S. (2011). Adsorption of CO<sub>2</sub> on nitrogen-enriched activated carbon and zeolite 13X. *Adsorption*, 17(1), 235-246.
- Bird, R. B., Stewart, W. E., & Lightfoot, E. N. (2002). *Transport Phenomena* (2nd ed.). New York: John Wiley & Sons, Inc.
- Boehm, H. P., Mair, G., Stoehr, T., De Rincón, A. R., & Tereczki, B. (1984). Carbon as a catalyst in oxidation reactions and hydrogen halide elimination reactions. *Fuel*, 63(8), 1061-1063.
- Bonnot, K., Tondeur, D., & Luo, L. A. (2006). Effects of Composition, Temperature and Purge on the Performance of the Cyclic Adsorption of CO<sub>2</sub> and CH<sub>4</sub> on Activated Carbon. *Chemical Engineering Research and Design*, 84(3), 192-208.

- Borah, J. M., Sarma, J., & Mahiuddin, S. (2011). Adsorption comparison at the  $\alpha$ -alumina/water interface: 3,4-Dihydroxybenzoic acid vs. catechol. *Colloids and Surfaces A: Physicochemical and Engineering Aspects*, 387(1–3), 50-56.
- Bota, K. B., & Abotsi, G. M. K. (1994). Ammonia: a reactive medium for catalysed coal gasification. *Fuel*, 73(8), 1354-1357.
- Brandani, F., Rouse, A., Brandani, S., & Ruthven, D. M. (2004). Adsorption Kinetics and Dynamic Behavior of a Carbon Monolith. *Adsorption*, 10(2), 99-109.
- Buzanowski, M. A., & Yang, R. T. (1989). Extended linear driving-force approximation for intraparticle diffusion rate including short times. *Chemical Engineering Science*, 44(11), 2683-2689.
- Can, M. Y., Kaya, Y., & Algur, O. F. (2006). Response surface optimization of the removal of nickel from aqueous solution by cone biomass of *Pinus sylvestris*. *Bioresource Technology*, 97(14), 1761-1765.
- Carta, G. (2003). Adsorption Calculations Using the Film Model Approximation for Intraparticle Mass Transfer. *Adsorption*, 9(1), 55-65.
- Carta, G., & Cincotti, A. (1998). Film model approximation for non-linear adsorption and diffusion in spherical particles. *Chemical Engineering Science*, 53(19), 3483-3488.
- Cavenati, S., Grande, C. A., & Rodrigues, A. E. (2004). Adsorption Equilibrium of Methane, Carbon Dioxide, and Nitrogen on Zeolite 13X at High Pressures. *Journal of Chemical & Engineering Data*, 49(4), 1095-1101.
- Cavenati, S., Grande, C. A., & Rodrigues, A. E. (2005). Upgrade of Methane from Landfill Gas by Pressure Swing Adsorption. *Energy & Fuels*, 19(6), 2545-2555.
- Cen, P., & Yang, R. T. (1985). Separation of a Five-Component Gas Mixture by Pressure Swing Adsorption. *Separation Science and Technology*, 20(9-10), 725-747.
- Cestari, A. R., Vieira, E. F. S., Vieira, G. S., & Almeida, L. E. (2006). The removal of anionic dyes from aqueous solutions in the presence of anionic surfactant using aminopropylsilica—A kinetic study. *Journal of Hazardous Materials*, 138(1), 133-141.
- Chaffee, A. L., Knowles, G. P., Liang, Z., Zhang, J., Xiao, P., & Webley, P. A. (2007). CO<sub>2</sub> capture by adsorption: Materials and process development. *International Journal of Greenhouse Gas Control*, 1(1), 11-18.
- Chahbani, M. H., & Tondeur, D. (2000). Mass transfer kinetics in pressure swing adsorption. *Separation and Purification Technology*, 20(2-3), 185-196.
- Chan, Y. N. I., Hill, F. B., & Wong, Y. W. (1981). Equilibrium theory of a pressure swing adsorption process. *Chemical Engineering Science*, 36(2), 243-251.
- Chihara, K., Suzuki, M., & Kawazoe, K. (1978). Adsorption rate on molecular sieving carbon by chromatography. *AIChE Journal*, 24(2), 237-246.

- Chilton, T. H., & Colburn, A. P. (1934). Mass Transfer (Absorption) Coefficients Prediction from Data on Heat Transfer and Fluid Friction. *Industrial & Engineering Chemistry*, 26(11), 1183-1187.
- Choi, W.-K., Kwon, T.-I., Yeo, Y.-K., Lee, H., Song, H., & Na, B.-K. (2003). Optimal operation of the pressure swing adsorption (PSA) process for CO<sub>2</sub> recovery. *Korean Journal of Chemical Engineering*, 20(4), 617-623.
- Chou, C.-T., & Chen, C.-Y. (2004). Carbon dioxide recovery by vacuum swing adsorption. *Separation and Purification Technology*, 39(1-2), 51-65.
- Chue, K. T., Kim, J. N., Yoo, Y. J., Cho, S. H., & Yang, R. T. (1995). Comparison of Activated Carbon and Zeolite 13X for CO<sub>2</sub> Recovery from Flue Gas by Pressure Swing Adsorption. *Industrial & Engineering Chemistry Research*, 34(2), 591-598.
- Clausse, M., Bonjour, J., & Meunier, F. (2004). Adsorption of gas mixtures in TSA adsorbers under various heat removal conditions. *Chemical Engineering Science*, 59(17), 3657-3670.
- Da Silva, F., Silva, J. A., & Rodrigues, A. r. (1999). A General Package for the Simulation of Cyclic Adsorption Processes. *Adsorption*, 5(3), 229-244.
- Dantas, T. L. P., Amorim, S. M., Luna, F. M. T., Silva, I. J., de Azevedo, D. C. S., Rodrigues, A. E., & Moreira, R. F. P. M. (2009). Adsorption of carbon dioxide onto activated carbon and nitrogen-enriched activated carbon: Surface changes, equilibrium, and modeling of fixed-bed Adsorption. *Separation Science and Technology*, 45(1), 73-84.
- Dantas, T. L. P., Luna, F. M. T., Silva Jr, I. J., de Azevedo, D. C. S., Grande, C. A., Rodrigues, A. E., & Moreira, R. F. P. M. (2011). Carbon dioxide-nitrogen separation through adsorption on activated carbon in a fixed bed. *Chemical Engineering Journal*, 169(1-3), 11-19.
- Dantas, T. L. P., Luna, F. M. T., Silva Jr, I. J., Torres, A. E. B., de Azevedo, D. C. S., Rodrigues, A. E., & Moreira, R. F. P. M. (2011). Modeling of the fixed - bed adsorption of carbon dioxide and a carbon dioxide - nitrogen mixture on zeolite 13X. *Brazilian Journal of Chemical Engineering*, 28, 533-544.
- Dastgheib, S. A., Karanfil, T., & Cheng, W. (2004). Tailoring activated carbons for enhanced removal of natural organic matter from natural waters. *Carbon*, 42(3), 547-557.
- Delgado, J. A., Uguina, M. A., Sotelo, J. L., & Ruiz, B. (2006). Fixed-bed adsorption of carbon dioxide-helium, nitrogen-helium and carbon dioxide-nitrogen mixtures onto silicalite pellets. *Separation and Purification Technology*, 49(1), 91-100.
- Delgado, J. A., Uguina, M. A., Sotelo, J. L., Ruiz, B., & Gomez, J. M. (2006). Fixed-bed adsorption of carbon dioxide/methane mixtures on silicalite pellets. *Adsorption*, 12(1), 5-18.

- Delgado, J. A., Uguina, M. A., Sotelo, J. L., Ruiz, B., & Rosario, M. (2007). Carbon Dioxide/Methane Separation by Adsorption on Sepiolite. *Journal of Natural Gas Chemistry*, 16(3), 235-243.
- Delgado, J. A., Uguina, M. A., Sotelo, J. L., Ruiz, B., & Rosario, M. (2007). Separation of carbon dioxide/methane mixtures by adsorption on a basic resin. *Adsorption*, 13(3-4), 373-383.
- Diagne, D., Goto, M., & Hirose, T. (1996). Numerical analysis of a dual refluxed PSA process during simultaneous removal and concentration of carbon dioxide dilute gas from air. *Journal of Chemical Technology & Biotechnology*, 65(1), 29-38.
- Ding, Y., & Alpay, E. (2000). Equilibria and kinetics of CO<sub>2</sub> adsorption on hydrotalcite adsorbent. *Chemical Engineering Science*, 55(17), 3461-3474.
- Do, D. D. (1998a). Adsorption analysis *Adsorption Analysis: Equilibria and Kinetics*. London: Imperial College Press.
- Do, D. D. (1998b). Analysis of Adsorption Kinetics in a Zeolite Particle *Adsorption Analysis: Equilibria and Kinetics*. London: Imperial College Press.
- Do, D. D., & Rice, R. G. (1986). Validity of the parabolic profile assumption in adsorption studies. *AIChE Journal*, 32(1), 149-154.
- Do, D. D., & Wang, K. (1998). A new model for the description of adsorption kinetics in heterogeneous activated carbon. *Carbon*, 36(10), 1539-1554.
- Do, H. D., & Do, D. D. (1998). Maxwell-Stefan analysis of multicomponent transient diffusion in a capillary and adsorption of hydrocarbons in activated carbon particle. *Chemical Engineering Science*, 53(6), 1239-1252.
- Doong, S. J., & Yang, R. T. (1986). Bulk separation of multicomponent gas mixtures by pressure swing adsorption: Pore/surface diffusion and equilibrium models. *AIChE Journal*, 32(3), 397-410.
- Doong, S. J., & Yang, R. T. (1987). Bidisperse pore diffusion model for zeolite pressure swing adsorption. *AIChE Journal*, 33(6), 1045-1049.
- Drage, T. C., Arenillas, A., Smith, K. M., Pevida, C., Piippo, S., & Snape, C. E. (2007). Preparation of carbon dioxide adsorbents from the chemical activation of urea-formaldehyde and melamine-formaldehyde resins. *Fuel*, 86(1-2), 22-31.
- Dreisbach, F., Staudt, R., & Keller, J. U. (1999). *Experimental investigation of the kinetics of adsorption of pure gases and binary gas mixtures on activated carbon*. Paper presented at the Fundamentals of Adsorption 6 (FoA6), Paris.
- Esteves, I. A. A. C., Lopes, M. S. S., Nunes, P. M. C., & Mota, J. P. B. (2008). Adsorption of natural gas and biogas components on activated carbon. *Separation and Purification Technology*, 62(2), 281-296.
- Farooq, S., & Ruthven, D. M. (1990). Heat effects in adsorption column dynamics. 2. Experimental validation of the one-dimensional model. *Industrial & Engineering Chemistry Research*, 29(6), 1084-1090.



- Farooq, S., Hassan, M. M., & Ruthven, D. M. (1988). Heat effects in pressure swing adsorption systems. *Chemical Engineering Science*, 43(5), 1017-1031.
- Farooq, S., Qinglin, H., & Karimi, I. A. (2001). Identification of Transport Mechanism in Adsorbent Micropores from Column Dynamics. *Industrial & Engineering Chemistry Research*, 41(5), 1098-1106.
- Fernandez, G. F., & Kenney, C. N. (1983). Modelling of the pressure swing air separation process. *Chemical Engineering Science*, 38(6), 827-834.
- Ferraro, V., Cruz, I. B., Jorge, R. F., Pintado, M. E., & Castro, P. M. L. (2013). Effects of Physical Parameters onto Adsorption of the Borderline Amino Acids Glycine, Lysine, Taurine, and Tryptophan upon Amberlite XAD16 Resin. *Journal of Chemical & Engineering Data*, 58(3), 707-717.
- Foo, K. Y., & Hameed, B. H. (2010). Insights into the modeling of adsorption isotherm systems. *Chemical Engineering Journal*, 156(1), 2-10.
- Frigon, N. L., & Mathews, D. (1997). *Practical Guide to Experimental Design*: John Wiley and Sons, New York, USA.
- Garcés, S. I., Villarroel-Rocha, J., Sapag, K., Korili, S. A., & Gil, A. (2013). Comparative Study of the Adsorption Equilibrium of CO<sub>2</sub> on Microporous Commercial Materials at Low Pressures. *Industrial & Engineering Chemistry Research*, 52(20), 6785-6793.
- García, S., Gil, M. V., Martín, C. F., Pis, J. J., Rubiera, F., & Pevida, C. (2011). Breakthrough adsorption study of a commercial activated carbon for pre-combustion CO<sub>2</sub> capture. *Chemical Engineering Journal*, 171(2), 549-556.
- Garg, U. K., Kaur, M. P., Garg, V. K., & Sud, D. (2008). Removal of Nickel(II) from aqueous solution by adsorption on agricultural waste biomass using a response surface methodological approach. *Bioresource Technology*, 99(5), 1325-1331.
- Ghafari, S., Aziz, H. A., Isa, M. H., & Zinatizadeh, A. A. (2009). Application of response surface methodology (RSM) to optimize coagulation-flocculation treatment of leachate using poly-aluminum chloride (PAC) and alum. *Journal of Hazardous Materials*, 163(2-3), 650-656.
- Gholami, M., & Talaie, M. R. (2009). Investigation of Simplifying Assumptions in Mathematical Modeling of Natural Gas Dehydration Using Adsorption Process and Introduction of a New Accurate LDF Model. *Industrial & Engineering Chemistry Research*, 49(2), 838-846.
- Glueckauf, E. (1955). Theory of chromatography. Part 10.-Formulae for diffusion into spheres and their application to chromatography. *Transactions of the Faraday Society*, 51(0), 1540-1551.
- Glueckauf, E., & Coates, J. I. (1947). 241. Theory of chromatography. Part IV. The influence of incomplete equilibrium on the front boundary of chromatograms and on the effectiveness of separation. *Journal of the Chemical Society (Resumed)*, 0(0), 1315-1321.

- Gomes, V. G., & Yee, K. W. K. (2002). Pressure swing adsorption for carbon dioxide sequestration from exhaust gases. *Separation and Purification Technology*, 28(2), 161-171.
- Gönen, F., & Aksu, Z. (2008). Use of response surface methodology (RSM) in the evaluation of growth and copper(II) bioaccumulation properties of *Candida utilis* in molasses medium. *Journal of Hazardous Materials*, 154(1-3), 731-738.
- Grande, C. A., & Rodrigues, A. E. (2004). Adsorption Kinetics of Propane and Propylene in Zeolite 4A. *Chemical Engineering Research and Design*, 82(12), 1604-1612.
- Grande, C. A., & Rodrigues, A. E. (2007). Layered Vacuum Pressure-Swing Adsorption for Biogas Upgrading. *Industrial & Engineering Chemistry Research*, 46(23), 7844-7848.
- Grande, C. A., & Rodrigues, A. E. (2008). Electric Swing Adsorption for CO<sub>2</sub> removal from flue gases. *International Journal of Greenhouse Gas Control*, 2(2), 194-202.
- Grande, C. A., & Rodrigues, A. r. E. (2005). Propane/Propylene Separation by Pressure Swing Adsorption Using Zeolite 4A. *Industrial & Engineering Chemistry Research*, 44(23), 8815-8829.
- Grande, C. A., Cavenati, S., Barcia, P., Hammer, J., Fritz, H. G., & Rodrigues, A. r. E. (2006). Adsorption of propane and propylene in zeolite 4A honeycomb monolith. *Chemical Engineering Science*, 61(10), 3053-3067.
- Grande, C. A., Lopes, F. V. S., Ribeiro, A. M., Loureiro, J. M., & Rodrigues, A. E. (2008). Adsorption of Off-Gases from Steam Methane Reforming (H<sub>2</sub>, CO<sub>2</sub>, CH<sub>4</sub>, CO and N<sub>2</sub>) on Activated Carbon. *Separation Science and Technology*, 43(6), 1338-1364.
- Gray, M. L., Soong, Y., Champagne, K. J., Baltrus, J., Stevens Jr, R. W., Toochinda, P., & Chuang, S. S. C. (2004). CO<sub>2</sub> capture by amine-enriched fly ash carbon sorbents. *Separation and Purification Technology*, 35(1), 31-36.
- Gray, M. L., Soong, Y., Champagne, K. J., Pennline, H., Baltrus, J. P., Stevens Jr, R. W., Filburn, T. (2005). Improved immobilized carbon dioxide capture sorbents. *Fuel Processing Technology*, 86(14-15), 1449-1455.
- Hameed, B. H., Tan, I. A. W., & Ahmad, A. L. (2008). Optimization of basic dye removal by oil palm fibre-based activated carbon using response surface methodology. *Journal of Hazardous Materials*, 158(2-3), 324-332.
- Hao, G.-P., Li, W.-C., Qian, D., & Lu, A.-H. (2010). Rapid Synthesis of Nitrogen-Doped Porous Carbon Monolith for CO<sub>2</sub> Capture. *Advanced Materials*, 22(7), 853-857.
- Hassan, M. M., Ruthven, D. M., & Raghavan, N. S. (1986). Air separation by pressure swing adsorption on a carbon molecular sieve. *Chemical Engineering Science*, 41(5), 1333-1343.
- Haul, R., & Stremming, H. (1984). Nonisothermal sorption kinetics in porous adsorbents. *Journal of Colloid and Interface Science*, 97(2), 348-355.

- Heydari-Gorji, A., & Sayari, A. (2011). CO<sub>2</sub> capture on polyethylenimine-impregnated hydrophobic mesoporous silica: Experimental and kinetic modeling. *Chemical Engineering Journal*, 173(1), 72-79.
- Himeno, S., Komatsu, T., & Fujita, S. (2005). High-Pressure Adsorption Equilibria of Methane and Carbon Dioxide on Several Activated Carbons. *Journal of Chemical & Engineering Data*, 50(2), 369-376.
- Himeno, S., Tomita, T., Suzuki, K., & Yoshida, S. (2007). Characterization and selectivity for methane and carbon dioxide adsorption on the all-silica DD3R zeolite. *Microporous and Mesoporous Materials*, 98(1-3), 62-69.
- Ho, M. T., Allinson, G. W., & Wiley, D. E. (2008). Reducing the Cost of CO<sub>2</sub> Capture from Flue Gases Using Pressure Swing Adsorption. *Industrial & Engineering Chemistry Research*, 47(14), 4883-4890.
- Ho, Y. S., Porter, J. F., & McKay, G. (2002). Equilibrium Isotherm Studies for the Sorption of Divalent Metal Ions onto Peat: Copper, Nickel and Lead Single Component Systems. *Water, Air, and Soil Pollution*, 141(1-4), 1-33.
- Ho, Y. S. (2004). Selection of optimum sorption isotherm. *Carbon*, 42(10), 2115-2116.
- Ho, Y. S. (2006). Review of second-order models for adsorption systems. *Journal of Hazardous Materials*, 136(3), 681-689.
- Hu, X., & Do, D. D. (1995). Validity of isothermality in adsorption kinetics of gases in bidispersed solids. *AIChE Journal*, 41(6), 1581-1584.
- Huang, C. C., & Fair, J. R. (1988). Study of the adsorption and desorption of multiple adsorbates in a fixed bed. *AIChE Journal*, 34(11), 1861-1877.
- Hwang, K. S., & Lee, W. K. (1994). The adsorption and desorption breakthrough behavior of carbon monoxide and carbon dioxide on activated carbon. Effect of total pressure and pressure-dependent mass transfer coefficients. *Separation Science and Technology*, 29(14), 1857-1891.
- Hwang, K. S., Jun, J. H., & Lee, W. K. (1995). Fixed-bed adsorption for bulk component system. Non-equilibrium, non-isothermal and non-adiabatic model. *Chemical Engineering Science*, 50(5), 813-825.
- Hwang, K. S., Son, Y. S., Park, S. W., Park, D. W., Oh, K. J., & Kim, S. S. (2010). Adsorption of Carbon Dioxide onto EDA-CP-MS41. *Separation Science and Technology*, 45(1), 85-93.
- Incropera, F. P., & Witt, D. P. D. (1996). *Fundamentals of Heat and Mass Transfer* (4th ed.). New York: John Wiley & Sons.
- Jadhav, P. D., Chatti, R. V., Biniwale, R. B., Labhsetwar, N. K., Devotta, S., & Rayalu, S. S. (2007). Monoethanol Amine Modified Zeolite 13X for CO<sub>2</sub> Adsorption at Different Temperatures. *Energy & Fuels*, 21(6), 3555-3559.
- Jansen, R. J. J., & van Bekkum, H. (1994). Amination and ammoxidation of activated carbons. *Carbon*, 32(8), 1507-1516.

- Jansen, R. J. J., & van Bekkum, H. (1995). XPS of nitrogen-containing functional groups on activated carbon. *Carbon*, 33(8), 1021-1027.
- Jee, J. G., Park, H. J., Haam, S. J., & Lee, C. H. (2002). Effects of Nonisobaric and Isobaric Steps on O<sub>2</sub> Pressure Swing Adsorption for an Aerator. *Industrial & Engineering Chemistry Research*, 41(17), 4383-4392.
- Jin, X., Malek, A., & Farooq, S. (2006). Production of Argon from an Oxygen-Argon Mixture by Pressure Swing Adsorption. *Industrial & Engineering Chemistry Research*, 45(16), 5775-5787.
- Kapoor, A., & Yang, R. T. (1989). Kinetic separation of methane-carbon dioxide mixture by adsorption on molecular sieve carbon. *Chemical Engineering Science*, 44(8), 1723-1733.
- Kapoor, A., & Yang, R. T. (1990). Surface diffusion on energetically heterogeneous surfaces-an effective medium approximation approach. *Chemical Engineering Science*, 45(11), 3261-3270.
- Karger, J., & Ruthven, D. M. (1992). *Diffusion in Zeolites and Other Microporous Solids* New York: Wiley.
- Kawazoe, K., Suzuki, M., & Chihara, K. (1974). Chromatographic study of diffusion in molecular-sieving carbon. *Journal of chemical engineering of Japan*, 7(3), 151-157.
- Khalighi, M., Farooq, S., & Karimi, I. A. (2012). Nonisothermal Pore Diffusion Model for a Kinetically Controlled Pressure Swing Adsorption Process. *Industrial & Engineering Chemistry Research*, 51(32), 10659-10670.
- Khuri, A. I., & Cornell, J. A. (1996). *Response Surfaces, Design and Analyses* (2nd ed.): Marcel Dekker Inc., New York.
- Kikkinides, E. S., Yang, R. T., & Cho, S. H. (1993). Concentration and recovery of carbon dioxide from flue gas by pressure swing adsorption. *Industrial & Engineering Chemistry Research*, 32(11), 2714-2720.
- Kim, D. H. (1990). Single effective diffusivities for dynamic adsorption in bidisperse adsorbents. *AIChE Journal*, 36(2), 302-306.
- Kim, M. B., Bae, Y. S., Choi, D.-K., & Lee, C.-H. (2006). Kinetic Separation of Landfill Gas by a Two-Bed Pressure Swing Adsorption Process Packed with Carbon Molecular Sieve: Nonisothermal Operation. *Industrial & Engineering Chemistry Research*, 45(14), 5050-5058.
- Kim, M.-B., Moon, J.-H., Lee, C.-H., Ahn, H., & Cho, W. (2004). Effect of heat transfer on the transient dynamics of temperature swing adsorption process. *Korean Journal of Chemical Engineering*, 21(3), 703-711.
- Knaebel, K. S., & Hill, F. B. (1985). Pressure swing adsorption: Development of an equilibrium theory for gas separations. *Chemical Engineering Science*, 40(12), 2351-2360.

- Knowles, G. P., Delaney, S. W., & Chaffee, A. L. (2006). Diethylenetriamine[propyl(silyl)]-Functionalized (DT) Mesoporous Silicas as CO<sub>2</sub> Adsorbents. *Industrial & Engineering Chemistry Research*, 45(8), 2626-2633.
- Ko, D., Siriwardane, R., & Biegler, L. T. (2003). Optimization of a Pressure-Swing Adsorption Process Using Zeolite 13X for CO<sub>2</sub> Sequestration. *Industrial & Engineering Chemistry Research*, 42(2), 339-348.
- Ko, D., Siriwardane, R., & Biegler, L. T. (2005). Optimization of Pressure Swing Adsorption and Fractionated Vacuum Pressure Swing Adsorption Processes for CO<sub>2</sub> Capture. *Industrial & Engineering Chemistry Research*, 44(21), 8084-8094.
- Körbahti, B. K. (2007). Response surface optimization of electrochemical treatment of textile dye wastewater. *Journal of Hazardous Materials*, 145(1-2), 277-286.
- Körbahti, B. K., & Rauf, M. A. (2008a). Application of response surface analysis to the photolytic degradation of Basic Red 2 dye. *Chemical Engineering Journal*, 138(1-3), 166-171.
- Körbahti, B. K., & Rauf, M. A. (2008b). Response surface methodology (RSM) analysis of photoinduced decoloration of toluidine blue. *Chemical Engineering Journal*, 136(1), 25-30.
- Körbahti, B. K., & Rauf, M. A. (2009). Determination of optimum operating conditions of carmine decoloration by UV/H<sub>2</sub>O<sub>2</sub> using response surface methodology. *Journal of Hazardous Materials*, 161(1), 281-286.
- Kumar, K. V., & Sivanesan, S. (2006). Selection of optimum sorption kinetics: Comparison of linear and non-linear method. *Journal of Hazardous Materials*, 134(1-3), 277-279.
- Kusic, H., Jovic, M., Kos, N., Koprivanac, N., & Marin, V. (2010). The comparison of photooxidation processes for the minimization of organic load of colored wastewater applying the response surface methodology. *Journal of Hazardous Materials*, 183(1-3), 189-202.
- Lai, C. C., & Tan, C. S. (1991). Approximate models for nonlinear adsorption in a packed-bed adsorber. *AIChE Journal*, 37(3), 461-465.
- Lamia, N., Wolff, L., Leflaive, P., Leinekugel-Le-Cocq, D., Sa Gomes, P., Grande, C. A., & Rodrigues, A. E. (2008). Equilibrium and fixed bed adsorption of 1-butene, propylene and propane over 13X Zeolite Pellets. *Separation Science and Technology*, 43(5), 1124-1156.
- Leci, C. L. (1996). Financial implications on power generation costs resulting from the parasitic effect of CO<sub>2</sub> capture using liquid scrubbing technology from power station flue gases. *Energy Conversion and Management*, 37(6-8), 915-921.
- Lee, C. H., Yang, J., & Ahn, H. (1999). Effects of carbon-to-zeolite ratio on layered bed H<sub>2</sub> PSA for coke oven gas. *AIChE Journal*, 45(3), 535-545.

- Lee, J., & Kim, D. H. (1998). High-order approximations for noncyclic and cyclic adsorption in a particle. *Chemical Engineering Science*, 53(6), 1209-1221.
- Lee, L. K., & Ruthven, D. M. (1979). Analysis of thermal effects in adsorption rate measurements. *Journal of the Chemical Society, Faraday Transactions 1*, 75(0), 2406-2422.
- Leinekugel-le-Cocq, D., Tayakout-Fayolle, M. I., Le Gorrec, Y., & Jallut, C. (2007). A double linear driving force approximation for non-isothermal mass transfer modeling through bi-disperse adsorbents. *Chemical Engineering Science*, 62(15), 4040-4053.
- LeVan, M. D., Carta, G., & Yon, C. M. (1999). Adsorption and ion exchange. In D. W. Green (Ed.), *Perry's Chemical Engineers' Handbook* (7th ed.). New York: McGrawHill.
- Li, P., & Tezel, F. H. (2008). Pure and Binary Adsorption Equilibria of Carbon Dioxide and Nitrogen on Silicalite. *Journal of Chemical & Engineering Data*, 53(11), 2479-2487.
- Liaw, C. H., Wang, J. S. P., Greenkorn, R. A., & Chao, K. C. (1979). Kinetics of fixed-bed adsorption: A new solution. *AIChE Journal*, 25(2), 376-381.
- Liow, J. L., & Kenney, C. N. (1990). The backfill cycle of the pressure swing adsorption process. *AIChE Journal*, 36(1), 53-65.
- Liu, H., & Ruthven, D. M. (Eds.). (1996). *Diffusion in Carbon Molecular Sieve*. Boston: Kluwer Academic Publishers.
- Liu, Y., Shi, J., Chen, J., Ye, Q., Pan, H., Shao, Z., & Shi, Y. (2010). Dynamic performance of CO<sub>2</sub> adsorption with tetraethylenepentamine-loaded KIT-6. *Microporous and Mesoporous Materials*, 134(1-3), 16-21.
- Liu, Y., Ye, Q., Shen, M., Shi, J., Chen, J., Pan, H., & Shi, Y. (2011). Carbon dioxide capture by functionalized solid amine sorbents with simulated flue gas conditions. *Environmental Science & Technology*, 45(13), 5710-5716.
- Loganathan, S., Tikmani, M., Edubilli, S., Mishra, A., & Ghoshal, A. K. (2014). CO<sub>2</sub> adsorption kinetics on mesoporous silica under wide range of pressure and temperature. *Chemical Engineering Journal*, 256(0), 1-8.
- Lopes, E. C. N., dos Anjos, F. S. C., Vieira, E. F. S., & Cestari, A. R. (2003). An alternative Avrami equation to evaluate kinetic parameters of the interaction of Hg(II) with thin chitosan membranes. *Journal of Colloid and Interface Science*, 263(2), 542-547.
- Lu, C., Bai, H., Wu, B., Su, F., & Hwang, J. F. (2008). Comparative Study of CO<sub>2</sub> Capture by Carbon Nanotubes, Activated Carbons, and Zeolites. *Energy & Fuels*, 22(5), 3050-3056.

- Lu, C., Su, F., Hsu, S. C., Chen, W., Bai, H., Hwang, J. F., & Lee, H.-H. (2009). Thermodynamics and regeneration of CO<sub>2</sub> adsorption on mesoporous spherical-silica particles. *Fuel Processing Technology*, 90(12), 1543-1549.
- Lu, Z. P., Loureiro, J. M., Rodrigues, A. E., & LeVan, M. D. (1993). Pressurization and blowdown of adsorption beds—II. Effect of the momentum and equilibrium relations on isothermal operation. *Chemical Engineering Science*, 48(9), 1699-1707.
- Lua, A. C., & Yang, T. (2009). Theoretical and experimental SO<sub>2</sub> adsorption onto pistachio-nut-shell activated carbon for a fixed-bed column. *Chemical Engineering Journal*, 155(1-2), 175-183.
- Macdonald, I. F., El-Sayed, M. S., Mow, K., & Dullien, F. A. L. (1979). Flow through Porous Media—the Ergun Equation Revisited. *Industrial & Engineering Chemistry Fundamentals*, 18(3), 199-208.
- Malek, A., & Farooq, S. (1996). Comparison of isotherm models for hydrocarbon adsorption on activated carbon. *AIChE Journal*, 42(11), 3191-3201.
- Mangun, C. L., Benak, K. R., Economy, J., & Foster, K. L. (2001). Surface chemistry, pore sizes and adsorption properties of activated carbon fibers and precursors treated with ammonia. *Carbon*, 39(12), 1809-1820.
- Maroto-Valer, M. M., Tang, Z., & Zhang, Y. (2005). CO<sub>2</sub> capture by activated and impregnated anthracites. *Fuel Processing Technology*, 86(14-15), 1487-1502.
- Mason, J. A., Sumida, K., Herm, Z. R., Krishna, R., & Long, J. R. (2011). Evaluating metal-organic frameworks for post-combustion carbon dioxide capture via temperature swing adsorption. *Energy & Environmental Science*, 4(8), 3030-3040.
- Mendes, A. I. M. M., Costa, C. A. V., & Rodrigues, A. r. E. (1996). Extension of the linear driving force-dusty gas model approximation to include surface or micropore diffusion. *Gas Separation & Purification*, 10(3), 141-148.
- Mendes, A. M. M., Costa, C. A. V., & Rodrigues, A. E. (1995). Linear driving force approximation for isothermal non-isobaric diffusion/convection with binary Langmuir adsorption. *Gas Separation & Purification*, 9(4), 259-270.
- Mitchell, J. E., & Shendalman, L. H. (1973). Study of heat-less adsorption in the model system CO<sub>2</sub> in He. *AIChE Symp. Ser.*, 69(134), 25–32.
- Mohamadinejad, H., Knox, J. C., & Smith, J. E. (2000). Experimental and numerical investigation of adsorption/desorption in packed sorption beds under ideal and nonideal flows. *Separation Science and Technology*, 35(1), 1-22.
- Monazam, E. R., Spenik, J., & Shadle, L. J. (2013). Fluid bed adsorption of carbon dioxide on immobilized polyethylenimine (PEI): Kinetic analysis and breakthrough behavior. *Chemical Engineering Journal*, 223(0), 795-805.

- Montgomery, D. C. (2005). *Design and Analysis of Experiments*: John Wiley and Sons, New York, USA.
- Moreira, R. F. P. M., Soares, J. L., Casarin, G. L., & Rodrigues, A. E. (2006). Adsorption of CO<sub>2</sub> on Hydrotalcite-like Compounds in a Fixed Bed. *Separation Science and Technology*, 41(2), 341-357.
- Mosca, A., Hedlund, J., Ridha, F., & Webley, P. (2008). Optimization of synthesis procedures for structured PSA adsorbents. *Adsorption*, 14(4-5), 687-693.
- Mulgundmath, V. P., Jones, R. A., Tezel, F. H., & Thibault, J. (2012). Fixed bed adsorption for the removal of carbon dioxide from nitrogen: Breakthrough behaviour and modelling for heat and mass transfer. *Separation and Purification Technology*, 85(0), 17-27.
- Mulgundmath, V., & Tezel, F. H. (2010). Optimisation of carbon dioxide recovery from flue gas in a TPSA system. *Adsorption*, 16(6), 587-598.
- Mutasim, Z. Z., & Bowen, J. H. (1991). Pressure swing adsorption in non-isothermal, non-equilibrium conditions : single adsorbate. *Chemical Engineering Research & Design*, 69, 108-118.
- Myer, R. H., & Montgomery, D. C. (2002). *Response Surface Methodology Process and Product Optimization using Designed Experiment* (2nd ed.): John Wiley and Sons, New York, USA.
- Na, B. K., Koo, K. K., Eum, H. M., Lee, H., & Song, H. (2001). CO<sub>2</sub> recovery from flue gas by PSA process using activated carbon. *Korean Journal of Chemical Engineering*, 18(2), 220-227. doi: 10.1007/bf02698463
- Nakao, S.-I., & Suzuki, M. (1983). Mass transfer coefficient in cyclic adsorption and desorption. *Journal of chemical engineering of Japan*, 16(2), 114-119.
- Ning, P., Li, F., Yi, H., Tang, X., Peng, J., Li, Y., Deng, H. (2012). Adsorption equilibrium of methane and carbon dioxide on microwave-activated carbon. *Separation and Purification Technology*, 98(0), 321-326.
- Ölmez, T. (2009). The optimization of Cr(VI) reduction and removal by electrocoagulation using response surface methodology. *Journal of Hazardous Materials*, 162(2-3), 1371-1378.
- Park, J. H., Beum, H. T., Kim, J. N., & Cho, S. H. (2002). Numerical Analysis on the Power Consumption of the PSA Process for Recovering CO<sub>2</sub> from Flue Gas. *Industrial & Engineering Chemistry Research*, 41(16), 4122-4131.
- Park, J. W., Lee, S. S., Choi, D. K., Lee, Y. W., & Kim, Y. M. (2002). Adsorption Equilibria of Toluene, Dichloromethane, and Trichloroethylene onto Activated Carbon Fiber. *Journal of Chemical & Engineering Data*, 47(4), 980-983.
- Patton, A., Crittenden, B. D., & Perera, S. P. (2004). Use of the Linear Driving Force Approximation to Guide the Design of Monolithic Adsorbents. *Chemical Engineering Research and Design*, 82(8), 999-1009.



- Perry, R. H., Green, D. W., & Maloney, J. O. (1997). *Perry's chemical engineers' handbook* (7th ed.): New York, McGraw-Hill.
- Pevida, C., Drage, T. C., & Snape, C. E. (2008). Silica-templated melamine-formaldehyde resin derived adsorbents for CO<sub>2</sub> capture. *Carbon*, 46(11), 1464-1474.
- Pevida, C., Plaza, M. G., Arias, B., Feroso, J., Rubiera, F., & Pis, J. J. (2008). Surface modification of activated carbons for CO<sub>2</sub> capture. *Applied Surface Science*, 254(22), 7165-7172.
- Plaza, M. G., Garcia, S., Rubiera, F., Pis, J. J., & Pevida, C. (2011). Evaluation of ammonia modified and conventionally activated biomass based carbons as CO<sub>2</sub> adsorbents in postcombustion conditions. *Separation and Purification Technology*, 80(1), 96-104.
- Plaza, M. G., Pevida, C., Arenillas, A., Rubiera, F., & Pis, J. J. (2007). CO<sub>2</sub> capture by adsorption with nitrogen enriched carbons. *Fuel*, 86(14), 2204-2212.
- Plaza, M. G., Pevida, C., Arias, B., Feroso, J., Casal, M. D., Martín, C. F., Pis, J. J. (2009). Development of low-cost biomass-based adsorbents for postcombustion CO<sub>2</sub> capture. *Fuel*, 88(12), 2442-2447.
- Plaza, M. G., Pevida, C., Martín, C. F., Feroso, J., Pis, J. J., & Rubiera, F. (2010). Developing almond shell-derived activated carbons as CO<sub>2</sub> adsorbents. *Separation and Purification Technology*, 71(1), 102-106.
- Plaza, M. G., Rubiera, F., Pis, J. J., & Pevida, C. (2010). Ammoxidation of carbon materials for CO<sub>2</sub> capture. *Applied Surface Science*, 256(22), 6843-6849.
- Plaza, M., Pevida, C., Arias, B., Casal, M., Martin, C., Feroso, J., Pis, J. (2009). Different Approaches for the Development of Low-Cost Adsorbents. *Journal of Environmental Engineering*, 135(6), 426-432.
- Porter, J. F., McKay, G., & Choy, K. H. (1999). The prediction of sorption from a binary mixture of acidic dyes using single- and mixed-isotherm variants of the ideal adsorbed solute theory. *Chemical Engineering Science*, 54(24), 5863-5885.
- Przepiórski, J., Skrodzewicz, M., & Morawski, A. W. (2004). High temperature ammonia treatment of activated carbon for enhancement of CO<sub>2</sub> adsorption. *Applied Surface Science*, 225(1-4), 235-242.
- Qinglin, H., Farooq, S., & Karimi, I. A. (2003a). Binary and ternary adsorption kinetics of gases in carbon molecular sieves. *Langmuir*, 19(14), 5722-5734.
- Qinglin, H., Farooq, S., & Karimi, I. A. (2004). Prediction of binary gas diffusion in carbon molecular sieves at high pressure. *AIChE Journal*, 50(2), 351-367.
- Qinglin, H., Sundaram, S. M., & Farooq, S. (2003b). Revisiting transport of gases in the micropores of carbon molecular sieves. *Langmuir*, 19(2), 393-405.
- Radosz, M., Hu, X., Krutkramelis, K., & Shen, Y. (2008). Flue-gas carbon capture on carbonaceous sorbents: Toward a low-cost multifunctional carbon filter for

“green” energy producers. *Industrial & Engineering Chemistry Research*, 47(10), 3783-3794.

- Raghavan, N. S., Hassan, M. M., & Ruthven, D. M. (1985). Numerical simulation of a PSA system. Part I: Isothermal trace component system with linear equilibrium and finite mass transfer resistance. *AIChE Journal*, 31(3), 385-392.
- Raghavan, N. S., Hassan, M. M., & Ruthven, D. M. (1986). Numerical simulation of a PSA system using a pore diffusion model. *Chemical Engineering Science*, 41(11), 2787-2793.
- Reynolds, S., Ebner, A., & Ritter, J. (2005). New Pressure Swing Adsorption Cycles for Carbon Dioxide Sequestration. *Adsorption*, 11(1), 531-536.
- Rezaei, F., & Grahn, M. (2012). Thermal Management of Structured Adsorbents in CO<sub>2</sub> Capture Processes. *Industrial & Engineering Chemistry Research*, 51(10), 4025-4034.
- Rezaei, F., & Webley, P. (2009). Optimum structured adsorbents for gas separation processes. *Chemical Engineering Science*, 64(24), 5182-5191.
- Rezaei, F., & Webley, P. (2010). Structured adsorbents in gas separation processes. *Separation and Purification Technology*, 70(3), 243-256.
- Ribeiro, A. M., Grande, C. A., Lopes, F. V. S., Loureiro, J. M., & Rodrigues, A. r. E. (2008). A parametric study of layered bed PSA for hydrogen purification. *Chemical Engineering Science*, 63(21), 5258-5273.
- Ribeiro, R. P., Sauer, T. P., Lopes, F. V., Moreira, R. F., Grande, C. A., & Rodrigues, A. E. (2008). Adsorption of CO<sub>2</sub>, CH<sub>4</sub>, and N<sub>2</sub> in activated carbon honeycomb monolith. *Journal of Chemical & Engineering Data*, 53(10), 2311-2317.
- Richardson, J. T., Peng, Y., & Remue, D. (2000). Properties of ceramic foam catalyst supports: pressure drop. *Applied Catalysis A: General*, 204(1), 19-32.
- Rinker, E. B., Ashour, S. S., & Sandall, O. C. (2000). Absorption of Carbon Dioxide into Aqueous Blends of Diethanolamine and Methyl-diethanolamine. *Industrial & Engineering Chemistry Research*, 39(11), 4346-4356.
- Rutherford, S. W., & Do, D. D. (2000a). Adsorption dynamics measured by permeation and batch adsorption methods. *Chemical Engineering Journal*, 76(1), 23-31.
- Rutherford, S. W., & Do, D. D. (2000b). Adsorption dynamics of carbon dioxide on a carbon molecular sieve 5A. *Carbon*, 38(9), 1339-1350.
- Ruthven, D. M. (1984). *Principles of Adsorption and Adsorption Processes*. New York: John Wiley & Sons.
- Ruthven, D. M., Farooq, S., & Knaebel, K. S. (1994). *Pressure Swing Adsorption*. New York: VCH Publishers.
- Ruthven, D. M., Lee, L.-K., & Yucel, H. (1980). Kinetics of non-isothermal sorption in molecular sieve crystals. *AIChE Journal*, 26(1), 16-23.

- Sabouni, R., Kazemian, H., & Rohani, S. (2013). Mathematical modeling and experimental breakthrough curves of carbon dioxide adsorption on metal organic framework CPM-5. *Environmental Science & Technology*, 47(16), 9372-9380.
- Sahu, J. N., Acharya, J., & Meikap, B. C. (2009). Response surface modeling and optimization of chromium(VI) removal from aqueous solution using Tamarind wood activated carbon in batch process. *Journal of Hazardous Materials*, 172(2-3), 818-825.
- Samanta, A., Zhao, A., Shimizu, G. K. H., Sarkar, P., & Gupta, R. (2011). Post-Combustion CO<sub>2</sub> Capture Using Solid Sorbents: A Review. *Industrial & Engineering Chemistry Research*, 51(4), 1438-1463.
- Serbezov, A. (1997). *Adsorptive separation of multicomponent gaseous mixtures*. (Ph.D. Dissertation), University of Rochester, Rochester.
- Serbezov, A., & Sotirchos, S. (1998). Mathematical modeling of multicomponent nonisothermal adsorption in sorbent particles under pressure swing conditions. *Adsorption*, 4(2), 93-111.
- Serbezov, A., & Sotirchos, S. V. (2001). On the formulation of linear driving force approximations for adsorption and desorption of multicomponent gaseous mixtures in sorbent particles. *Separation and Purification Technology*, 24(1-2), 343-367.
- Serna-Guerrero, R., & Sayari, A. (2010). Modeling adsorption of CO<sub>2</sub> on amine-functionalized mesoporous silica. 2: Kinetics and breakthrough curves. *Chemical Engineering Journal*, 161(1-2), 182-190.
- Serna-Guerrero, R., Belmabkhout, Y., & Sayari, A. (2010a). Further investigations of CO<sub>2</sub> capture using triamine-grafted pore-expanded mesoporous silica. *Chemical Engineering Journal*, 158(3), 513-519.
- Serna-Guerrero, R., Belmabkhout, Y., & Sayari, A. (2010b). Modeling CO<sub>2</sub> adsorption on amine-functionalized mesoporous silica: 1. A semi-empirical equilibrium model. *Chemical Engineering Journal*, 161(1-2), 173-181.
- Sevilla, M., & Fuertes, A. B. (2011). Sustainable porous carbons with a superior performance for CO<sub>2</sub> capture. *Energy & Environmental Science*, 4(5), 1765-1771.
- Shafeeyan, M. S., Daud, W. M. A. W., Houshmand, A., & Arami-Niya, A. (2011). Ammonia modification of activated carbon to enhance carbon dioxide adsorption: Effect of pre-oxidation. *Applied Surface Science*, 257(9), 3936-3942.
- Shafeeyan, M. S., Daud, W. M. A. W., Houshmand, A., & Shamiri, A. (2010). A review on surface modification of activated carbon for carbon dioxide adsorption. *Journal of Analytical and Applied Pyrolysis*, 89(2), 143-151.
- Shafeeyan, M. S., Wan Daud, W. M. A., & Shamiri, A. (2014). A review of mathematical modeling of fixed-bed columns for carbon dioxide adsorption. *Chemical Engineering Research and Design*, 92(5), 961-988.

- Shafeeyan, M. S., Wan Daud, W. M. A., Houshmand, A., & Arami-Niya, A. (2012). The application of response surface methodology to optimize the amination of activated carbon for the preparation of carbon dioxide adsorbents. *Fuel*, *94*(0), 465-472.
- Shen, C., Grande, C. A., Li, P., Yu, J., & Rodrigues, A. E. (2010). Adsorption equilibria and kinetics of CO<sub>2</sub> and N<sub>2</sub> on activated carbon beads. *Chemical Engineering Journal*, *160*(2), 398-407.
- Shendalman, L. H., & Mitchell, J. E. (1972). A study of heatless adsorption in the model system CO<sub>2</sub> in He, I. *Chemical Engineering Science*, *27*(7), 1449-1458.
- Sherwood, T. K., Pigford, R. L., & Wilke, C. R. (1975). *Mass Transfer*. Singapore: McGraw-Hill Book Company.
- Shokrollahi, A., Alizadeh, A., Malekhosseini, Z., & Ranjbar, M. (2011). Removal of bromocresol green from aqueous solution via adsorption on ziziphus nummularia as a new, natural, and low-cost adsorbent: Kinetic and thermodynamic study of removal process. *Journal of Chemical & Engineering Data*, *56*(10), 3738-3746.
- Siahpoosh, M., Fatemi, S., & Vatani, A. (2009). Mathematical modeling of single and multi-component adsorption fixed beds to rigorously predict the mass transfer zone and breakthrough curves. *Iranian Journal of Chemistry & Chemical Engineering*, *28*(3), 25-44.
- Simo, M., Brown, C. J., & Hlavacek, V. (2008). Simulation of pressure swing adsorption in fuel ethanol production process. *Computers & Chemical Engineering*, *32*(7), 1635-1649.
- Sircar, S. (2006). Basic Research Needs for Design of Adsorptive Gas Separation Processes. *Industrial & Engineering Chemistry Research*, *45*(16), 5435-5448.
- Sircar, S., & Hufton, J. R. (2000a). Intraparticle adsorbate concentration profile for linear driving force model. *AIChE Journal*, *46*(3), 659-660.
- Sircar, S., & Hufton, J. R. (2000b). Why does the linear driving force model for adsorption kinetics work? *Adsorption*, *6*(2), 137-147.
- Sircar, S., & Kratz, W. C. (1988). Simultaneous production of hydrogen and carbon dioxide from steam reformer off-gas by pressure swing adsorption. *Separation Science and Technology*, *23*(14-15), 2397-2415.
- Siriwardane, R. V., Shen, M.-S., Fisher, E. P., & Poston, J. A. (2001). Adsorption of CO<sub>2</sub> on molecular sieves and activated carbon. *Energy & Fuels*, *15*(2), 279-284.
- Sjostrom, S., & Krutka, H. (2010). Evaluation of solid sorbents as a retrofit technology for CO<sub>2</sub> capture. *Fuel*, *89*(6), 1298-1306.
- Soloman, P. A., Ahmed Basha, C., Velan, M., Balasubramanian, N., & Marimuthu, P. (2009). Augmentation of biodegradability of pulp and paper industry wastewater by electrochemical pre-treatment and optimization by RSM. *Separation and Purification Technology*, *69*(1), 109-117.

- Srinivasan, R., Auvil, S. R., & Schork, J. M. (1995). Mass transfer in carbon molecular sieves—an interpretation of Langmuir kinetics. *The Chemical Engineering Journal and the Biochemical Engineering Journal*, 57(2), 137-144.
- Stevens, L., Williams, K., Han, W. Y., Drage, T., Snape, C., Wood, J., & Wang, J. (2013). Preparation and CO<sub>2</sub> adsorption of diamine modified montmorillonite via exfoliation grafting route. *Chemical Engineering Journal*, 215–216(0), 699-708.
- Stöhr, B., Boehm, H. P., & Schlögl, R. (1991). Enhancement of the catalytic activity of activated carbons in oxidation reactions by thermal treatment with ammonia or hydrogen cyanide and observation of a superoxide species as a possible intermediate. *Carbon*, 29(6), 707-720.
- Su, F., Lu, C., Kuo, S. C., & Zeng, W. (2010). Adsorption of CO<sub>2</sub> on amine-functionalized Y-type zeolites. *Energy & Fuels*, 24(2), 1441-1448.
- Suzuki, M. (1990). *Adsorption Engineering*. Tokyo: Kodansha/Elsevier.
- Takamura, Y., Narita, S., Aoki, J., Hironaka, S., & Uchida, S. (2001). Evaluation of dual-bed pressure swing adsorption for CO<sub>2</sub> recovery from boiler exhaust gas. *Separation and Purification Technology*, 24(3), 519-528.
- Thote, J. A., Iyer, K. S., Chatti, R., Labhsetwar, N. K., Biniwale, R. B., & Rayalu, S. S. (2010). In situ nitrogen enriched carbon for carbon dioxide capture. *Carbon*, 48(2), 396-402.
- Tsai, M. C., Wang, S. S., & Yang, R. T. (1983). Pore-diffusion model for cyclic separation: Temperature swing separation of hydrogen and methane at elevated pressures. *AIChE Journal*, 29(6), 966-975.
- Tsai, M. C., Wang, S. S., Yang, R. T., & Desai, N. J. (1985). Temperature-swing separation of hydrogen-methane mixture. *Industrial & Engineering Chemistry Process Design and Development*, 24(1), 57-62.
- Van Der Vaart, R., Huiskes, C., Bosch, H., & Reith, T. (2000). Single and mixed gas adsorption equilibria of carbon dioxide/methane on activated carbon. *Adsorption*, 6(4), 311-323.
- Vargas, A. M. M., Cazetta, A. L., Kunita, M. H., Silva, T. L., & Almeida, V. C. (2011). Adsorption of methylene blue on activated carbon produced from flamboyant pods (*Delonix regia*): Study of adsorption isotherms and kinetic models. *Chemical Engineering Journal*, 168(2), 722-730.
- Veawab, A., Tontiwachwuthikul, P., & Chakma, A. (1999). Corrosion Behavior of Carbon Steel in the CO<sub>2</sub> Absorption Process Using Aqueous Amine Solutions. *Industrial & Engineering Chemistry Research*, 38(10), 3917-3924. doi: 10.1021/ie9901630
- Vinke, P., van der Eijk, M., Verbree, M., Voskamp, A. F., & van Bekkum, H. (1994). Modification of the surfaces of a gasactivated carbon and a chemically activated carbon with nitric acid, hypochlorite, and ammonia. *Carbon*, 32(4), 675-686.

- Wahby, A., Ramos-Fernández, J. M., Martínez-Escandell, M., Sepúlveda-Escribano, A., Silvestre-Albero, J., & Rodríguez-Reinoso, F. (2010). High-surface-area carbon molecular sieves for selective CO<sub>2</sub> adsorption. *ChemSusChem*, 3(8), 974-981.
- Wakao, N., & Funazkri, T. (1978). Effect of fluid dispersion coefficients on particle-to-fluid mass transfer coefficients in packed beds: Correlation of sherwood numbers. *Chemical Engineering Science*, 33(10), 1375-1384.
- Wakao, N., Kaguei, S., & Funazkri, T. (1979). Effect of fluid dispersion coefficients on particle-to-fluid heat transfer coefficients in packed beds: Correlation of nusselt numbers. *Chemical Engineering Science*, 34(3), 325-336.
- Wang, J., Stevens, L. A., Drage, T. C., & Wood, J. (2012). Preparation and CO<sub>2</sub> adsorption of amine modified Mg–Al LDH via exfoliation route. *Chemical Engineering Science*, 68(1), 424-431.
- Wehner, J. F., & Wilhelm, R. H. (1956). Boundary conditions of flow reactor. *Chemical Engineering Science*, 6(2), 89-93.
- Welty, J. R., Wicks, C. E., Wilson, R. E., & Rorrer, G. (2000). *Fundamentals of Momentum*, John Wiley and Sons, New York.
- Xiao, P., Zhang, J., Webley, P., Li, G., Singh, R., & Todd, R. (2008). Capture of CO<sub>2</sub> from flue gas streams with zeolite 13X by vacuum-pressure swing adsorption. *Adsorption*, 14(4-5), 575-582.
- Xu, X., Song, C., Andresen, J. M., Miller, B. G., & Scaroni, A. W. (2002). Novel polyethylenimine-modified mesoporous molecular sieve of MCM-41 type as high-capacity adsorbent for CO<sub>2</sub> capture. *Energy and Fuels*, 16(6), 1463-1469.
- Xu, X., Song, C., Miller, B. G., & Scaroni, A. W. (2005). Adsorption separation of carbon dioxide from flue gas of natural gas-fired boiler by a novel nanoporous "molecular basket" adsorbent. *Fuel Processing Technology*, 86(14-15), 1457-1472.
- Yang, J., & Lee, C. H. (1998). Adsorption dynamics of a layered bed PSA for H<sub>2</sub> recovery from coke oven gas. *AIChE Journal*, 44(6), 1325-1334.
- Yang, J., Lee, C. H., & Chang, J. W. (1997). Separation of hydrogen mixtures by a two-bed pressure swing adsorption process using zeolite 5A. *Industrial & Engineering Chemistry Research*, 36(7), 2789-2798.
- Yang, J., Park, M. W., Chang, J. W., Ko, S.-M., & Lee, C. H. (1998). Effects of pressure drop in a PSA process. *Korean Journal of Chemical Engineering*, 15(2), 211-216.
- Yang, R. T. (1987). *Gas Separation by Adsorption Processes*. Boston: Butterworth.
- Yang, R. T., & Doong, S. J. (1985). Gas separation by pressure swing adsorption: A pore-diffusion model for bulk separation. *AIChE Journal*, 31(11), 1829-1842.
- Yetilmezsoy, K., Demirel, S., & Vanderbei, R. J. (2009). Response surface modeling of Pb(II) removal from aqueous solution by *Pistacia vera* L.: Box-Behnken experimental design. *Journal of Hazardous Materials*, 171(1-3), 551-562.

- Yong, Z., Mata, V., & Rodrigues, A. r. E. (2002). Adsorption of carbon dioxide at high temperature—a review. *Separation and Purification Technology*, 26(2–3), 195-205.
- Zhang, R., & Ritter, J. A. (1997). New approximate model for nonlinear adsorption and diffusion in a single particle. *Chemical Engineering Science*, 52(18), 3161-3172.
- Zhang, Z., & Zheng, H. (2009). Optimization for decolorization of azo dye acid green 20 by ultrasound and H<sub>2</sub>O<sub>2</sub> using response surface methodology. *Journal of Hazardous Materials*, 172(2-3), 1388-1393.
- Zhang, Z., Xu, M., Wang, H., & Li, Z. (2010). Enhancement of CO<sub>2</sub> adsorption on high surface area activated carbon modified by N<sub>2</sub>, H<sub>2</sub> and ammonia. *Chemical Engineering Journal*, 160(2), 571-577.
- Zhang, Z., Zhang, W., Chen, X., Xia, Q., & Li, Z. (2010). Adsorption of CO<sub>2</sub> on zeolite 13X and activated carbon with higher surface area. *Separation Science and Technology*, 45(5), 710-719.
- Zhao, X. X., Xu, X. L., Sun, L. B., Zhang, L. L., & Liu, X. Q. (2009). Adsorption behavior of carbon dioxide and methane on alpo4-14: A neutral molecular sieve. *Energy & Fuels*, 23(3), 1534-1538.
- Zhao, Y., Shen, Y., Bai, L., & Ni, S. (2012). Carbon dioxide adsorption on polyacrylamide-impregnated silica gel and breakthrough modeling. *Applied Surface Science*, 261(0), 708-716.

## LIST OF PUBLICATIONS

### Academic Journal

- **Mohammad Saleh Shafeeyan**, Wan Mohd Ashri Wan Daud, Ahmad Shamiri, “A review of mathematical modeling of fixed-bed columns for carbon dioxide adsorption”, *Chemical Engineering Research and Design*, 92 (2014), Pages 961-988.
- **Mohammad Saleh Shafeeyan**, Wan Mohd Ashri Wan Daud, Amirhossein Houshmand, Arash Arami Niya, “The application of response surface methodology to optimize the amination of activated carbon for the preparation of carbon dioxide adsorbents”, *Fuel* 94 (2012), Pages 465-472.
- **Mohammad Saleh Shafeeyan**, Wan Mohd Ashri Wan Daud, Ahmad Shamiri, “A semi-empirical model to predict adsorption equilibrium of carbon dioxide on ammonia modified activated carbon”, *Chemical Engineering Research and Design*, (2015), Under Review.
- **Mohammad Saleh Shafeeyan**, Wan Mohd Ashri Wan Daud, Ahmad Shamiri, “Modeling of carbon dioxide adsorption onto ammonia-modified activated carbon: Kinetic analysis and breakthrough behavior”, *Fuel*, (2015), Under Review.
- Amirhossein Houshmand, **Mohammad Saleh Shafeeyan**, Arash Arami Niya, Wan Mohd Ashri Wan Daud, , “Modification of activated carbon using nitration followed by reduction for carbon dioxide capture”, *Bulletin of the Korean chemical society*, 2015, Accepted, Article in press.



- Amirhossein Houshmand, **Mohammad Saleh Shafeeyan**, Arash Arami Niya, Wan Mohd Ashri Wan Daud, , “Anchoring a halogenated amine on the surface of a microporous activated carbon for carbon dioxide capture”, Journal of the Taiwan Institute of Chemical Engineers, 44 (2013), Pages 774-779.
- Amirhossein Houshmand, Wan Mohd Ashri Wan Daud, Min-Gyu Lee, **Mohammad Saleh Shafeeyan**, “Carbon dioxide capture with amine-grafted activated carbon”, Water, Air, & Soil Pollution, 223 (2012), Pages 827-835.

#### **Conference Proceeding**

- **Mohammad Saleh Shafeeyan**, Wan Mohd Ashri Wan Daud, Amirhossein Houshmand, Arash Arami Niya, “Statistical modeling and optimization of amination conditions of activated carbon for carbon dioxide adsorption using response surface methodology”, 3rd International Conference on Chemical, Biological and Environmental Engineering (IPCBEE), Singapore, 2011.



Contents lists available at ScienceDirect

Chemical Engineering Research and Design

IChemE

journal homepage: [www.elsevier.com/locate/cherd](http://www.elsevier.com/locate/cherd)

## A review of mathematical modeling of fixed-bed columns for carbon dioxide adsorption

Mohammad Saleh Shafeeyan, Wan Mohd Ashri Wan Daud\*, Ahmad Shamiri

Department of Chemical Engineering, Faculty of Engineering, University of Malaya, 50603 Kuala Lumpur, Malaysia

### ABSTRACT

Carbon dioxide emissions must be stabilized to mitigate the unfettered release of greenhouse gases into the atmosphere. The removal of carbon dioxide from flue gases, an important first step in addressing the problem of CO<sub>2</sub> emissions, can be achieved through adsorption separation technologies. In most adsorption processes, the adsorbent is in contact with fluid in a fixed bed. Fixed-bed column mathematical models are required to predict the performance of the adsorptive separation of carbon dioxide for optimizing design and operating conditions. A comprehensive mathematical model consists of coupled partial differential equations distributed over time and space that describe material, energy, and the momentum balances together with transport rates and equilibrium equations. Due to the complexities associated with the solution of a coupled stiff partial differential equation system, the use of accurate and efficient simplified models is desirable to decrease the required computational time. The simplified model is primarily established based on the description of mass transfer within adsorption systems. This paper presents a review of efforts over the last three decades toward mathematical modeling of the fixed-bed adsorption of carbon dioxide. The nature of various gas–solid equilibrium relationships as well as different descriptions of the mass transfer mechanisms within the adsorbent particle are reviewed. In addition to mass transfer, other aspects of adsorption in a fixed bed, such as heat and momentum transfer, are also studied. Both single- and multi-component CO<sub>2</sub> adsorption systems are discussed in the review.

© 2013 The Institution of Chemical Engineers. Published by Elsevier B.V. All rights reserved.

**Keywords:** Adsorption; Carbon dioxide; Fixed bed; Modeling; Mass transfer; Linear driving force approximation

### Contents

1. Introduction .....	962
2. Overview of the prediction of adsorption column dynamics .....	962
3. Development and analysis of a mathematical model .....	963
3.1. Fluid phase material balance .....	963
3.2. Complexity of kinetic models .....	976
3.2.1. Local equilibrium model .....	976
3.2.2. Mass transfer resistance models .....	977
3.3. Energy balance .....	982
3.3.1. Gas phase energy balance .....	983
3.3.2. Solid-phase energy balance .....	983
3.3.3. Wall energy balance .....	983
3.4. Momentum balance .....	984
4. Conclusion .....	984
Acknowledgments .....	985
References .....	985

\* Corresponding author. Tel.: +60 3 79675297; fax: +60 3 79675319.

E-mail addresses: [ms.shafeeyan@gmail.com](mailto:ms.shafeeyan@gmail.com) (M.S. Shafeeyan), [ashri@um.edu.my](mailto:ashri@um.edu.my) (W.M.A. Wan Daud).

Received 16 March 2013; Received in revised form 22 July 2013; Accepted 19 August 2013

0263-8762/\$ – see front matter © 2013 The Institution of Chemical Engineers. Published by Elsevier B.V. All rights reserved.  
<http://dx.doi.org/10.1016/j.cherd.2013.08.018>



## The application of response surface methodology to optimize the amination of activated carbon for the preparation of carbon dioxide adsorbents

Mohammad Saleh Shafeeyan, Wan Mohd Ashri Wan Daud\*, Amirhossein Houshmand, Arash Arami-Niya

Department of Chemical Engineering, Faculty of Engineering, University of Malaya, 50603 Kuala Lumpur, Malaysia

### ARTICLE INFO

#### Article history:

Received 19 May 2011

Received in revised form 12 November 2011

Accepted 14 November 2011

Available online 30 November 2011

#### Keywords:

Activated carbon

Amination

Carbon dioxide adsorption

Response surface methodology

Optimization

### ABSTRACT

In this comparative study, the application of response surface methodology (RSM) in predicting and optimizing the amination conditions of activated carbon adsorbent toward CO<sub>2</sub> adsorption was investigated. The adsorbents were prepared based on the central composite design (CCD) with three independent variables (i.e., amination temperature, amination time, and the use of pre-heat treated (HTA) or pre-oxidized (OXA) sorbent as the starting material), and the responses studied were CO<sub>2</sub> adsorption and desorption capacity. Two quadratic models were developed to calculate the optimum amination conditions of activated carbon that provide a compromise between the studied responses (dependent variables). From the analysis of variance (ANOVA), the temperature of ammonia treatment was found to be the most important factor; it had a positive influence on CO<sub>2</sub> adsorption capacity but a negative effect on desorption capacity. The optimal point indicated by numerical optimization corresponded to an OXA sorbent that had been aminated at 425 °C for 2.1 h. The activated carbon modified at optimum conditions had a CO<sub>2</sub> adsorption capacity of 26.47 mg/g and a CO<sub>2</sub> desorption capacity of 95.4%. The experimental values of the responses were in good agreement with the amounts predicted by the regression models, indicating that the developed models could adequately predict the responses from the amination variables. The stable adsorption/desorption performance of the optimal activated carbon adsorbent during cyclical operations showed its potential for practical applications.

© 2011 Elsevier Ltd. All rights reserved.

### 1. Introduction

Carbon dioxide (CO<sub>2</sub>) is one of the most important greenhouse gases, and it is primarily released during the combustion of fossil fuels (coal, oil, and natural gas). Power plants that generate electricity from carbon-based fuels are responsible for approximately 1/3 of all anthropogenic CO<sub>2</sub> emissions [1]. The growing environmental concern over global warming and climate change has prompted a global research effort to stabilize the atmospheric concentration of CO<sub>2</sub> and mitigate the unfettered release of greenhouse gases into the atmosphere [2,3]. To date, the most common method for capturing CO<sub>2</sub> from gas streams is low temperature absorption with liquid solvents. Because this process has serious drawbacks, such as an energy-intensive regeneration process and a tendency to corrode process equipment, there is a need to develop alternative energy-efficient separation techniques [2,4–6].

The removal of CO<sub>2</sub> with solid adsorbents may be a more attractive approach than conventional liquid absorbents because it could reduce the cost associated with the capture step. However, the success of this approach is dependent on the development of an easily

regenerated and durable adsorbent with high CO<sub>2</sub> selectivity and adsorption capacities [4,7,8]. One of the most widely used adsorbents for CO<sub>2</sub> capture from flue gas streams is activated carbon. Activated carbon has a number of attractive characteristics, such as its high adsorption capacity, high hydrophobicity, low cost, and low energy requirement for regeneration [1,9].

Introducing basic nitrogen functionalities into the carbon surface through reactions with nitrogen-containing reagents (e.g., ammonia) can increase the capacity of activated carbon to adsorb CO<sub>2</sub> [10–14]. However, the graphitic surface of carbon does not demonstrate a high reactivity toward ammonia. Therefore, carbon is usually oxidized prior to introducing N-containing functionalities to the carbon surface [15,16]. This oxidation-amination process may also enlarge pores and increase surface basicity [17]; such changes in the carbon structure and surface chemistry can increase CO<sub>2</sub> adsorption capacity [12,14].

Most of the processes that produce CO<sub>2</sub> in product streams occur at elevated temperatures (up to 100 °C), and the stream must be cooled before separation takes place. Therefore, developing an adsorbent with a high adsorption capacity at relatively high temperatures can drastically reduce the cooling cost of separation and make CO<sub>2</sub> capture from power plants feasible [7,12]. The CO<sub>2</sub> capture capacity of activated carbon is a combination of both physical and chemical adsorption (i.e., the capacity is governed by

\* Corresponding author. Tel.: +60 3 79675297; fax: +60 3 79675319.

E-mail addresses: [ms.shafeeyan@gmail.com](mailto:ms.shafeeyan@gmail.com) (M.S. Shafeeyan), [ashri@um.edu.my](mailto:ashri@um.edu.my) (W.M.A. Wan Daud).

## Modification of Activated Carbon Using Nitration Followed by Reduction for Carbon Dioxide Capture

Mohammad Saleh Shafeeyan,<sup>\*,\*</sup> Amirhossein Houshmand,<sup>‡</sup> Arash Arami-Niya,<sup>‡</sup> Hosain Razaghizadeh,<sup>‡</sup> and Wan Mohd Ashri Wan Daud<sup>‡</sup>

<sup>\*</sup>Department of Chemical Engineering, Faculty of Engineering, University of Malaya, Kuala Lumpur 50603, Malaysia. \*E-mail: ms.shafeeyan@gmail.com

<sup>‡</sup>Faculty of Environment and Energy, Research and Science Branch, Islamic Azad University, Tehran, Iran  
Received August 11, 2014, Accepted November 10, 2014

Activated carbon (AC) samples were modified using nitration followed by reduction to enhance their CO<sub>2</sub> adsorption capacities. Besides characterization of the samples, investigation of CO<sub>2</sub> capture performance was conducted by CO<sub>2</sub> isothermal adsorption, temperature-programmed (TP) CO<sub>2</sub> adsorption, cyclic CO<sub>2</sub> adsorption-desorption, and dynamic CO<sub>2</sub> adsorption tests. Almost all modified samples showed a rise in the amount of CO<sub>2</sub> adsorbed when the comparison is made in unit surface area. On the other hand, some of the samples displayed a capacity superior to that of the parent material when compared in mass unit, especially at elevated temperatures. Despite ~65% decrease in the surface area, TP-CO<sub>2</sub> adsorption of the best samples exhibited increases of ~10 and 70% in CO<sub>2</sub> capture capacity at 30 and 100 °C, respectively.

**Keywords:** Activated carbon, Surface modification, Anchoring, Amino groups, Nitration

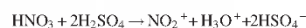
### Introduction

Carbon dioxide is the most significant greenhouse gas that contributes to global warming. This is due to its high emission rate.<sup>1</sup> CO<sub>2</sub> capture and sequestration (CCS) is one of the possible strategies for mitigating the amount of emitted CO<sub>2</sub>. However, these approaches are considered as short-term solutions.<sup>2</sup> Adsorption is the viable method among the various methods currently in use or undergoing investigation for the initial stage of CCS (*i.e.*, CO<sub>2</sub> capture). Adsorption does not have the drawbacks of amine scrubbing as with most conventional technique for CO<sub>2</sub> capture and has lower energy requirement.<sup>3–12</sup> Adsorption capacity of an adsorbate such as CO<sub>2</sub> is determined by the surface area, pore size, adsorbent's surface chemistry, temperature, and partial pressure/concentration of the adsorbate.<sup>12,13</sup> In this regard, surface functional groups may strongly increase the adsorption capacity via the creation of specific interactions between the adsorbent and the adsorbate. However, it is worth noting that textural characteristics have a governing effect on the capacity, whereas surface chemistry has an influencing effect.<sup>14</sup>

Activated carbon (AC) is a suitable adsorbent that has a number of advantages over other porous materials.<sup>10,12,15–18</sup> Modification of AC in terms of surface chemistry has received great attention in producing adsorbents with high capture capacity. It is widely accepted that nitrogen functionalities, in the form of amino or other nitrogen groups, enhance CO<sub>2</sub> adsorption capacity on the AC surface.<sup>4,12,13,19–28</sup> There are a number of methods that can be used to modify the AC surface with nitrogen functionalities (amino groups, in particular), including impregnation with amine-containing compounds,<sup>12,13,22</sup> amination,<sup>13,19–21</sup> silylation with aminosilanes, nitration followed by reduction, anchoring diamines/

polyamines, anchoring halogenated amines, surface-initiated polymerization of ethylenimine and its derivatives, and plasma treatment. The possible techniques for modifying AC with amino groups have been reviewed.<sup>29</sup>

Nitration followed by reduction as one of these potential methods has been studied in this work. Nitration of AC with the mixture of nitric acid and sulfuric acid (the so-called nitrating mixture<sup>30</sup> or mixed acid<sup>31</sup>) creates –NO<sub>2</sub> groups directly attached to the benzene ring of the AC surface.<sup>30–32</sup> Electrophilic aromatic substitution is believed to be the mechanism of nitration<sup>31,33,34</sup>; sulfuric acid is stronger than nitric acid and can protonate the latter with the following reaction:



Nitronium ion (NO<sub>2</sub><sup>+</sup>), which is an electrophile center for nitration, is produced by the above reaction.<sup>30,31,34</sup> This ion is highly reactive and can attach to the aromatic rings with activating or deactivating groups.<sup>35</sup> Theoretically, nitric acid alone is not able to nitrate the benzene ring.<sup>30</sup> However, some studies show that it can produce a small amount of NO<sub>2</sub><sup>+</sup> by electrophilic aromatic substitution.<sup>31,34–36</sup> Reduction of nitro groups to amino groups may be carried out via a variety of methods. Na<sub>2</sub>S<sub>2</sub>O<sub>4</sub><sup>33,34</sup> or iron powder<sup>37</sup> has been employed for reduction of nitrated AC.

### Experimental

**Materials.** The starting material for experimental study was a commercial AC produced from palm shell by Bravo Green Sdn Bhd, Malaysia. After sieving to the size range of 500–850 μm, it was washed with distilled water to remove



## Anchoring a halogenated amine on the surface of a microporous activated carbon for carbon dioxide capture

Amirhossein Houshmand, Mohammad Saleh Shafeeyan, Arash Arami-Niya, Wan Mohd Ashri Wan Daud \*

Department of Chemical Engineering, Faculty of Engineering, University of Malaya, 50603 Kuala Lumpur, Malaysia

### ARTICLE INFO

#### Article history:

Received 13 July 2012  
Received in revised form 9 January 2013  
Accepted 13 January 2013  
Available online 16 March 2013

#### Keywords:

Activated carbon  
Surface modification  
Anchoring  
Amino groups  
Halogenated amine

### ABSTRACT

Activated carbon (AC) surface may be modified by grafting amine-containing compounds to improve the CO<sub>2</sub> adsorption capacity. Two solid sorbents were prepared by anchoring a halogenated amine, *i.e.*, 2-chloroethylamine hydrochloric acid (CEA) on the surface of a microporous AC using a two-stage modification. At the first stage, the samples of AC were oxidized by nitric acid to increase the amount of oxygen surface groups and at the second stage, the oxidized samples were modified by anchoring CEA on the surface to produce a superior CO<sub>2</sub> adsorbent. The oxidized samples were compared with the acid proximate and ultimate analysis, nitrogen adsorption–desorption at –196 °C (77 K) and temperature programmed desorption (TPD) to decide on the best oxidation conditions. The amine-modified samples were analyzed in terms of texture, surface chemistry and CO<sub>2</sub> adsorption. The latter was studied using isothermal CO<sub>2</sub> capture, temperature-programmed (TP) CO<sub>2</sub> adsorption and cyclic operation. The modified samples had a lower surface area than the parent sample. The best modified sample presented an increase of 45% in CO<sub>2</sub> capture capacity at 100 °C. Based on unit surface area, the modified samples showed great CO<sub>2</sub> capture capacities, compared to the virgin sample. Moreover, the modified samples presented a less dependency of CO<sub>2</sub> capacity on temperature. This indicates that the adsorption mechanism shifts from physisorption to chemisorption by increasing temperature.

© 2013 Taiwan Institute of Chemical Engineers. Published by Elsevier B.V. All rights reserved.

### 1. Introduction

Climate change and global warming as a concern of this century is led by emission of greenhouse gases such as carbon dioxide, methane, chlorofluorocarbons (CFCs), ozone and nitrous oxide into the atmosphere [1,2].

Greenhouse effects of chlorofluorocarbons and methane are much higher than carbon dioxide when they are compared in mass unit [2]. However, CO<sub>2</sub> is by far the most important contributor to the global warming due to its high emitted amount by using fossil fuels, which supply around 98% of energy requirement worldwide [3]. According to IPCC, global average of anthropogenic CO<sub>2</sub> emission in the last decade of twentieth century was around 27 × 10<sup>9</sup> metric tons per year [4].

Growth in demand for energy in 21st century with the consideration of the point that fossil fuel is still the major source of energy caused a great attraction toward developing solutions to mitigate anthropogenic CO<sub>2</sub> emission.

Three general strategies can be thought to cut down the released amount of CO<sub>2</sub> [2]. The first one is increasing energy efficiency, which decreases “energy intensity”. The second is using energy sources other than fossil fuels to decrease “carbon intensity” and the last one is capture and sequestration of CO<sub>2</sub> (CCS).

CCS can be considered as a short- or mid-term, but not long-term, solution to the global warming problem, while new sources of energy such as nuclear, solar and biomass, are matured and developed enough to replace fossil fuels safely and economically [5,6]. Different approaches are currently being developed for both stages of CCS. For sequestration of CO<sub>2</sub>, a variety of geoengineering technologies including storage in terrestrial ecosystems, geological formation (*e.g.* emptied fields of oil and gas and deep saline formations) and deep ocean are possible [7,8]. CO<sub>2</sub> capture is the first and most consuming stage of CCS [2]. It takes approximately 70–80% of CCS total cost [8].

Several methods including absorption (amine scrubbing), adsorption, cryogenic distillation and membrane separation are under use and progressive development for CO<sub>2</sub> capture [6,9,10]. Of these ways, absorption by different amine solutions has been higher developed compared with other methods and so is the most conventional one. However, it has several drawbacks such as being energy sensitive (due to high energy requirement for regeneration step), corrosion, solvent degradation (causing restricted lifetime),

\* Corresponding author. Tel.: +60 3 79675297; fax: +60 3 79675319.

E-mail addresses: [amir.hshmd@gmail.com](mailto:amir.hshmd@gmail.com) (A. Houshmand), [ms.shafeeyan@gmail.com](mailto:ms.shafeeyan@gmail.com) (M.S. Shafeeyan), [arash.araminiya@gmail.com](mailto:arash.araminiya@gmail.com) (A. Arami-Niya), [ashri@um.edu.my](mailto:ashri@um.edu.my) (W.M.A.W. Daud).

## Carbon Dioxide Capture with Amine-Grafted Activated Carbon

Amirhossein Houshmand ·  
Wan Mohd Ashri Wan Daud · Min-Gyu Lee ·  
Mohammad Saleh Shafeeyan

Received: 7 February 2011 / Accepted: 25 July 2011 / Published online: 4 August 2011  
© Springer Science+Business Media B.V. 2011

**Abstract** There are several possible methods by which amine groups can be grafted on the surface of activated carbon (AC) to improve their capacity for CO<sub>2</sub> adsorption. Ethylenediamine and diethylenetriamine were selected as amino compounds for anchoring on the surface of an oxidized AC. Oxidation of AC was carried out by concentrated nitric acid. For each amino compound, two “in-solvent” and “solvent-free” methods with a number of grafting times were studied. Nitrogen adsorption–desorption at 77 K and proximate and ultimate analysis were used to determine physical and chemical characteristics of the samples. Temperature-programmed (TP) CO<sub>2</sub> adsorption test from 30°C to 120°C were performed to investigate the effect of modification on CO<sub>2</sub> capture. The modification clearly had a negative

effect on the textural characteristics of the samples, so the samples showed a less CO<sub>2</sub> uptake at lower temperatures. However, the decrease of capture capacity with increasing temperature is to somewhat softer for amine-grafted samples, so that they have a capacity comparable to the parent sample or even more than that at elevated temperatures. This property may give the new adsorbents this opportunity to be used at flue gas temperature with a higher efficiency. CO<sub>2</sub> capture capacity per unit surface area of all the amine-modified samples, however, was significantly improved, compared to the parent sample presenting a great influence of amino groups on the CO<sub>2</sub> capture capacity. Moreover, the used amine compounds and grafting methods were compared in terms of adsorbent characteristics and CO<sub>2</sub> uptake curves. Cyclic adsorption–desorption tests showed a satisfactory regeneration for the modified samples.

A. Houshmand · W. M. A. W. Daud (✉) · M. S. Shafeeyan  
Department of Chemical Engineering,  
Faculty of Engineering, University of Malaya,  
50603 Kuala Lumpur, Malaysia  
e-mail: ashri@um.edu.my

A. Houshmand  
e-mail: amir.hshmd@gmail.com

M. S. Shafeeyan  
e-mail: ms.shafeeyan@gmail.com

M.-G. Lee  
Department of Chemical Engineering,  
Pukyong National University,  
Busan 608-739, Republic of Korea  
e-mail: mglee@pknu.ac.kr

**Keywords** Activated carbon · Surface modification · Amine grafting · Ethylenediamine · Diethylenetriamine

### 1 Introduction

Energy consumption continues to grow worldwide in this century. Considering that fossil fuel is still the major source of energy, a great attention has been concentrated on developing solutions to mitigate anthropogenic CO<sub>2</sub> emission. Available methods

## Statistical Modeling and Optimization of Amination Conditions of Activated Carbon for Carbon Dioxide Adsorption Using Response Surface Methodology

Mohammad Saleh Shafeeyan<sup>1</sup>, Wan Mohd Ashri Wan Daud<sup>1+</sup>, Amirhossein Houshmand<sup>1</sup> and Arash Arami-Niya<sup>1</sup>

<sup>1</sup>Department of Chemical Engineering, Faculty of Engineering, University of Malaya, 50603 Kuala Lumpur, Malaysia

**Abstract.** The surface modification of activated carbon with gaseous ammonia for obtaining an efficient carbon dioxide (CO<sub>2</sub>) adsorbent was optimized using the response surface methodology. The variables chosen were amination temperature, amination time, and the use of pre-heat treated (HTA) or pre-oxidized (OXA) sorbent as the starting material, while the responses were CO<sub>2</sub> adsorption and desorption capacity. Among process parameters studied, amination temperature was found to have the most significant effect on both the studied responses. Quadratic models developed for the two responses studied (dependent variables) indicated the optimum conditions could be obtained by using OXA sorbent with amination temperature of 425 °C and amination time of 2.1 h. The activated carbon modified at optimum condition showed CO<sub>2</sub> adsorption capacity of 26.1 mg/g and CO<sub>2</sub> desorption capacity of 94.9%. The experimental values of the responses at the optimum condition were found to agree satisfactorily with the amounts predicted by the models.

**Keywords:** Activated carbon, Ammonia modification, Carbon dioxide adsorption, Response surface methodology, Optimization

### 1. Introduction

Carbon dioxide (CO<sub>2</sub>) is one of the most important greenhouse gases, and it is primarily released during the combustion of fossil fuels (coal, oil, and natural gas). The growing environmental concern over global warming and climate change has prompted a global research effort to stabilize the atmospheric concentration of CO<sub>2</sub> and mitigate the unfettered release of greenhouse gases into the atmosphere [1]. The removal of CO<sub>2</sub> with solid adsorbents may be a more attractive approach than conventional liquid absorbents because it could reduce the cost associated with the capture step. However, the success of this approach is dependent on the development of an easily regenerated and durable adsorbent with high CO<sub>2</sub> selectivity and adsorption capacities [2]. One of the most widely used adsorbents for CO<sub>2</sub> capture from flue gas streams is activated carbon.

Introducing basic nitrogen functionalities into the carbon surface through reactions with nitrogen-containing reagents (e.g., ammonia) can increase the capacity of activated carbon to adsorb CO<sub>2</sub> [3]. However, the graphitic surface of carbon does not demonstrate a high reactivity toward ammonia. Therefore, carbon is usually oxidized prior to introducing N-containing functionalities to the carbon surface [4]. In the case of high-temperature adsorption, although the role of surface chemistry and the presence of basic nitrogen functionalities is more considerable [5], only the optimization of textural properties is well reached in literature. Although the effect of surface chemistry modification on CO<sub>2</sub> adsorption performance depends on the modification conditions, as far as we know, no study has been done to optimize these modification conditions.

Accordingly, in the present study, RSM based on central composite design (CCD) was used to design experiments, build models and determine the optimum modification conditions for desirable responses. The main objective of this work was to investigate the effect of modification parameters (amination temperature,

<sup>+</sup> Corresponding author. Tel.: (+60 3 79675297); fax: (+60 3 79675319).  
E-mail address: (ms.shafeeyan@gmail.com).